Thesis Presented for the degree of Doctor of Philosophy

Investigating the Parameter Space of Viable Models for $f(R)$ Gravity

Author:
Sulona Kandhai

Supervisors:
Prof. Peter Dunsby
Dr. Alvaro de la Cruz - Dombriz
Prof. Amanda Weltman

October 5, 2019

Abstract

The accelerated expansion of spacetime intuitively points to the existence of new, unknown energy fields pervading the universe, but it is has also spurred the growth of the research field of modified gravity theories. Of these, $f(R)$ theories of gravity is the first and simplest modification to General Relativity, and have been studied extensively for their astrophysical and cosmological predictions. Power law $f(R)$ modifications have been shown to exhibit desirable characteristics, producing the late time accelerated expansion as well as satisfying local tests of gravity. However, there is wide degeneracy among models in this class, and they are known to suffer from cosmological instabilities, which could lead to curvature singularities at finite times. This thesis addresses questions directly relating to model degeneracy and sudden singularities. Cosmologies and cosmological perturbations, resulting from a *general broken power law* modification to GR are generated, studied and evolved. Simulations are performed using 1+3 space time decomposition of the field equations and a dynamical systems approach to $f(R)$ cosmology. The parameter space of this model, which includes the Hu-Sawicki [6], Starobinsky [96] and Miranda [7] $f(R)$ forms as subclasses, is investigated. It is found that there are regions in the parameter space which are completely singular and bound by continuous curves. We also investigate regions of the parameter space in which the attractive nature of gravity is preserved, and find that these regions intersect. The results of a Markov Chain Monte Carlo analysis significantly narrowed the viable region of the exponent parameter space of the general power law $f(R)$ model. Current cosmological distance data; SNIa (Union 2), BAO (6dFGS, BOSS, SDSS, WiggleZ) as well as the LRG power spectrum (SDSS DR9), were used to obtain these constraints. The best fits are compared with the ΛCDM model, and leads to the conclusion that this class is still a candidate for the gravitational interaction.

Declaration

The work presented in this thesis is based partly on collaborations with my supervisors Prof. Peter Dunsby (University of Cape Town) and Dr. Alvaro de la Cruz-Dombriz (University of Cape Town), with Dr. Diego Saez Gomez (University of Lisbon).

Part of this work has been published in the papers

- A. de la Cruz-Dombriz, P. K. S. Dunsby, V. C. Busti, S. Kandhai, *On tidal forces in f(R) theories of gravity, Phys.Rev. D89 (2014) no.6, 064029* [parts in Chapter 3]

- A. de la Cruz-Dombriz, P. K. S. Dunsby, S. Kandhai, D. Saez-Gomez, *Theoretical and observational constraints of viable f(R) theories of gravity*, Physical Review D 93, 084016 (2016) [parts in Chapters 3, 5 & 6]

The following Dropbox link contains a folder with the scripts used to generate the results presented in Chapters 5, 6 and 7: https://www.dropbox.com/sh/0rvo5mpshnkyfv7/AABsoVkV3RhYm8MXHrM48-K0a?dl=0

I hereby declare that the work presented here has not previously been submitted to this or any other university for a degree, and that it represents my own work.

Sulona Kandhai

Acknowledgements

To my supervisors, I have nothing but respect and appreciation for the role you played in my journey. Thank you to Prof. Peter Dunsby; you were a brave and patient supervisor, who introduced me thoroughly to the research realm, and for that I am so very grateful. Thank you for sharing your knowledge and ideas, guiding me through this process and encouraging me throughout, even when I didn't believe in myself. I learnt tremendously from your example, and have to recognise that this would have been impossible without you.

Thank you to Dr. Álvaro dela Cruz Dombriz for being so generous with your expertise and just as kind in your critique. Thank you for your comments, suggestions and support throughout the research and writing. It was a pleasure to work with you. Also, thank you for being instrumental in organising my Spanish exchange in 2017.

Thank you to Prof. Amanda Weltman, for taking me under your wing in 2018. I sincerely appreciated your kindness, in some rather strange and difficult moments, and for giving me the opportunity to work with your group. I learned an incredible amount in that short time and count myself lucky to have been a part of it.

I would like to thank Dr. Diego Saez Gomez and Vinicius Busti for very useful discussions and collaboration in the first stages of my research. Thanks to David Bacon for hosting me at the University of Portsmouth in 2014, and for extremely insightful explanations about aspects of large scale structure. Thanks to the National Research Foundation and the UCT Science Faculty for seeing potential in and funding the bulk of my Ph.D, and to Amanda for taking care of me in the final year. It's impossible to make a Ph.D with no funding! Thanks to the Erasmus A4U program for the opportunity to work and stay at IFT, Universidad Autónoma de Madrid. I would like to acknowledge Prof. Juan Garcia-Bellido for kindly hosting me, and for illuminating discussions on the ISW effect.

Thanks to my friends and allies, you know who you are. You were an essential, irreplaceable part of the Ph.D era. You held my hands, heard my stories, poured my drinks, fed me, let me crash, picked me up and kept me moving. Thank you for indulging and accepting my craziness, and for all the fascinating conversations and wonderful memories.

Thanks to my grandparents for their love, which they sent, strong, though from far away. You have always been my most enthusiastic and faithful cheerleaders, and I deeply appreciate this life you

have afforded and supported. Thanks to Aju Mama, in many ways, my inspiration from the very beginning.

Thanks to my parents, my first peoples, Noddy and Preeti Sharan, whose love and support form the foundation of every journey I've ever embarked upon, and whose fire and energy continue to school and astound me. Thank you to Shejali for literally getting me through those final days. If it weren't for you, I might still be writing.

Contents

Chapter 1

The questions and approach

During my MSc. I was involved in a project studying the dynamics of a viable theory for $f(R)$ gravity, especially related to simulating the expansion history for a specific class of $f(R)$ theories, known as the Hu-Sawicki model [1].

The theory, designed to mimic closely the behaviour of the ΛCDM model[1], without an explicit "cosmological constant", is popular because it also, by construction, will produce correct predictions for the gravitational field in high density regions of space.

At that stage, the focus of the study was on a "dynamical systems" analysis of the $f(R)$ modification to gravity[2]. The equations governing the expansion of space time are recast in terms of a set of new variables - following a method detailed in papers like [2], [3], [4], [5]. These new variables transform the system into a set of autonomous, first order differential equations. Minimising these equations reveals a set of stationary points in the phase space, representing the exact asymptotic solutions to the cosmological equations. This type of analysis provides important information about the model under investigation [6], regarding the existence of critical states of universal evolution. Much of it was not new, since it turns out that many of the fixed points exist for most of the "viable"[3] $f(R)$ power law theories. There are stable and unstable de Sitter fixed points, representing solutions which expand exponentially. All radiation-like expanding fixed point solutions were unstable, and a non analytic matter like expanding fixed point, with saddle instability was also identified. Several trajectories connecting a radiation like fixed point with a de Sitter stable fixed point, passing closely to the matter saddle point were found to exist. This confirms that the model is an appropriate candidate, producing a chronologically correct expansion behaviour.

The main difficulty of this project was how long it took to find a set of model parameters for which the integration of the dynamical system could be performed, in order to determine the exact expansion history. The models are highly sensitive to parameter choices due to the occurrence of

[1] In Chapter 2, we describe the ΛCDM parametrisation of the big bang theory, and the fact that it is desirable to mimic its behaviour.

[2] This method is presented in Section 5.1

[3] The viability of models in this context is discussed in detail in Section 3.2.4

real cosmological singularities [4]. This problem lead to the question of whether or not there exists some region of the parameter space of the Hu-Sawicki model which is completely *free* of singularities. Locating this "region"[5] would significantly simplify analysis of such models as well as possibly help to reduce the parameter space of the entire class.

Once obtaining a set of parameters, quite accidentally, which *was* free of singular behaviour, the Hubble rate and its dynamic derivative, the deceleration parameter were determined to construct a first order background expansion history. A comparison to the ΛCDM model confirmed that the two are essentially the same for all redshifts, except at very late times; the Hubble constant, H_0, and deceleration parameter, q_0, evaluated for the present epoch are inconsistent with their observed values. A naturally interesting point to address is to find the set of model parameters which provide the *closest* mimicking of the observed data.

I performed an analysis to do this using SNIa data to constrain the parameters of the Hu Sawicki model, at a background level. This formed the framework for much of the rest of the research contained within, especially regarding the understanding and handling of sudden singularities.

However, beyond that, a far more interesting question developed, being: Is there a way to constrain the whole $f(R)$ space of theories, in some way, using observational data? Such an analysis has the potential to effectively delete a large chunk of the $f(R)$ model market, and possibly lead to ruling them out completely, and would thus be an important step in this branch of modified gravity theories. The space of all $f(R)$ theories would mathematically include all possible general functions of the Ricci scalar. And no doubt over the last few years several papers have appeared attempting to constrain or rule out subsets of the $f(R)$ theory space. But seeing as the whole problem began at an analysis of the HS model, the class of broken power law theories, which are by construct successful, should be a good place to start; in considering whether or not in this class of models a special region of the space gave particularly suitable fits to observational data.

We therefore considered a general broken power law model having a form given in [7], which we shall describe in Chapter 5. In constraining the parameter space of this model, we may be able to draw some useful conclusions on the best value of the exponent of the Ricci scalar in $f(R)$ theories. And since this is supported by cosmological data, it could significantly reduce the viable power law parameter space that need be considered in $f(R)$ cosmology. If we could, for example, conclusively say that the power of the Ricci scalar in $f(R)$ theories having a power law correction is preferred by certain groups of data to be $n = 1$, this could simplify the cosmology equations for such theories when studying other phenomena that could assess the suitability of the theory.

Once again the difficulty with sudden singularities in the $f(R)$ scenario entered our parameter optimisation MCMC scheme (see Section 5.2). And to understand them, especially in the case of the HS model, we, as others have before, for example [8], resorted to the equivalence between

[4]The appearance of these singularities is discussed in Section 3.2.4

[5]This may also correspond to a special relationship between the parameters.

chameleon like $f(R)$ theories and the scalar tensor gravity modification. I present the conditions for this equivalence when I discuss scalar tensor theories in Chapter 3, and show the potentials of the scalar field in both of the models which we studied in Chapter 5, where the occurrence of the singularity becomes clear. We also give an analytic expression, for a special case of HS model, giving the relationship between the model parameters to guarantee a regular expansion history[6]. But in general, to deal with these singularities, we constructed an effective filter, which on detecting some singular-like behaviour, we avoided them, by assigning a large χ^2 parameter to the parameter optimisation routine. I give a break down of this method in Section 5.4.3, and some curious results on the regions of singularities in the phase space are presented. In the final stages of the project, we simply set a prior on the ranges of the parameters, in each model, which avoid problematic regions.

The rest of this thesis is set out to clarify the steps taken to answer the questions highlighted in these introductory paragraphs. I give a short history and description of cosmology, its development and briefly present important results in GR in the next chapter, leading to a discussion of current cosmological observation data, and the ΛCDM model. I also review $f(R)$ gravity, as an alternative to GR, after motivating the modification of GR in the first place, and specifically in the metric formalism, give the system of equations determining the background cosmological evolution. In Chapter 4, I write down the details of cosmological perturbations and cite the equations which we used, in the 1+3 covariant gauge invariant formalism to investigate the evolution of perturbations in $f(R)$ gravity. Chapters 5, 6 and 7 comprise the unique presentation of the results obtained in this project. Chapter 5 details the models under scrutiny, the approach taken to solve the problem, and the data used. Chapter 6 presents constraints on parameters of a general viable broken power law model, obtained by minimising residuals with respect to the background SNIa and BAO data. Chapter 7 complements the results of Chapter 6, with a set of constraints on the same parameters obtained by considering the linear matter power spectrum of Luminous Red Galaxies (LRGs). The results of the total analysis point to a preferred value for the exponent of the Ricci scalar in this class of theories, significantly constraining its parameter space.

[6]In general, this is not possible, and we made use of numeric methods to find the spaces where singularities are most likely to be found.

Chapter 2

Foundational Concepts in Cosmology

The study of cosmology lies on two fundamental assumptions. The first is the assumption that General Relativity successfully describes the interaction between the geometry of space time and the matter content of the universe. The second is an assumption known as the Cosmological Principle, without which much of the road comprising modern cosmology cannot be paved [9], [10]. The Cosmological Principle states that the Universe is homogeneous and isotropic at cosmologically relevant scales. This notion, powerful as it is, is backed up to a high degree by the isotropy of the Cosmic Microwave Background (CMB), and it is a widely accepted premise in the field, except where the investigation is to question its validity. However, our mere presence, enabling our scientific questioning of the universe, requires matter having clumped, stars being formed, and general non homogeneity at smaller scales. In order to move forward cosmologists are faced with the task of separating the dynamics of small scale and large scale evolution of the observable universe. We impose the background of homogeneity and isotropy, and then upon this background we can introduce perturbations to describe the seeds of the inhomogeneity we observe. However, before we get there, the gravitational interaction, which is the only force we know able to act over large distances, must be understood. This chapter focuses on introducing Cosmology using General Relativity (GR), so that we can continue the discussion of alternatives to GR.

2.1 Concepts in General Relativity

General Relativity is a theory which was born out of the need to unify Special Relativity and the gravitational force. The description of gravity previously contained within it the idea of action at a distance and the instantaneous influence of one body on another, which is incompatible with Special Relativity.

Einstein's main concerns were i) The motion of a body in space seems not to depend on its internal nature, and that all bodies fall in the same way in a gravitational field ii) that the laws of physics observed by any person is invariant of where that person is and iii) that the results of a non

gravitational experiment performed in a laboratory, is independent of the motion of that laboratory. Under the premise that the above three statements are true, the idea that all motion of particles are satisfying some minimised criterion, inspired Einstein to propose that what we perceive as the gravitational interaction is actually our motion (and that of all bodies) along the geodesics of a curved space time. Further to this, he attempted to address Mach's concerns about Special Relativity; the idea the space and time and matter are all inseparably intertwined, and that the motion of a particle must be determined relative to the motion of all other matter in the universe, for in an empty universe, it would be impossible to know what acceleration or rotation means [10].

This lead to the discovery of rules relating to a General Relativity, describing how the gravitational force fits into relativity of motion, along with the development of tensor calculus, and the Einstein field equations. These are given by,

$$G_{\mu\nu} = \kappa T_{\mu\nu}, \tag{2.1}$$

mathematically stating that the space time geometry of the metric is related locally to the matter contained in the space time, and vice versa, which revolutionised the way we think about space and time and gravity. $\kappa = 8\pi G/c^4$, where G is Newton's gravitational constant, c is the speed of light, and $G_{\mu\nu}$ is the Einstein tensor,

$$G_{\mu\nu} \equiv R_{\mu\nu} - \frac{1}{2} g_{\mu\nu} R. \tag{2.2}$$

Here, $R_{\mu\nu}$ is the Ricci tensor, and R is the Ricci scalar, giving measures of the curvature of the given space-time considered, specified by the metric $g_{\mu\nu}$. The Einstein tensor encapsulates the dependence on the curvature of the space time metric $g_{\mu\nu}$. The right hand side of equation (2.1) is proportional to the stress energy momentum tensor, $T_{\mu\nu}$ defined below by expression (2.31), describing the properties and interactions of fluid matter embedded in space time.

One of the cornerstones of relativity, and the foundation of general relativity is the inability to distinguish between two observers, and that their physical experience of the world and any measurements of observables made by observers are equal and should be governed by the same laws of Physics. This progressed the development of tensor calculus in the need to be inclusive of all possible coordinate systems by which physical solutions can be expressed in our universe, and to prioritize those quantities which are invariant of coordinate choice. A test particle subject to no other external forces, falling along the geodesics of a curved space time, will essentially be parallel transported across the space-time manifold, and the motion, x^μ, of this test particle is determined by the geodesic equation:

$$\ddot{x}^\mu + \Gamma^\mu{}_{\nu\lambda} \dot{x}^\nu \dot{x}^\lambda = 0, \tag{2.3}$$

where the metric connection is given by the Christoffel symbol, defined by the partial derivatives of

the metric as

$$\Gamma^{\mu}{}_{\nu\lambda} = \frac{1}{2} g^{\mu\rho}(\partial_\nu g_{\lambda\rho} + \partial_\lambda g_{\rho\nu} - \partial^\rho g_{\nu\lambda}). \tag{2.4}$$

Note that the parallel transportation of a vector on a manifold of arbitrary curvature, which, under no external forces, is the trajectory of a test particle, also requires a carefully defined covariant derivative satisfying

$$\nabla_\alpha g_{\mu\nu} = 0. \tag{2.5}$$

The parallel transport of a vector along a closed loop in a manifold leads to a characterisation of the curvature of that manifold; in a curved space-time, requiring that the start and end points are exactly equal would lead to a change in the orientation of the vector, and if the orientation is controlled (as it is in parallel transport), the start and end points will be different. This same phenomenon can also be identified through the deflection of two particles, initially parallel, falling along their respective geodesics. The geodesic deviation equation describes this deflection by considering the relative separation between two geodesics, using as basis vectors the unit tangent to the geodesic, q, and a unit vector orthogonal to the tangent, s. In this set up, we can describe the relative "acceleration" between two geodesics, mathematically, and this gives a measure of the curvature of the space time in that region. Specifically, it shows how congruent adjacent geodesics shift in the presence of a gravitational field,

$$A^\mu = R^{\mu}{}_{\nu\alpha\beta} u^\nu u^\alpha n^\beta, \tag{2.6}$$

where $A^\mu = \frac{\partial^2 x^\mu}{\partial q^2}$ is the acceleration, $n^\mu = \frac{\partial x^\mu}{\partial s}$ illustrating that the relative acceleration between two neighbouring geodesics is proportional to the curvature of the manifold, controlled by the Riemann tensor,

$$R^{\mu}{}_{\nu\alpha\beta} = \partial_\alpha \Gamma^\mu_{\nu\beta} - \partial_\beta \Gamma^\mu_{\nu\alpha} + \Gamma^\mu_{\sigma\alpha}\Gamma^\sigma_{\nu\beta} - \Gamma^\mu_{\sigma\beta}\Gamma^\sigma_{\nu\alpha}, \tag{2.7}$$

where $\Gamma^{\alpha}{}_{\beta\mu}$ is the Levi Civita connection. The physical implication of the deviation given by Equation (2.6), especially for extended bodies, would be the generation of a tidal effect, as matter particles are forced along geodesics curved by a gravitational field.

The Riemann tensor has a set of symmetry properties, which define a group of identities known as the Bianchi identities;

$$R_{\alpha[\beta\mu\nu]} = 0, \tag{2.8}$$

$$R_{\alpha\beta\mu\nu} = R_{[\alpha\beta][\mu\nu]} = R_{\mu\nu\alpha\beta}, \tag{2.9}$$

equation (2.8) is known as the first Bianchi identities. The following symmetry in its derivatives,

$$\nabla_{[\sigma} R_{\alpha\beta]\mu\nu} = 0, \tag{2.10}$$

gives the second Bianchi identities. Contracting (2.10) twice we obtain the *twice contracted Bianchi identities*,

$$\nabla_\alpha R^\alpha_\mu + \nabla_\beta R^\beta_\mu - \nabla_\mu R = 0, \tag{2.11}$$

which imply

$$\nabla^\alpha G_{\alpha\beta} = 0, \tag{2.12}$$

stating that the Einstein tensor, $G_{\alpha\beta}$, is conserved on any generic curved manifold. Equation (2.12) examined in conjunction with Equation (2.1) leads to

$$\nabla^\alpha T_{\alpha\beta} = 0, \tag{2.13}$$

which is the continuity equation, stating the conservation of energy.

It is now common to teach cosmology including a modification to Einstein's equations (2.1), which includes a cosmological constant such that

$$G_{\mu\nu} = \kappa T_{\mu\nu} - \Lambda g_{\mu\nu}. \tag{2.14}$$

This makes it possible for the generation of a late time accelerated epoch of cosmological expansion, which is actually required from the theory of gravity if SNIa observations, cosmic microwave measurements and the big bang model is to be upheld. We will come back to this point later. In the development below for the rest of Chapter 1, we shall assume the inclusion of the cosmological constant, Λ, on the right hand side of the Einstein Field Equations. It is essential to require that Λ is invariant in space and time,

$$\nabla_\mu \Lambda = 0. \tag{2.15}$$

2.2 1+3 Decomposition of Space-time

The 1+3 decomposition is an analytic approach to studying the equations of motion in a gravitational field, that has the advantage of being physically intuitive, and is especially useful in extended gravity theories, like $f(R)$ models, where the modification may be considered as a separate fluid source, as will be seen in the next chapter.

2.2.1 Kinematics

In the 1+3 approach, a choice of a preferred family of world lines, representing specific types of observers, is made, and this choice is identified by the 4 velocity field of a fundamental observer, u_α. In the plasma of the early universe, this velocity represents an average velocity of the matter contained, which is uniquely defined by the temperature of primordial "fireball", and at late times, the universe will exhibit a clustering of families of world lines, indicating a preferred average motion of matter at a given point. The choice of this vector field, or *frame* is the starting point of any analysis in this formalism, we take it to be the matter frame.

The four velocity is defined to be

$$u^{\alpha} = \frac{dx^{\alpha}}{d\tau} \quad , u^{\alpha}u_{\alpha} = -1. \tag{2.16}$$

From our modern observer perspective, this could be taken to be the unique 4-velocity which cancels the dipole in the cosmic microwave background.

Once the frame is chosen, given the velocity u^{α} of a time-like observer, the following unique projection tensors are defined by:
i) projecting parallel to the 4 velocity vector for any tensor V,

$$V^{\alpha}{}_{\beta} = -u^{\alpha}u_{\beta} \implies V^{\alpha}{}_{\sigma}V^{\sigma}{}_{\beta} = V^{\alpha}{}_{\beta} \quad , \quad V^{\alpha}{}_{\alpha} = 1 \quad , \quad V_{\alpha\beta}u^{\beta} = u_{\alpha}, \tag{2.17}$$

ii) and projecting orthogonal to the 4 velocity, onto the instantaneous rest frame of this observer:

$$h_{\alpha\beta} = g_{\alpha\beta} + u_{\alpha}u_{\beta} \implies h^{\alpha}{}_{\sigma}h^{\sigma}{}_{\beta} = h^{\alpha}{}_{\beta} \quad , \quad h^{\alpha}{}_{\alpha} = 3 \quad , \quad h_{\alpha\beta}u^{\beta} = 0. \tag{2.18}$$

Thus, a space time can be separated into hypersurfaces, where the projection tensor $h_{\alpha\beta}$ defines the spatial part of the instantaneous rest spaces of the chosen observer, and we can choose any affine parameter running along the world lines to represent "time".

Using the four dimensional volume element with the splitting described above, u_{α} and $h_{\alpha\beta}$ are used to form the volume element projected onto the instantaneous rest spaces,

$$\eta_{\alpha\beta\gamma} = u^{\sigma}\eta_{\sigma\alpha\beta\gamma} \implies \eta_{\alpha\beta\gamma} = \eta_{[\alpha\beta\gamma]} \quad , \quad \eta_{\alpha\beta\gamma}u^{\gamma} = 0. \tag{2.19}$$

Furthermore, for a generic tensor $T^{\mu\nu}{}_{\alpha\beta}$ i) the *covariant time derivative* parallel to the fundamental world line is defined by,

$$\dot{T}^{\mu\nu}{}_{\alpha\beta} = u^{\sigma}\nabla_{\sigma}T^{\mu\nu}{}_{\alpha\beta}, \tag{2.20}$$

and ii) the *orthogonal covariant spatial derivative* with total projection on all the indices is,

$$\tilde{\nabla}_{\sigma}T^{\mu\nu}{}_{\alpha\beta} = h^{\mu}{}_{\gamma}h^{\nu}_{\kappa}h^{\theta}{}_{\alpha}h^{\rho}{}_{\beta}h^{\chi}{}_{\sigma}\nabla_{\chi}T^{\gamma\kappa}{}_{\theta\rho}, \tag{2.21}$$

where a tilde denotes the fact that if there is a non-zero vorticity component of the 4-velocity then the above derivative must be distinguished from the 3D proper covariant derivative.

Further useful vector and tensor relations, and projections are summarised below, where angle brackets denote both the orthogonal projection of vectors, and their covariant derivatives with respect to time;

$$v^{\langle\alpha\rangle} = h^{\alpha}{}_{\beta}v^{\beta}, \quad \dot{v}^{\langle\alpha\rangle} = h^{\alpha}{}_{\beta}\dot{v}^{\beta}, \tag{2.22}$$

and the orthogonally projected symmetric trace-free part of tensors, and their derivatives, as

$$T^{\langle\mu\nu\rangle} = \left[h^{(\mu}{}_{\alpha}h^{\nu)}{}_{\beta} - \frac{1}{3}h^{\mu\nu}h_{\alpha\beta}\right]T^{\alpha\beta}, \quad \dot{T}^{\langle\mu\nu\rangle} = \left[h^{(\mu}{}_{\alpha}h^{\nu)}{}_{\beta} - \frac{1}{3}h^{\mu\nu}h_{\alpha\beta}\right]\dot{T}^{\alpha\beta}. \tag{2.23}$$

The projected time and space covariant derivatives of projection tensors $V_{\alpha\beta}$, $h_{\alpha\beta}$ and volume element $\eta_{\alpha\beta\gamma}$ all vanish, given the above definitions, yielding

$$\tilde{\nabla}_\gamma V_{\alpha\beta} = \tilde{\nabla}_\gamma h_{\alpha\beta} = \tilde{\nabla}_\gamma \eta_{\alpha\beta} = 0 \tag{2.24}$$

$$\dot{V}_{\langle\alpha\beta\rangle} = \dot{h}_{\langle\alpha\beta\rangle} = \dot{\eta}_{\langle\alpha\beta\gamma\rangle} = 0, \tag{2.25}$$

$$\tag{2.26}$$

and,

$$\dot{h}_{\alpha\beta} = 2u_{(\alpha}\dot{u}_{\beta)}, \tag{2.27}$$

$$\dot{\eta}_{\alpha\beta\gamma} = 3\dot{u}^\sigma \eta_{\sigma[\alpha\beta}u_{\gamma]} = 0. \tag{2.28}$$

Splitting the first covariant derivative of the 4-velocity u_β into its irreducible parts yields

$$\nabla_\alpha u_\beta = -u_\alpha \dot{u}_\beta + \tilde{\nabla}_\alpha u_\beta = -u_\alpha \dot{u}_\beta + \frac{1}{3}\Theta h_{\alpha\beta} + \sigma_{\alpha\beta} + \omega_{\alpha\beta}, \tag{2.29}$$

where the scalar corresponding to the *volume expansion rate* is given by $\Theta = \tilde{\nabla}_\alpha u^\alpha$, with $H = \Theta/3$. The symmetric trace-free tensor corresponding to the *rate of shear*, is $\sigma_{\alpha\beta} = \tilde{\nabla}_{\langle a}\, u_{\beta\rangle}$, accounting for how the fluid is deformed as it moves, with $\sigma_{\alpha\beta} = \sigma_{(\alpha\beta)}$, $\sigma_{\alpha\beta}u^\beta = 0$ and $\sigma^\alpha{}_\alpha = 0$. Finally, $\omega_{\alpha\beta} = \tilde{\nabla}_{[\alpha}u_{\beta]}$ defines the *skew symmetric vorticity tensor*, describing the rotation of matter relative to some "non rotating frame", with $\omega_{\alpha\beta} = \omega_{[\alpha\beta]}$ and $\omega_{\alpha\beta}u^\beta = 0$. The vorticity vector is defined by

$$\omega^\alpha = \frac{1}{2}\eta^{\alpha\beta\mu}\omega_{\beta\mu}, \quad \text{such that} \quad \omega_\alpha u^\alpha = 0, \omega_{\alpha\beta}\omega^\beta = 0. \tag{2.30}$$

2.2.2 Fluid Sources

The physical properties of the matter content is described by the stress energy momentum tensor, which, in general for a time-like observer, having 4-velocity u_μ, is

$$T_{\mu\nu} = \rho u_\mu u_\nu + q_{(\mu}u_{\nu)} + q_{(\nu}u_{\mu)} + p h_{\mu\nu} + \pi_{\mu\nu}, \tag{2.31}$$

$$q_\mu u^\mu = 0, \qquad \pi_\mu{}^\mu = 0, \qquad \pi_{\mu\nu} = \pi_{\nu\mu}, \qquad \pi_{\mu\nu}u^\nu = 0, \tag{2.32}$$

where, the *relativistic energy density* relative to u^α is,

$$\rho = T_{\alpha\beta}u^\alpha u^\beta, \tag{2.33}$$

the *isotropic pressure* is

$$p = \frac{1}{3}T_{\alpha\beta}h^{\alpha\beta}, \tag{2.34}$$

the *relativistic momentum density*, or *energy flux* relative to u^α, is

$$q_\alpha = -T_{\beta\mu}u^\beta h^\mu{}_\alpha, \tag{2.35}$$

and *projected symmetric trace free anisotropic stress* tensor is

$$\pi_{\alpha\beta} = T_{\mu\nu} h^{\mu}{}_{\langle\alpha} h^{\nu}{}_{\beta\rangle}. \tag{2.36}$$

The physics will be contained in the specification of an equation of state which relates the quantities above.

It is fairly typical to consider, at least at first, the stress energy momentum tensor corresponding to that of a single component perfect fluid, with density ρ, pressure p and an equation of state as the ratio of the two; $w = p/\rho$ such that:

$$q^{\alpha} = \pi_{\alpha\beta} = 0 \implies T_{\mu\nu} = (p+\rho)u_{\mu}u_{\nu} + P g_{\mu\nu}. \tag{2.37}$$

To get the correct kind of behaviour of the matter contents, a set of energy conditions are imposed, taking the following relational form:

$$T^{(M)}_{\alpha\beta} u^{\alpha} u^{\beta} \equiv \rho > 0, \tag{2.38}$$

$$(\rho + p) > 0, \tag{2.39}$$

$$(\rho + 3p) > 0. \tag{2.40}$$

Equation (2.38) forms the *Weak Energy Condition*, requiring merely that the energy density of matter measured by any observer is strictly non negative. Equations (2.39) and (2.40) encode the *Strong Energy Condition*,

$$T^{(M)}_{\alpha\beta} u^{\alpha} u^{\beta} \geq \frac{1}{2} T^{(M)} u^{\gamma} u_{\gamma}, \tag{2.41}$$

which is required to ensure the attractive character of the gravity[1], furthermore that the matter will move in the direction of a positive pressure gradient. Additionally, it is required that the following bounds on the isentropic speed of sound in the fluid are satisfied:

$$0 \leq c_s^2 \leq 1, \quad c_s^2 \equiv \left(\frac{\partial p}{\partial \rho}\right)_{s=\text{const}}, \tag{2.42}$$

and this condition is known as the *Dominant Energy Condition*, required to ensure that the speed of sound in the fluid is at most the speed of light, preserving causality [11], and that it must be at least zero, ensuring the matter is stable.

2.2.3 Curvature

The 1+3 decomposition of the curvature decouples the symmetric trace free part, $C_{\alpha\beta\mu\nu}$ and the symmetric traceful parts $M_{\alpha\beta\mu\nu}$, of the Riemann curvature:

$$R_{\alpha\beta\mu\nu} = C_{\alpha\beta\mu\nu} + M_{\alpha\beta\mu\nu}. \tag{2.43}$$

[1]It is well known that many modified gravity theories result in the emergence of a scalar field which violate all the energy conditions, allowing negative energy density or large negative pressure, which is useful in the context of the Dark Energy problem.

The symmetric trace free part is known as the Weyl curvature, linked to the matter only through the Riemann curvature, it describes the "at a distance" effects of the gravitational field, determining non local dynamics [46], defined as

$$C^{\alpha\beta}{}_{\mu\nu} = R^{\alpha\beta}{}_{\mu\nu} - 2g^{[\alpha}{}_{[\mu}R^{\beta]}{}_{\nu]} + \frac{1}{3}Rg^{[\alpha}{}_{[\mu}\,g^{\beta]}{}_{\nu]}. \tag{2.44}$$

The Riemann tensor passes its symmetries (2.8) and (2.10) directly to the Weyl tensor, and furthermore its traceless nature lends the following property

$$C_{\alpha\beta\mu\nu} = C_{[\alpha\beta][\mu\nu]}, \qquad C^{\alpha}_{\beta\mu\alpha} = 0 = C_{\alpha[\beta\mu\nu]}. \tag{2.45}$$

In order to write completely the decomposition of the Riemann tensor we require the decomposition of the Weyl curvature tensor $C_{\alpha\beta\mu\nu}$, which represents long range, non-local gravitational dynamics occurring over a distance, for example tidal forces and gravitational waves [46]. In this scenario, the motion of the matter fluid is determined by the geodesic deviation equation for time-like curves, and the motion of radiation is determined by null congruences. The Weyl curvature may be further split, in analogy to the decomposition of the Maxwell field strength tensor [11] , into what is known as "gravito-electric" and "gravito-magnetic" parts, which are symmetric and traceless,
the electric part:

$$E_{\mu\nu} = C_{\mu\alpha\nu\beta}u^{\alpha}u^{\beta} \implies E^{\mu}{}_{\mu} = 0, \quad E_{\mu\nu} = E_{(\mu\nu)}, \quad E_{\mu\nu}u^{\nu} = 0, \tag{2.46}$$

the magnetic part:

$$H_{\mu\nu} = \frac{1}{2}\eta_{\mu\alpha\nu}C^{\alpha\beta}{}_{\nu\sigma}u^{\sigma} \implies H^{\mu}{}_{\mu} = 0, \quad H_{\mu\nu} = H_{(\mu\nu)}, \quad H_{\mu\nu}u^{\nu} = 0, \tag{2.47}$$

such that

$$C_{\alpha\beta\mu\nu} = C^{E}_{\alpha\beta\mu\nu} + C^{H}_{\alpha\beta\mu\nu}. \tag{2.48}$$

Then, the complete 1+3 decomposition for the Riemann tensor, in terms of both thermodynamic and geometric quantities defined above, is given by

$$R^{\alpha\beta}{}_{\mu\nu} = R^{\alpha\beta}_{P}{}_{\mu\nu} + R^{\alpha\beta}_{I}{}_{\mu\nu} + R^{\alpha\beta}_{E}{}_{\mu\nu} + R^{\alpha\beta}_{H}{}_{\mu\nu}, \tag{2.49}$$

where

$$R^{\alpha\beta}_{P}{}_{\mu\nu} = \frac{2}{3}(\rho + 3p - 2\Lambda)u^{[\alpha}u_{[\mu}h^{\beta]}{}_{\nu]} + \frac{2}{3}(\rho + \Lambda)h^{[\alpha}{}_{[\mu}h^{\beta]}{}_{\nu]}, \tag{2.50}$$

$$R^{\alpha\beta}_{I}{}_{\mu\nu} = -2u^{[\alpha}h^{\beta]}{}_{[\mu}q_{\nu]} - 2u_{[\mu}h^{[\alpha}{}_{\nu]}q^{\beta]} - 2u^{[\alpha}u_{[\mu}\pi^{\beta]}{}_{\nu]} + 2h^{[\alpha}{}_{[\mu}\pi^{\beta]}{}_{\nu]}, \tag{2.51}$$

$$R^{\alpha\beta}_{E}{}_{\mu\nu} = 4u^{[a}u_{[c}E^{\beta]}{}_{\nu} + 4h^{[\alpha}{}_{\mu}E^{\beta]}{}_{\nu]}, \tag{2.52}$$

$$R^{\alpha\beta}_{H}{}_{\mu\nu} = 2\eta^{\alpha\beta\gamma}u_{[\mu}H_{\nu]\gamma} + 2\eta_{\mu\nu\gamma}u^{[\alpha}H^{\beta]\gamma}, \tag{2.53}$$

and P and I represent the perfect and imperfect fluid components, and E and H represent the electric and magnetic parts of the Weyl curvature tensor.

2.2.4 Propagation and Constraint Equations

The Einstein equations, and its integrability conditions in the 1+3 covariant split formalism results in three sets of equations relevant to a cosmological model.

1. Ricci identities

The first set of propagation equations result from the Ricci identities for the velocity vector field u^α,

$$2\nabla_{[\alpha}\nabla_{\beta]}u^\mu = R_{\alpha\beta}{}^{\mu}{}_{\nu}u^\nu. \tag{2.54}$$

Using the derivative (2.29) in (2.14), and then splitting each of the orthogonal and parallel projections into their respective trace, symmetric trace-free and skew-symmetric parts, the following three propagation equations, and three constraint equations are obtained:

1. The Raychaudhuri Equation

$$\dot{\Theta} - \tilde{\nabla}_\alpha \dot{u}^\alpha = -\frac{1}{3}\Theta^2 + (\dot{u}_\alpha \dot{u}^\alpha) - 2\sigma^2 + 2\omega^2 - \frac{1}{2}(\rho + 3p) + \Lambda, \tag{2.55}$$

describing the acceleration. From this equation we can understand mathematically the attractive character of gravity, and the anti attractive nature of the cosmological constant.

2. The vorticity propagation equation

$$\dot{\omega}^{\langle\alpha\rangle} - \frac{1}{2}\eta^{\alpha\beta\mu}\tilde{\nabla}_\beta \dot{u}_\mu = -\frac{2}{3}\Theta\omega^\alpha + \sigma^\alpha{}_\beta\omega^\beta, \tag{2.56}$$

describing any rotational modes.

3. The shear propagation equation

$$\dot{\sigma}^{\langle\alpha\beta\rangle} - \tilde{\nabla}^{\langle\alpha}\dot{u}^{\beta\rangle} = -\frac{2}{3}\Theta\sigma^{\alpha\beta} + \dot{u}^{\langle\alpha}\dot{u}^{\beta\rangle} - \sigma^{\langle\alpha}{}_\mu\sigma^{\beta\rangle\mu} - \omega^{\langle\alpha}w^{\beta\rangle} - (E^{\alpha\beta} - \frac{1}{2}\pi^{\alpha\beta}), \tag{2.57}$$

illustrating how the "electric" part of the Weyl curvature $E_{\alpha\beta}$ generates a shearing, resulting in a change in the motion of the fluid.

4. The shear divergence constraint,

$$0 = (C_1)^\alpha = \tilde{\nabla}_\beta\sigma^{\alpha\beta} - \frac{2}{3}\tilde{\nabla}^\alpha\Theta + \eta^{\alpha\beta\nu}\left[\tilde{\nabla}_\beta\omega_\nu + 2\dot{u}_\beta\omega_\mu\right] + q^\alpha, \tag{2.58}$$

or the (0α) constraint, shows how the momentum flux is related to the dynamics of the spatial expansion.

5. The vorticity divergence constraint

$$0 = (C_2) = \tilde{\nabla}_\alpha\omega^\alpha - \dot{u}_\alpha\omega^\alpha. \tag{2.59}$$

6. The gravito-magnetic $H_{\alpha\beta}$ constraint,

$$0 = (C_3)^{\alpha\beta} = H^{\alpha\beta} + 2\dot{u}^{\langle\alpha}\omega^{\beta\rangle} - \eta^{\mu\nu\langle\alpha}\tilde{\nabla}_\mu\sigma^{\beta\rangle}{}_\nu + \tilde{\nabla}^{\langle\alpha}\omega^{\beta\rangle}. \tag{2.60}$$

showing the relationship between the Weyl curvature, the vorticity and shear.

2. Twice-contracted Bianchi identities

The second set of equations to be considered result from the twice-contracted Bianchi identities. The constraint obtained by projecting parallel to u^α yields

7. The energy conservation equation:

$$\dot{\rho} + \tilde{\nabla}_\alpha q^\alpha = -\Theta(\rho + p) - 2\dot{u_\alpha} q^\alpha - \sigma_{\alpha\beta}\pi^{\alpha\beta}, \tag{2.61}$$

and by projecting orthogonally to u^α yields

8. The conservation of momentum equation:

$$\dot{q}^{\langle\alpha\rangle} + \tilde{\nabla}^\alpha p + \tilde{\nabla}_\beta \pi^{\alpha\beta} = -\frac{4}{3}\Theta q^\alpha - \sigma^\alpha{}_\beta q^\beta - (\rho + p)\dot{u}^\alpha - \dot{u}_\beta \pi^{\alpha\beta} - \eta^{\alpha\beta\mu}\omega_\beta q_\nu. \tag{2.62}$$

For the case of a perfect fluid, as is ours, the above conservation equations reduce to

$$\dot{\rho} = -\Theta(\rho + p), \tag{2.63}$$

$$\tilde{\nabla}_\alpha p = -(\rho + p)\dot{u}_\alpha. \tag{2.64}$$

3. Once contracted Bianchi identities

Contracting the first set of Bianchi identities (2.8) provide further constraint and propagation equations. The propagation equations from this contraction are listed below.

9. The gravito-electric $\dot{E}$ propagation equation:

$$\begin{aligned}(\dot{E}^{\langle\alpha\beta\rangle} + \frac{1}{2}\dot{\pi}^{\langle\alpha\beta\rangle}) - \eta^{\mu\nu\langle\alpha}\tilde{\nabla}_\mu H^{\beta\rangle}{}_\nu + \frac{1}{2}\tilde{\nabla}^{\langle\alpha} q^{\beta\rangle} \\ = -\frac{1}{2}(\rho + p)\sigma^{\alpha\beta} - \Theta\left(E^{\alpha\beta} + \frac{1}{6}\pi^{\alpha\beta}\right) + 3\sigma^{\langle\alpha}{}_\mu\left(E^{\beta\rangle\mu} - \frac{1}{6}\pi^{\beta\rangle\mu}\right) \\ - \dot{u}^{\langle\alpha} q^{\beta\rangle} + \eta^{\mu\nu\langle\alpha}\left[2\dot{u}_\mu H^{\beta\rangle}{}_\nu + \omega_\mu\left(E^{\beta\rangle}{}_\nu + \frac{1}{2}\pi^{\beta\rangle}{}_\nu\right)\right].\end{aligned} \tag{2.65}$$

10. The gravito-magnetic $\dot{H}$ propagation equation:

$$\begin{aligned}\dot{H}^{\langle\alpha\beta\rangle} + \eta^{\mu\nu\langle\alpha}\tilde{\nabla}_\mu\left(E^{\beta\rangle}{}_\nu - \frac{1}{2}\pi^{\beta\rangle}{}_\nu\right) = &-\Theta H^{\alpha\beta} + 3\sigma^{\langle\alpha}{}_\mu H^{\beta\rangle\mu} + \frac{3}{2}\omega^{\langle\alpha} q^{\beta\rangle} \\ &- \eta^{\mu\nu\langle\alpha}\left[2\dot{u}_\mu E^{\beta\rangle}{}_\nu - \frac{1}{2}\sigma^{\beta\rangle}{}_\mu q_\nu - \omega_\mu H^{\beta\rangle}{}_\nu\right].\end{aligned} \tag{2.66}$$

The constraint equations arising from the single contraction of the Bianchi identities at (2.8) are

11. The gravito-electric divergence constraint:

$$\begin{aligned}0 = (C_4)^\alpha = &\tilde{\nabla}_\beta\left(E^{\alpha\beta} + \frac{1}{2}\pi^{\alpha\beta}\right) - \frac{1}{3}\tilde{\nabla}^\alpha\rho + \frac{1}{3}\Theta q^\alpha - \frac{1}{2}\sigma^\alpha{}_\beta q^\beta - 3\omega_\beta H^{\alpha\beta} \\ &- \eta^{\alpha\beta\mu}\left[\sigma_{\beta\nu}H^\nu{}_\mu - \frac{3}{2}\omega_\beta q_\mu\right].\end{aligned} \tag{2.67}$$

12. The gravito-magnetic divergence (div H) constraint:

$$0 = (C_5)^\alpha = \tilde{\nabla}_\beta H^{\alpha\beta} + (\rho + p)\omega^\alpha + 3\omega_\beta \left(E^{\alpha\beta} - \frac{1}{6}\pi^{\alpha\beta} \right) \tag{2.68}$$

$$+ \eta^{\alpha\beta\mu} \left[\frac{1}{2}\tilde{\nabla}_\beta q_\mu + \sigma_{\beta\nu}(E^\nu{}_\mu + \frac{1}{2}\pi^\nu{}_\mu) \right]. \tag{2.69}$$

The above propagation and constraint equations are closed by specifying the equation of state of the fluid source, or sources, which amounts to choosing restrictions on the thermodynamic properties of the matter. Particularly relevant for late time cosmological considerations is that of pressure-less non relativistic matter, dust, with $p = q_\alpha = \pi_{\alpha\beta} = 0 \implies \dot{u}_\alpha = 0$. The kinematics and thermodynamics above formalize the physical interaction and evolution of the matter and gravitational fields in general relativity. We will pick up this thread again, when considering the 1+3 decomposition in the fourth order gravity framework, and extend the above system to include a second geometric source term arising from higher order curvature terms included in the gravitational action.

2.3 Friedmann Robertson Walker Metric

One of the most progressive stances on our place in the universe, and certainly one underpinning cosmology, is the notion that we, as observers of the vast universe, are negligibly different from any other observers of the same universe. It is known as the Copernican principle, and formalised mathematically by assuming that the 4 dimensional universe apparent to us is spatially isotropic and homogeneous, and that all points are equivalent, on large enough scales.

The observation of isotropy of spatial distribution of extra-galactic radio sources in the sky [12], [13], and especially the extreme isotropy of the CMB, and the precision of these measurements, are widely used as evidence for the spatial isotropy of the observed universe. Assuming the Copernican principle, implies that every observer at any location will observe this level of isotropy, therefore we need a space-time which exhibits spherical symmetry around us, and about *every* point. A universe with this property will also be spatially homogeneous, and is called a Robertson-Walker space-time, of which Minkowski and de Sitter space-times are both special cases. Geometrically, a homogeneous and isotropic space-time is described by maximally symmetric spatial sections, given by the Friedmann-Lemaitre-Roberston-Walker metric,

$$ds^2 = -dt^2 + a(t)^2 q_{ij} dx^i dx^j, \tag{2.70}$$

such that q_{ij} represents any maximally symmetric 3-metric, having Gaussian curvature κ.

2.3.1 Background Cosmology

Setting the background cosmology means selecting a suitable metric for the space time – one that locally satisfies our requirements of observation –, and selecting the kind of matter contained in the universe. From the Einstein field equations in general relativity, we can then find equations of motion for the scale factor, and hence the expansion rate, for the universe. Using spherical coordinates, we have

$$ds^2 = -dt^2 + a^2 \left[\frac{dr^2}{1 - kr^2} + r^2 d\Omega \right]. \tag{2.71}$$

Above, $d\Omega = d\theta + \sin^2\theta d\phi$, and the spatial curvature, k, determines the shape of the spatial sections; $k > 0$ gives a positive **spherical (closed)** curvature to surfaces of constant time, $k < 0$ gives **hyperbolic (open)** hyper-surfaces of constant time, and $k = 0$ gives **flat** surfaces of constant time. Throughout this thesis we assume that the spatial sections are flat, $k = 0$. Note that the choice $k = 0$ is not an initial condition, but rather should be viewed as an approximation which is consistent with measurements of $\Omega_k = -k/H^2a^2$ being very close to zero [14].

The scale factor $a(t)$ describes the way physical distances depend on time. It characterises how the *comoving* distance between two fluid points comoving with the expanding fluid, relates to the proper distance, between those two fluid points, as the universe evolves:

$$D(t) = a(t)\chi, \tag{2.72}$$

such that χ is the constant comoving distance and $D(t)$ gives the proper distance determined by the expansion of the universe. The scale factor is a key measure in the study of cosmology, it can be likened to the roll of position in mechanics; its derivatives define dynamical quantities such as the Hubble rate of expansion of the universe $H(t)$,

$$H(t) \equiv \frac{\dot{a}(t)}{a(t)}, \tag{2.73}$$

and the deceleration parameter

$$q(t) \equiv -\frac{\ddot{a}a}{\dot{a}^2}, \tag{2.74}$$

together almost completely specifying an expansion history for a given model. The scale factor is normalized such that its present value is equal to one, $a_0 = 1$, so $H_0 = H(a = 1)$ is the present value of the Hubble rate, known as the Hubble constant.

The dynamics of the scale factor as a function of time in an FLRW universe may be obtained by substituting the metric at (2.71) and the energy momentum tensor for a perfect fluid at (2.37) into the Einstein equations. Two independent dynamical equations emerge, the first known as the Friedmann equation,

$$H^2 = \left(\frac{\dot{a}(t)}{a(t)} \right)^2 = \frac{8\pi G}{3} \sum_i \rho_i - \frac{\kappa}{a^2}, \tag{2.75}$$

and the second, known as the Raychaudhuri equation,

$$\frac{\ddot{a}(t)}{a(t)} = -\frac{4\pi G}{3}\sum_i \rho_i(1+3w_i). \tag{2.76}$$

ρ represents the energy densities of any possible matter fields present in the model; radiation ρ_γ, pressure-less non-relativistic matter ρ_m etc. $w_i = \frac{P_i}{\rho_i}$ represents the equation of state for a given material, where P is defined uniquely through fundamental considerations of particle behaviour, for a given fluid type. Non-relativistic matter, dust, is known to be pressure-less, such that $w_m = 0$, and a fluid containing only photons has an equation of state $w_\gamma = \frac{1}{3}$. Equations (2.75) and (2.76) are known as the cosmological field equations corresponding to an FLRW metric, the former solving the evolution of the scale factor, and the latter describing how the expansion rate evolves with time. In these simple cosmologies, two parameters control the solution; w, the equation of state, specifying the matter content, and k, indicating the shape of the universe. Using the critical density, $\rho_{cr} = \frac{3H^2}{8\pi G}$, which gives the density required for an spatially flat universe, we are able to express these densities as fractional densities of the critical density itself,

$$\Omega_i = \frac{\rho_i}{\rho_{cr}}, \tag{2.77}$$

such that the Friedmann equation becomes a constraining equation for the densities of energy content of such an asymptotically flat universe,

$$\sum_i \Omega_i = 1. \tag{2.78}$$

Finding solutions for the scale factor, one of the main exercises in the field of modelling in cosmology, requires knowledge of the way the matter content of the Universe evolves with time. The continuity equation, parametrised by the form of matter filling the universe, also given by (2.13), may be recovered by differentiating the Friedmann equation and substituting into the Raychaudhuri equation, obtaining:

$$\dot{\rho}_i + 3H(1+w_i)\rho_i = 0. \tag{2.79}$$

Above, we assume that each of the fluids involved are perfect, moreover, that each evolves separately from the next. There are only a few analytic solutions of the equations (2.75) and (2.79) and these correspond to simple single fluid energy contents. Solving these equations together, the scale dependence of the different forms of energy density, ρ, which feature in the stress energy momentum tensor may be obtained. It is straight forward to show that the density of a pressure-free, non-relativistic type of matter scales as $\rho \propto a^{-3}$, and that for radiation, $\rho \propto a^{-4}$.

The scale evolution of the density of such single fluids may then be input into the Friedmann equation to find evolution of the scale factor with time. Analytically, given a constant equation of state, with $w \neq -1$, it is straight forward to find

$$a = \left(\frac{3(1+w)}{2}H_0 t\right)^{\frac{2}{3w+3}}. \tag{2.80}$$

Substituting $w = \frac{1}{3}$ for a radiation dominated universe gives $a(t) = \sqrt{2H_0 t}$, where as for dust $w = 0$ yields $a(t) = \left(\frac{3H_0 t}{2}\right)^{2/3}$. Even though these solutions correspond to very special cases, they are to a large extent extremely useful in studying various epochs of the universe where it is reasonable to assume that one of the types of energy density dominate drastically over any other forms of energy present. The matter energy density today is about a factor of 10^4 more significant than the energy density of radiation. Over the last thirty years, as it became clear through observations that a time independent, spatially homogeneous fluid has overtaken the matter content, driving the observed accelerated expansion of the universe, a cosmological constant was considered as a mysterious additional form of energy density. If a cosmological constant is the dominant energy content, we find $a(t) = e^{H_0 t}$ as a solution for the scale factor, resulting in an exponential expansion of the universe.

2.4 Distance measures in FLRW cosmology

The Universe, as we see it, is effectively only an instance of its whole evolution. Describing it comes down to a handful of observables, which come from measurements of objects we can see, consisting of magnitudes of fluxes, angular sizes in the sky, and the motion and variation of these observables. Below, I briefly recount the definition of the distances used in cosmology (an essential inferred observable), and the part they play in various measurements and data analyses.

Hubble's law, which is the first order term of a Taylor expansion of the scale factor around the present epoch (t_0, where $a(t_0 = 1)$), gives a linear relation between the recession velocity of an object and its distance, where the Hubble parameter, H is the constant of proportionality, which while constant in space, varies with time.

$$v = Hd. \tag{2.81}$$

We can define a characteristic time for the age of the universe given by the inverse of the present value of the Hubble parameter

$$t_H = \frac{1}{H_0} = 9.78 \times 10^9 h^{-1} \text{ yr} , \tag{2.82}$$

and we define the Hubble *distance* as being the distance travelled by light for the duration of the age of the universe:

$$D_H = \frac{c}{H_0} = 3000 h^{-1} \text{ Mpc}, \tag{2.83}$$

where h is a parameter related to the definition of the Hubble rate as $H_0 = 100h$ kms^{-1}Mpc^{-1}, such that we can constrain dimensionless h alone. The above quantities set a scale for our Universe, and it is common to work in units which set them equal to one; $c = t_H = D_H = 1$, which we also choose to do.

The *comoving* distance, defined as the distance normalised by the expansion of the universe, is given by the integration along a light ray of the distance travelled divided by the scale factor

$$\chi = c\int_t^{t_0} \frac{\mathrm{c}dt'}{a(t')}. \tag{2.84}$$

Distances in cosmology depend on what kind of geometry we assume the universe to have, hence the value that k, the curvature parameter in the metric, plays an important role. Letting $\Omega_k = -kD_H^2$, the radial integral, assuming the observer is at zero, gives an expression for the comoving distance in each scenario:

$$\chi = \int_0^{D_M} \frac{\mathrm{d}r}{\sqrt{1-kr^2}} = \begin{cases} \frac{D_H}{\sqrt{\Omega_k}} \sinh^{-1}\left(\sqrt{\Omega_k}\frac{D_M}{D_H}\right) & \text{for } \Omega_k > 0 \\ D_M & \text{for } \Omega_k = 0 \\ \frac{D_H}{\sqrt{|\Omega_k|}} \sin^{-1}\left(\sqrt{|\Omega_k|}\frac{D_M}{D_H}\right) & \text{for } \Omega_k < 0. \end{cases}$$

where D_M is the "proper" motion distance. In a Euclidean geometry, the comoving distance and the "proper" motion distance are equivalent, however any curvature will generate a deviation between the two. We can now define three important distance measures.

The *angular diameter distance*, a measure based on the apparent proper size of an object on the sky, is given by

$$D_A = \frac{D_M}{1+z}, \tag{2.85}$$

where redshifts are usually determined from the emission spectrum of the object. The angular diameter distance is a significant observable, when objects of known size are identified. Baryon Acoustic Oscillations are an important example, which I will discuss in Chapter 5. Given the total incoming flux from an object, we can use the relationship between bolometric flux, F, and bolometric luminosity, L, to define

$$D_L \equiv \sqrt{\frac{L}{4\pi S}},$$

what is known as the *luminosity distance* of an object, D_L. Since the surface brightness of an object in recession is reduced by a factor of $(z+1)^{-4}$ while the angular area decreases like D_A^{-2}, we have the following relationship between luminosity distance and angular diameter distance

$$D_L = (1+z)D_M = (1+z)^2 D_A.$$

Luminosity distances are especially important in the observations and analyses of point source objects. Supernovae, which comprise important background data in any expansion history study of our Universe or model universes alike, are primarily identified through their spectral redshifts and their luminosity distances, which translate to another important measurable in astronomy, known as the distance modulus. The distance modulus, d, based on the *absolute magnitude* definition of the brightness of celestial objects is defined as follows: Given the apparent magnitude of an object, m, its absolute magnitude, M, which is its apparent magnitude normalised at a distance of 10 pc from

the source, so that $m = M + d$, the distance modulus, d, can be related to the luminosity distance via

$$d \equiv 5 \log \left(\frac{D_L}{10 \text{ pc}} \right).$$

Later, in a statistical analysis, we consider the distance moduli of supernovae of type Ia, to gain background constraints on a specific model for $f(R)$ gravity.

2.5 The Concordance Model

Modern era cosmologists find themselves in a complicated love-hate relationship with what has come to be known as the concordance model of cosmology. It is a parameterisation of the Big Bang Theory containing an inflationary scenario at early times, Cold Dark Matter thought to have driven structure formation, and a cosmological constant for Dark Energy, supposed to drive the late time accelerated expansion of space. It is probably the best fitting model with the multitude of cosmological data we have at our disposal today.

But in reality both dark matter and dark energy still require robust description; it is the task of this generation of cosmologists to find a better grasp, intuitively and scientifically, of what exactly the nature of the these two mysterious energy components are. Below, I include some of the main points of the conversation regarding this model; outlining the evidence and the shortcomings.

2.5.1 Evidence for Dark Matter

The period from 1930 to 1980 was a trial for the existence of dark matter [15], [16]. It started with the discrepancy between the luminous mass of galaxy clusters, specifically the Coma cluster, and the apparent mass predicted by their motions. This came to be known as the missing mass discrepancy, brought to attention by Zwicky in 1933 [17]. With the observation of the galaxy rotation curve for M31, which was the subject of much research for at least a few decades, it became clear that something was missing, when a flattening of the rotation curve was noted. This phenomenon suggests higher densities of matter than observed, and is consistent with the idea that the baryonic luminous part of the galaxy is embedded in a "halo" of dark matter. This dark matter has a density profile that decreases as $1/r^2$. In 1978, X-ray observations of the Virgo cluster [18] revealed an enormous dark matter component, and triggered a phase of research in galaxy clusters which provided insights into the fact that the potential wells associated with clusters of galaxies are far deeper than those inferred by a galaxy cluster comprising only of baryonic matter [19]. This was confirmed by weak lensing measurements. By 1980, it was widely accepted in astronomy that dark matter was a newly identified form of clustering matter density, existing in large haloes around galaxies and galaxy clusters. A few years later, upper limits on CMB anisotropies ruled out a cosmic fluid having only adiabatic baryonic fluctuations, the idea of a massive neutrino lead to the theory of hot dark matter. However, hot dark matter fails to construct the observed large scale structure today, and cold dark matter,

which evolves more slowly with time, was the preferred dark matter candidate. While consensus has been established regarding the existence of cold dark matter, the search for the perfect dark matter candidate, or components, continues [20].

2.5.2 Evidence for Λ, the cosmological constant

Evidence for dark energy first cropped up in the 1980s. Measurements of temperature anisotropies in the CMB pointed strongly to the initial curvature being extremely close to zero, exhibiting spatial flatness, while the total amount of matter is constrained to about 26.8% dark matter and 4.9% baryonic matter, as a percentage of the critical density required for flatness. This implies the existence of an additional form of pressure-less matter making up nearly 68.3% of the total energy density of the universe; making a case for dark energy. There was also a rather large discrepancy between the estimates of the ages of the oldest globular clusters, pinned at between 12 and 14 billion years, and the age of a spatially flat matter dominated universe. Then, in the early 90s, when research showed that a CDM dominated universe was incompatible with observations of the large scale clustering of galaxies, a cosmological constant was considered in an attempt to explain clustering in a range of scales. Later in that same decade was when the evidence for dark energy became especially compelling, it became impossible to ignore the necessity for a non clustering energy density in the modern interpretation of cosmology. Major evidences are:

- Measurements of distances and redshifts of Supernovae Type Ia indicate the universe is expanding at an accelerated rate, and are distinctly more consistent with a universe containing a cosmological constant, than a flat matter dominated universe. Data constrains the equation of state of the dominant fluid energy density is $w = p/\rho \approx -1.068^{+0.080}_{-0.082}$ [21], [22]

- Data from CMB anisotropies and large scale galaxy clustering prefer a model containing a cosmological constant energy density having equation of state $w = -1.10 \pm 0.14$, such that the fractional energy density $\Omega_\Lambda = 0.725 \pm 0.016$ [23], [24], [25]

- Cross correlating the Integrated Sachs Wolfe (ISW) effect measured from the CMB with large scale structure surveys [26] favour an equation of state for dark energy to be around $w = -1.01^{+0.30}_{-0.40}$ at around 4 σ [27].

- Tracking the evolution of the number densities of galaxy clusters as a function of redshift, and therefore time, indicates that it is very unlikely that the universe is flat and matter dominated. In fact the number densities of clusters indicate accelerated expansion at least out to a redshift of 2.

See [28] for an excellent and detailed summary of evidence for dark energy. In any case, the above arguments, stated together, display what seems like an agreement or concordance with the

requirement for both dark matter and dark energy in amounts that are consistent with each piece of evidence, leading to the ΛCDM parametrisation. This model, containing mostly dark energy as a cosmological constant, and second mostly cold dark matter, is called the Concordance model for this reason, and it seems cosmology is now its fight to lose. However, there are several points of weakness in this model, which still promises continued work and excitement for young physicists, and I list them below, as it is *this* section which forms a large part of the motivation for the rest of the thesis, and I am quite sure, many theses to come.

2.6 Shortcomings of ΛCDM

In sharp contrast with the success of the ΛCDM model on very large cosmological scales (X-ray, weak and strong lensing observations of galaxy clusters, the angular power spectrum of the cosmic microwave background, the matter density power spectrum as well as the luminosity distances of supernova), several discrepancies on smaller scales do exist, regarding the nature of dark matter.

- Baryons and dark matter are thought to have very different production mechanisms; cold dark matter is thought to be produced via thermal production, where as baryons are known to be produced non-thermally. However, the energy densities of dark matter and baryons track very closely. This is called the coincidence problem of dark matter [29].

- Galaxies are observed to rotate like a solid body of uniform density at the bulge, implying a dark matter density core at the centre of galaxies. However, N-body simulations determine the density profile of cold dark matter in galaxies to exhibit cuspy behaviour near the centre of the dark matter halo, such that the density increases sharply as we reach the centre. Therefore, there is a discrepancy in dark matter simulations and observational inference [30].

- Another problem rooted in a disagreement between simulations of galaxy formation in the CDM paradigm and observations is known as the missing satellites problem [31]. Simulations predict that a ΛCDM dominated universe would result in numerous dwarf galaxies orbiting the main galaxy. When applied to the Milky Way, it is predicted that our home galaxy should have about 500 satellite galaxies gravitationally bound, however, we only observe about 30 such galaxies. It has been proposed as a solution to this problem that these dwarf galaxies consist completely of dark matter, having very little or no stars at all.

In addition to the issues on small scale, mainly issues for Dark Matter to answer to, the cosmological constant is itself a problematic quantity. Besides having very little fundamental motivation for its inclusion in the theory other than to fix the late time acceleration of the Universe's expansion, it suffers a terrible phenomenological issue, known as he cosmological constant problem, as its

inferred value is about 120 orders of magnitude smaller than its value predicted by particle physics. The cosmological constant also suffers a coincidence problem; its energy density is the same order of magnitude today as the matter density today. Given that these two quantities evolve in completely different ways, based on their apparently completely different nature, the coincidence of their present values gives pause for thought on whether a cosmological constant is the best interpretation of dark energy.

Chapter 3

$f(R)$ Gravity

Dark energy is one of the most fascinating problems of our time. It represents an absolute unknown quantity, availing a single clue : the apparent accelerated expansion of the universe at the present time.

Modifications to GR emerged almost immediately upon its acceptance by the scientific community, in 1919 when Weyl toyed with the inclusion of higher order curvature invariants in the Einstein-Hilbert action. While this and other attempts were driven by curiosity alone, the physical motivation for such exercises was yet to come. For a while, the high energy, strong gravity regime of physics stimulated interested in higher order theories of gravity, where it was shown that, unlike GR, higher order theories are renormalisable [32], and taking quantum corrections into account requires higher order curvature invariants in the gravitational action [33], [34], [35], [36]; and in such cases the modification to GR would be effective only at scales on the order of the Planck length in the primordial universe [37] or near extremely dense objects [38]. The low energy, late time implications of a modified theory of gravity only became a field of interest later in the 20th century, when the revelation that over 75% of the energy density of the universe may be unknown, came to light from projects such as High-Z Supernova search team (1994), Sloan Digitial Sky Survey (2000) and the Wilkinson Microwave Anisotropy Probe (2001) to name a few [39], [40], [41].

Dark energy signals new forms of energy density or additional physics, or both. While the ΛCDM model, a widely accepted description of the universe —containing two dark forms of energy, Dark matter and Dark energy and a physically unexplained period of rapid inflation— does very well to describe the Universe we live in and matches many observations, it suffers several well known drawbacks. Since, there is no reason to dismiss a more general theory of gravity than GR, the idea that the observed accelerated expansion of the universe emerges as a low energy, large scale artefact of such a theory should not, and can not, be ignored.

Extending General Relativity amounts to making one or more generalisations of the following form; (i) adding fields, (ii) including higher order derivatives of the curvature or curvature related invariants, and, or (iii) adding dimensions to the spacetime. These modifications resulted in the explosion of the

field of extended gravity theories [42], [43] far richer than GR in complexity, such as the Lovelock theories featuring field equations second order in the metric [44], Gauss-bonnet theories [45], [46], [47], scalar-tensor theories [48], [49], [50], [51] , Tensor-Vector-Scalar (TeVeS) [52], [53], [54], theories with extra dimensions [55], and Dvali-Gabadadze-Porrati (DGP) [56] theories for gravity. In this chapter we focus our attention on a class of theories that gained popularity after the discovery of the accelerating universe, however had been considered in the context of inflation [37], which involves introducing a generic function of the Ricci scalar into the action from which Einstein's field equations are derived. We give a detailed review of the motivation behind it, its appeal and difficulties, and present general results in $f(R)$ gravity. We also consider the equivalence between $f(R)$ theories and a subclass of scalar-tensor theories; namely Brans-Dicke gravity.

3.1 Scalar -Tensor Theories

Probably the first competitor to Einstein's GR, was Nordström's 1912 conformally flat scalar theory of gravity. In 1937, Dirac showed by allowing the gravitational coupling, G, to vary slowly over cosmological time scales, there was a relationship that naturally emerged, between the cosmological constants and the fundamental physical constants. This idea was developed by Jordan, a little over a decade later, using a scalar field to describe the gravitational coupling. In his theory, the gravitational scalar field behaved like a matter field, and satisfied a conservation law which was added to the theory, [57], [58]. By 1961, these ideas, thanks to Brans and Dicke [59], culminated into a complete gravitational theory, containing a scalar field, which, together with the metric tensor, is responsible for the gravitational interaction. The so-called Brans - Dicke theory is indeed considered to be the prototype of alternative theories to General Relativity [58].

Thereafter, scalar field considerations towards viable alternatives to general relativity, which include Brans-Dicke theory as a sub class, developed into branches of research including scalar fields coupled non-minimally to curvature and induced gravity. Further popularity of a gravitational scalar field stems from the fact that such a field is actually a vital part of theories such as supergravity, superstring and M-theories. Scalar fields have also been essential in the development of inflationary scenarios following the increasing support of an inflationary epoch to cure several well known shortcomings of the big bang theory. Thus, it appears, the scalar field, has yet a large role to play in at least theoretical cosmology and gravitational physics.

In this section we review the action of general scalar tensor theories, their resulting field equations, and their relation to fourth order gravity. This is an interesting point for this work, since while the bulk of the considerations may be done from a purely metric fourth order gravity perspective, viewing a given theory, from within a scalar tensor framework offers insight into the physical dynamics of the effective scalar field potential, which when faced with solutions containing singularities, proved useful. We therefore present a discussion of the equivalence between $f(R)$ gravity and scalar-tensor

gravity.

3.1.1 Field Equations of Scalar-Tensor Gravity

Scalar-tensor theories of gravity include Brans-Dicke, Galileons, $f(R)$, quintessence and Horndeski theories as subclasses. The general Lagrangian for a scalar tensor theory has the form [42],

$$\mathcal{L} = \frac{1}{16\pi}\sqrt{-g}\left[f(\phi)R - g(\phi)\nabla_\mu\phi\nabla^\mu\phi - 2\lambda(\phi)\right] + \mathcal{L}_M(\Psi, h(\phi)g_{\mu\nu}), \tag{3.1}$$

where f, g, h and λ are all arbitrary functions of the scalar field ϕ. We may absorb the function $h(\phi)$ into the metric following the conformal transformation

$$h(\phi)g_{\mu\nu} \to g_{\mu\nu}. \tag{3.2}$$

The resulting frame is known as the Jordan frame, wherein the scalar field and matter are independent, the motion of test particles are coupled to geodesics, and the weak equivalence principle is satisfied for massless test particles. The effects of this transformation on the arbitrary functions f, g, h and λ, maybe absorbed by a redefinition of these functions. By setting $f(\phi) \to \phi$, we can write the Lagrangian density as

$$\mathcal{L} = \frac{1}{16\pi}\sqrt{-g}\left[\phi R - \frac{\omega(\phi)}{\phi}\nabla_\mu\phi\nabla^\mu\phi - 2\Lambda(\phi)\right] + \mathcal{L}_M(\Psi, g_{\mu\nu}), \tag{3.3}$$

where $\omega(\phi)$ is another arbitrary function, which is called the coupling parameter, and the function Λ is a generalisation of the cosmological constant. Variation of the action with respect to the metric tensor leads to the following equation

$$\phi G_{\mu\nu} + \left[\Box\phi + \frac{1}{2}\frac{\omega}{\phi}(\nabla\phi)^2 + \Lambda\right]g_{\mu\nu} - \nabla_\mu\nabla_\nu\phi - \frac{\omega}{\phi}\nabla_\mu\phi\nabla_\nu\phi = 8\pi T_{\mu\nu}. \tag{3.4}$$

Now, the scalar field is also an independent dynamical quantity, and varying the action with respect to ϕ yields an additional field equation

$$(2\omega + 3)\Box\phi + \omega'(\nabla\phi)^2 + 4\Lambda - 2\phi\Lambda' = 8\pi T, \tag{3.5}$$

where the primes indicate derivatives with respect to the scalar field ϕ. Scalar-tensor theories are known to be conformally equivalent to general relativity. Under conformal transformations, we may find a metric that obeys a set of field equations like the Einstein equations, such that the scalar degree of freedom sources a matter field, which does not couple to the geodesics like ordinary matter. Anyhow, the conformal equivalence with GR means that such theories can be studied using familiar framework and intuition.

3.1.2 Brans-Dicke Theory

Brans-Dicke like theories were first studied in an attempt to mathematically include Mach's principle in a theory consistent with GR. In Brans-Dicke theories the gravitational coupling is not a constant but takes the form of a scalar field, which is position dependent and in principle feels the distance scaled effects of all the matter contained in the universe [58], [59]. Renewed interest in the theory was due to the discovery that string theories contain a low energy limit which is given by a Brans-Dicke Lagrangian [60]. And yet further interest was fueled by the fact that $f(R)$ theories, which due to the chameleon mechanism [61] are once again contenders as models for weak field gravity, are dynamically equivalent to Brans-Dicke theories.

The action for Brans-Dicke theories in the Jordan frame, may be obtained from Equation (3.3), by sending $\omega \to$ constant with $\Lambda \to 0$, and is given in terms of the metric $g_{\mu\nu}$ and the scalar ϕ by

$$S_{BD} = \frac{1}{16}\int d^4x\sqrt{-g}\left[\phi R - \frac{\omega}{\phi}g^{\mu\nu}\nabla_\mu\phi\nabla_\nu\phi - V(\phi)\right] + S_M. \tag{3.6}$$

Here S_M is the action of any matter fields present, and ω characterises the dimensionless Brans-Dicke parameter. ϕ couples directly to the scalar curvature, but not to the matter fields. We can identify the potential $V(\phi)$ as a general form of the "cosmological constant", but it may not in fact be a constant, and may reduce to an effective mass for the scalar field defined by its derivatives with respect to ϕ:

$$m^2 = \frac{1}{2\omega+3}\left(\phi\frac{d^2V}{d\phi^2} - \frac{dV}{d\phi}\right). \tag{3.7}$$

Variation with respect to the metric yields the following field equations

$$G_{\mu\nu} = \frac{8\pi}{\phi}T^{(M)}_{\mu\nu} + \frac{\omega}{\phi^2}\left(\nabla_\mu\phi\nabla_\nu\phi - \frac{1}{2}g_{\mu\nu}\nabla^\alpha\phi\nabla_\alpha\phi\right) + \frac{1}{\phi}\left(\nabla_\mu\nabla_\nu\phi - g_{\mu\nu}\Box\phi\right) - \frac{V}{2\phi}g_{\mu\nu}, \tag{3.8}$$

as usual,

$$T^M_{\mu\nu} = \frac{-2}{\sqrt{-g}}\frac{\delta}{\delta g^{\mu\nu}}\sqrt{-g}\mathcal{L}^M. \tag{3.9}$$

In this theory, the gravitational coupling is identified as the inverse of the scalar field,

$$G_{eff} = \frac{1}{\phi}, \tag{3.10}$$

making it a function of spacetime. In order to obtain a positive gravitational coupling and to guarantee the attractive character of gravity, we require that $\phi > 0$. If we then vary the action with respect to ϕ, we obtain an equation which looks like an equation of motion for the scalar field,

$$\frac{2\omega}{\phi}\Box\phi + R - \frac{\omega}{\phi^2}\nabla^\alpha\phi\nabla_\alpha\phi - \frac{dV}{d\phi} = 0. \tag{3.11}$$

Using the trace of the field equations, we may eliminate R, resulting in the dynamical equation for the Brans Dicke scalar field, ϕ :

$$\Box\phi = \frac{1}{2\omega+3}\left(8\pi T^M + \phi\frac{dV}{d\phi} - 2V\right). \tag{3.12}$$

This dynamical equation may also be derived from 3.5. The Brans-Dicke parameter is a free parameter of the theory. Values of $\omega = 1$ are consistent with results in string theory, but in order to satisfy local solar system tests of gravity, ω is preferred to be large. In fact, the larger ω is, the more closely Brans-Dicke theory resembles general relativity. The latest most stringent statements on values for ω come from the Cassini probe, and was found to satisfy $\omega > 40000$, and it is this fine tuning of ω which renders BD theories unattractive. However, as we will discuss later, this fine tuning may be avoided altogether, if the mass of the scalar field is large [62], [63].

3.2 Introduction to $f(R)$ gravity

Our choice to focus on $f(R)$ models follows intensive research related to cosmology applications of modified gravity theories, and the growth of a wider understanding of the consequences and limitations of these theories. They have been the subject of some reasonable amount attention over the last few decades, and this interest gave birth to a plethora of investigations into simple $f(R)$ models, the cosmologies which they govern, as well as some understanding into the caveats associated with these theories [58], [64], [14], [65], [66].

From understanding why $f(R)$ gravity, even in its apparently simple form, is the first general stable modification to the E-H action that can be made [33], [32], to constructing stable and well behaved cosmologies, which come close to mimicking our observed universe, and our favourite best fit model, the field has evolved substantially. And the questions we are asking are continuously updated.

$f(R)$ models were first considered as a means to facilitate the early time rapid inflation we require in the big bang theory [37], and more recently as a mechanism to generate the late time accelerated epoch of universal expansion. These theories result from a straight forward modification of the Einstein-Hilbert action, where the Ricci scalar is replaced with a general function of the Ricci scalar;

$$S = \int [f(R)]\sqrt{-g}d^4x, \tag{3.13}$$

$\kappa = 8\pi G$, where G is the gravitational coupling constant, g is the determinant of the metric, R is the Ricci scalar, and we take $c = \hbar = 1$.

The $f(R)$ inflationary theories have survived the onslaught of cosmological data and are able to predict the slope of the primordial power spectrum of matter density perturbations.

The renewed interest also brought to light the scalar tensor theory equivalence with $f(R)$ gravity, and that such an action was also able to produce the accelerated expansion, which was being sought at the time, eg. [67]. Early studies were pessimistic about $f(R)$ gravity; arguing that these theories are automatically ruled out since solar system constraints required that the Brans Dicke parameter be greater than 40000 [68], while other results concluded that $f(R)$ going like a power law of R could

not produce standard cosmological evolution [69], [70], both for large and small values of the Ricci scalar. It was claimed that $f(R)$ theories did not contain a phase of matter like expansion ($t^{2/3}$), when it was found that typically a radiation like expansion era ($t^{1/2}$) preceded a phase of dark energy expansion, eg. [71]. Since then, understanding of the dynamics of these models and the various general restrictions which can be placed has developed significantly, and several models have been proposed which are able to sustain a period of matter like expansion, for example [6], [72], [73], [74].

In the sections that follow, I shall discuss the details of these theories, in some cases more deeply than others; I will review the derivation of the field equations, discuss the FLRW solutions corresponding to viable theories, as well as what exactly makes a theory viable in the first place.

$f(R)$ models for gravity are very useful to consider in this context, in that the generality they grant is fairly wide, and their resulting field equations yield rich and interesting phenomenologies, providing ways to reproduce whatever dynamics we desire. They are also arguably the most straight forward modification to GR that can be made, meaning their solutions, when the form of f is chosen well[1], are tractable and their exact solutions can give insight into this class of theories as well as GR. Probably the most attractive advantage is that in $f(R)$ theories it is possible to avoid the Ostrogradsky instability, from which many other higher-order modifications to the gravitational Lagrangian suffer.

The generalised form of the Lagrangian included in equation (3.13) supersedes the addition of even higher order quadratic curvature invariants such as $R^{\mu\nu}R_{\mu\nu}$ or $R^{\mu\nu\alpha\beta}R_{\mu\nu\alpha\beta}$, which in fact will reduce to a function of R, $f(R)$, when considering a maximally symmetric, four dimensional space time (such as the one which we will occupy ourselves with for the entirety of this work). The first generalisation of the Einstein-Hilbert action would be to replace the linear gravitational component of the Lagrangian with quadratic contractions of the Riemann tensor, $R^2, R^{\mu\nu}R_{\mu\nu}, R^{\mu\nu\alpha\beta}R_{\mu\nu\alpha\beta}$ and $\varepsilon^{\mu\nu\sigma\gamma}R_{\mu\nu\alpha\beta}R^{\alpha\beta}_{\sigma\gamma}$, resulting in the following gravitational Lagrangian :

$$\mathcal{L}_g = \sqrt{-g}f(R, R^{\alpha\beta}R_{\alpha\beta}, R^{\mu\nu\alpha\beta}R_{\mu\nu\alpha\beta}...). \tag{3.14}$$

However, considering the fact that the derivative of the Gauss-Bonnet invariant and $\varepsilon^{\mu\nu\sigma\gamma}R_{\mu\nu\alpha\beta}R^{\alpha\beta}_{\sigma\gamma}$ go to zero in four dimensional spacetimes :

$$(\delta/\delta g_{ab})\int d^4x\sqrt{-g}(R^{\mu\nu\alpha\beta}R_{\mu\nu\alpha\beta} - 4R^{\mu\nu}R_{\mu\nu} + R^2) = 0, \tag{3.15}$$

$$(\delta/\delta g_{ab})\int d^4x\sqrt{-g}\varepsilon^{\mu\nu\sigma\gamma}R_{\mu\nu\alpha\beta}R^{\alpha\beta}_{\sigma\gamma} = 0, \tag{3.16}$$

as well as the following result due to the symmetries of the Riemann tensor, in maximally symmetric space times,

$$(\delta/\delta g_{ab})\int d^4x\sqrt{-g}(3R^{ab}R_{ab} - R^2) = 0, \tag{3.17}$$

it is possible to express the quadratic invariants $R^{\mu\nu}R_{\mu\nu}$ or $R^{\mu\nu\alpha\beta}R_{\mu\nu\alpha\beta}$ in terms of R^2, (a proof of these identities may be found in [75], p134). This conveniently allows any Lagrangian involving

[1]We discuss the various viability considerations which must be made in Section 3.2.4.

these higher order quadratic invariants to be expressed in general in the form of a generic power law function of R, or $f(R)$, as given by Equation (3.13).

This first correction to the Einstein-Hilbert action became especially popular as a candidate to describe the accelerated expansion of the universe without the need for a cosmological constant, as in the ΛCDM model, or an additional unknown source in the stress energy tensor. This theory gives rise to a gravitational field propagated by a spin-2 massless graviton, as well as massive scalar degree of freedom which couples to density, resulting in an effective long range *fifth force*, which can facilitate the late time acceleration observed, given a suitably chosen form for the function, $f(R)$.

3.2.1 Branches of $f(R)$ formalisms

The governing field equations for a general $f(R)$ theory may be derived by varying the modified action (3.13) in three different ways which result in three different formalisms within the $f(R)$ framework.

The so called *metric formalism* considers the only independent variable to be the metric itself, and the action,

$$S_{met} = \frac{1}{2\kappa}\int d^4x\sqrt{-g}f(R) + S_m(g_{\mu\nu},\psi) \tag{3.18}$$

is varied with respect to the metric alone, yielding the following field equations (which will be derived in Section 3.2.2)

$$f'(R)R_{\mu\nu} - \frac{1}{2}f(R)g_{\mu\nu} - [\nabla_\mu\nabla_\nu - g_{\mu\nu}\Box]\, f'(R) = \kappa T_{\mu\nu}. \tag{3.19}$$

These equations are fourth order with respect to the metric, and the matter fluids are described by

$$T_{\mu\nu} = \frac{-2}{\sqrt{-g}}\frac{\delta S_M}{\delta g^{\mu\nu}}. \tag{3.20}$$

Here, ∇_μ is the covariant derivative corresponding to the Levi-Civita connection of the metric, $\Box = \nabla^\mu\nabla_\mu$, and primes denote differentiation with respect to R the Ricci scalar.

In what is known as the *Palatini formalism*, the action from which we begin (3.18) remains the same, however, we assume that the connection is an independent quantity as well as the metric, and the action must then be varied with respect to both independently:

$$S_{Pal} = \frac{1}{2\kappa}\int d^4x\sqrt{-g}f(\mathcal{R}) + S_m(g_{\mu\nu},\psi), \tag{3.21}$$

where the Riemann tensor and the Ricci tensor are constructed with the independent connection, and, in this section, we denote the difference between the metric Ricci scalar, R, and the Ricci scalar constructed with this independent connection as $\mathcal{R} = g^{\mu\nu}\mathcal{R}_{\mu\nu}$. Making use of the formula

$$\delta\mathcal{R}_{\mu\nu} = \bar{\nabla}_\gamma\delta\Gamma^\gamma{}_{\mu\nu} - \bar{\nabla}_\nu\delta\Gamma^\gamma{}_{\mu\gamma}, \tag{3.22}$$

varying (3.21) with respect to both the metric and the connection yields

$$f'(\mathcal{R})\mathcal{R}_{(\mu\nu)} - \frac{1}{2}f(\mathcal{R})g_{\mu\nu} = \kappa T_{\mu\nu}, \tag{3.23}$$

$$-\bar{\nabla}_\gamma\left(\sqrt{-g}f'(\mathcal{R})g^{\mu\nu}\right) + \bar{\nabla}_\sigma\left(\sqrt{-g}f'(\mathcal{R})g^{\sigma(\mu}\right)\delta^{\nu)}_\gamma = 0. \tag{3.24}$$

Here, $\bar{\nabla}_\mu$ represents the covariant derivative defined with the independent connection used in the variation.

The important point is that when $f(\mathcal{R}) = \mathcal{R}$ in the Palatini formalism and when $f(R) = R$ in the metric formalism, both theories reduce to GR, and produce the same physics. However, they deviate significantly as soon as a more general function is used in the Lagrangian, in terms of the resulting physical theories. It is not yet clear which of these approaches is preferred.

While, in the Palatini formalism, the connection is considered independent from the metric, it does not appear explicitly in the Lagrangian. The Lagrangian density corresponding to the matter fields is independent of the connection itself, and the covariant derivatives of the matter fields are defined as usual with the Levi-Civita connection. In fact it is possible to eliminate the independent connection entirely from the field equations of Palatini $f(R)$ gravity, since the independent connection is not actually related to the geometry. In this sense, the Palatini formalism is still a metric theory [65].

The more general, and significantly more complicated, approach to the variation of the $f(R)$ action is known as *metric affine* $f(R)$, where the geometric properties of the independent connection manifest in its coupling to the matter fields present in the theory. In this way, we generalise both of the afore mentioned approaches, taking both the metric and the connection to be independent variables, and also allowing the matter to depend explicitly on the connection.

However, all things considered, for the research performed and presented for this thesis, it is the metric approach which we choose to be the underlying formalism of our study into viable $f(R)$ theories.

3.2.2 Field equations of Metric $f(R)$ gravity

In this section, the derivation of the field equations in metric gravity is presented and explained.

Starting with the action for a general function for $f(R)$ as the Lagrangian density in a vacuum given by equation (3.13) to satisfy the variational principle

$$\delta\int d^4x\sqrt{-g}f(R) = 0, \tag{3.25}$$

where we think of $f(R)$ as being R plus a corrective term $g(R)$, such that when $g(R) \to 0$ we regain GR. Varying this action in a locally inertial frame, we obtain

$$\begin{aligned}\delta\int\sqrt{-g}f(R) &= \int\left[\delta(\sqrt{-g}f(R)) + \sqrt{-g}\delta f(R)\right]d^4x \\ &= \int\sqrt{-g}\left[f'(R)R_{\mu\nu} - \frac{1}{2}g_{\mu\nu}f(R)\right]\delta g^{\mu\nu}d^4x + \int\sqrt{-g}f'(R)g^{\mu\nu}\delta R_{\mu\nu}d^4x,\end{aligned} \tag{3.26}$$

where the primes indicate a derivative with respect to scalar curvature, R. Using the fact that

$$\begin{aligned} g^{\mu\nu}\delta R_{\mu\nu} &= g^{\mu\nu}\partial_\alpha(\delta\Gamma^\alpha{}_{\mu\nu}) - g^{\mu\alpha}\partial_\alpha(\delta\Gamma^\nu{}_{\mu\nu}) \\ &= \partial_\alpha(g^{\mu\nu}\delta\Gamma^\alpha{}_{\mu\nu} - g^{\mu\alpha}\delta\Gamma^\nu{}_{\mu\nu}) = \partial_\alpha W^\alpha, \end{aligned} \tag{3.27}$$

where we define W^α to be

$$W^\alpha \equiv g^{\mu\nu}\delta\Gamma^\alpha{}_{\mu\nu} - g^{\mu\alpha}\delta\Gamma^\nu{}_{\mu\nu}, \tag{3.28}$$

we can write the second integral of (3.26) as:

$$\begin{aligned} \int \sqrt{-g}f'(R)g^{\mu\nu}\delta R_{\mu\nu}d^4x &= \int \sqrt{-g}f'(R)\partial_\alpha W^\alpha d^4x \\ &= \int \partial_\alpha\left[\sqrt{-g}f'(R)W^\alpha\right]d^4x - \int \partial_\alpha\left[\sqrt{-g}f'(R)\right]W^\alpha d^4x. \end{aligned} \tag{3.29}$$

The first term in (3.29) represents the total divergence of the field, and assuming the fields go to zero at infinity, we obtain

$$\int \sqrt{-g}f'(R)g^{\mu\nu}\delta R_{\mu\nu}d^4x = \int \partial_\alpha\left[\sqrt{-g}f'(R)\right]W^\alpha d^4x. \tag{3.30}$$

The quantity W^α can be determined simply by considering the variation of the connection $\Gamma^\alpha{}_{\mu\nu}$.

$$\Gamma^\sigma{}_{\mu\nu} = \frac{1}{2}g^{\sigma\delta}\left[g_{\delta\mu,\nu} + g_{\delta\nu,\mu} - g_{\mu\nu,\delta}\right] \ , \tag{3.31}$$

Varying the above quantity, we have

$$\begin{aligned} \delta\Gamma^\alpha{}_{\mu\nu} &= \delta\left[\frac{1}{2}g^{\alpha\beta}\left(\partial_\mu g_{\beta\nu} + \partial_\nu g_{\mu\beta} - \partial_\beta g_{\mu\nu}\right)\right] \\ &= \frac{1}{2}g^{\alpha\beta}\left[\partial_\mu(\delta g_{\beta\nu}) + \partial_\nu(\delta g_{\mu\beta}) - \partial_\beta(\delta g_{\mu\nu})\right]. \end{aligned} \tag{3.32}$$

In a locally inertial frame, the covariant derivative of the metric vanishes, so we obtain

$$\delta\Gamma^\nu{}_{\mu\nu} = \frac{1}{2}g^{\nu\beta}\partial_\mu(\delta g_{\nu\beta}). \tag{3.33}$$

Using this fact, and contracting (3.32) with the metric, we have:

$$\begin{aligned} g^{\mu\nu}\delta\Gamma^\alpha{}_{\mu\nu} &= \frac{1}{2}g^{\mu\nu}\left[-\partial_\mu(g_{\beta\nu}\delta g^{\beta\alpha}) - \partial_\nu(g_{\mu\beta}\delta g^{\alpha\beta}) - g^{\alpha\beta}\partial_\beta(\delta g_{\mu\nu})\right] \\ &= \frac{1}{2}\partial^\alpha(g_{\mu\nu}\delta g^{\mu\nu}) - \partial^\mu(g_{\beta\mu}\delta g^{\nu\beta}) \end{aligned} \tag{3.34}$$

$$\text{and} \quad \Rightarrow g^{\mu\alpha}\delta\Gamma^\nu{}_{\mu\nu} = -\frac{1}{2}\partial^\alpha(g_{\nu\beta}\delta g^{\nu\beta}). \tag{3.35}$$

With this, we may substitute for the respective expressions into (3.28), and thus (3.30) becomes:

$$\int \sqrt{-g}f'(R)g^{\mu\nu}\delta R_{\mu\nu}\ d^4x = \int \partial_\alpha\left[\sqrt{-g}f'(R)\right]\left[\partial^\mu(g_{\mu\nu}\delta g^{\alpha\nu}) - \partial^\alpha(g_{\mu\nu}\delta g^{\mu\nu})\right]\ d^4x. \tag{3.36}$$

Integrating the expression given by (3.36) by parts, and once again neglecting the terms corresponding to total divergence, we obtain:

$$\int \sqrt{-g} f'(R) g^{\mu\nu} \delta R_{\mu\nu} \; d^4x = \int g_{\mu\nu} \partial^\alpha \partial_\alpha [\sqrt{-g} f'(R)] \delta g^{\mu\nu} \; d^4x - \int g_{\mu\nu} \partial^\mu \partial_\alpha [\sqrt{-g} f'(R)] \delta g^{\alpha\nu} \; d^4x. \tag{3.37}$$

Thus, the variation of (3.13) gives

$$\delta \int \sqrt{-g} f(R) \; d^4x = \int \sqrt{-g} \left[f'(R) R_{\mu\nu} - \frac{1}{2} f(R) g_{\mu\nu} \right] \delta g^{\mu\nu} \; d^4x \tag{3.38}$$

$$+ \int \left[g_{\mu\nu} \partial^\alpha \partial_\alpha (\sqrt{-g} f'(R)) - g_{\alpha\nu} \partial^\mu \partial_\alpha (\sqrt{-g} f'(R)) \right] \delta g^{\mu\nu} \; d^4x. \tag{3.39}$$

Now, we obtain the fourth order vacuum field equations for $f(R)$ gravity by setting the variation equal to zero, to minimise:

$$f'(R) R_{\mu\nu} - \frac{1}{2} f(R) g_{\mu\nu} = (\nabla_\mu \nabla_\nu - g_{\mu\nu} \Box) \, f'(R) \tag{3.40}$$

For aesthetic appeal, we may add and subtract $\frac{1}{2} f'(R) g_{\mu\nu} R$ from the left hand side of (3.40), leading to a set of equations which look very much like the Einstein Field Equations

$$f'(R) R_{\mu\nu} + \frac{1}{2} f'(R) g_{\mu\nu} R - \frac{1}{2} f'(R) g_{\mu\nu} R - \frac{1}{2} f(R) g_{\mu\nu} = (\nabla_\mu \nabla_\nu - g_{\mu\nu} \Box) \, f'(R). \tag{3.41}$$

Collecting the terms in the following way,

$$R_{\mu\nu} - \frac{1}{2} g_{\mu\nu} R \equiv G_{\mu\nu} = \frac{1}{f'(R)} \left[(\nabla_\mu \nabla_\nu - g_{\mu\nu} \Box) \, f'(R) + \frac{1}{2} g_{\mu\nu} [f(R) - f'(R) R] \right]. \tag{3.42}$$

we find the Einstein tensor equal to a combination of terms in $f(R)$.

The right hand side of (3.42) may be considered an effective stress energy tensor, behaving as a source for the modified field. This new source term is dubbed the *curvature fluid*, $T^{curv}_{\mu\nu}$. Of course, this idea is not to be taken literally, and we should be aware that actually the resulting theory is completely different from GR. However, intuitively, it lends a useful perspective; the vacuum itself contains a source that is generated by the geometry, in an otherwise Einstein-like field.

For a universe including matter, we have

$$S = \int \sqrt{-g} \, [f(R) + \mathcal{L}_m] \, d^4x, \tag{3.43}$$

$\mathcal{L}_m$ is the Lagrangian for all matter sources present. Following the same prescription as above, the $f(R)$ modified field equations are obtained in a universe containing matter fields:

$$f'(R) R_{\mu\nu} - \frac{1}{2} f(R) g_{\mu\nu} - (\nabla_\mu \nabla_\nu - g_{\mu\nu} \Box) \, f'(R) = T^{matter}_{\mu\nu} \tag{3.44}$$

Here, as usual $T^M_{\mu\nu}$, the stress energy tensor for the matter components is defined by

$$T_{\mu\nu} = \frac{-2}{\sqrt{-g}} \frac{\delta S_M}{\delta g^{\mu\nu}}. \tag{3.45}$$

We can, once again, rearrange the above set of equations to resemble the Einstein field equations with an additional source term, comprising the higher order curvature contributions:

$$R_{\mu\nu} - \frac{1}{2}g_{\mu\nu}R = G_{\mu\nu} = T^{(curv)}_{\mu\nu} + \frac{1}{f'(R)}T^{(matter)}_{\mu\nu}, \tag{3.46}$$

so that, when the stress energy tensor for the curvature fluid is exactly zero, we recover GR. An effective gravitational coupling can then be defined as $G_{eff} \equiv G/f'(R)$. The coupling is required to be positive, in analogy to requiring that the graviton is not a ghost, in scalar tensor gravity, and this amounts to the following condition on the form of $f(R)$

$$f'(R) > 0, \tag{3.47}$$

which we touch on again later.

The trace of the field equations at (3.44) is given by

$$f'(R)R + 3\Box f'(R) - 2f(R) = \kappa T, \tag{3.48}$$

$T = g^{\mu\nu}T^{(matter)}_{\mu\nu}$. The trace equation makes obvious the distinction between $f(R)$ gravity and GR, where we have $R = -\kappa T$. In this case, a vanishing of ordinary matter sources does not imply a vanishing of Ricci curvature, hinting at the importance of the additional field, $df/dR = f'(R) \equiv f_R$ and the roll it plays in the resultant physics of the given universe. In fact, we can interpret the trace equation as being an equation of motion for this emergent scalar degree of freedom, f_R, which is sometimes called the scalaron.

For maximally symmetric solutions of the above equation, where we have surfaces of constant curvature; $R = constant$, considering $T_{\mu\nu} = 0$, (3.48) reduces to

$$f_R R - 2f(R) = 0 \tag{3.49}$$

which is just an algebraic expression for R. When $R = 0$ is a root of the above equation, then the field equations at (3.44) become $R_{\mu\nu} = 0$ corresponding to isotropic, homogeneous and flat Minkowski spacetime. When $R = const$ is taken to be a root of (3.49), the field equations (3.44) become $R_{\mu\nu} = g_{\mu\nu}C/4$. This root gives an interesting and desirable result, as it represents exponential expansion of space time, similar to the behaviour of a GR universe plus a cosmological constant.

3.2.3 $f(R)$ gravity from a Scalar - Tensor Perspective

Performing coordinate transformations, normalizations or variable redefinitions is standard in classical mechanics, if it lends to the convenience of computation and interpretation. Finding equivalence between theories is a tool which comes in handy, especially when a toy theory is being investigated. For the sake of definiteness, we can say that two theories are thought to be equivalent if after an appropriate redefinition, or transformation, or renormalization, their field equations, or the action

from which these are derived, are identical. In this case, the dynamics of the equivalent theories are indistinguishable, and previous progress of understanding on one theory will shed light on a theory which is found to be a dynamically equivalent, alternative representation to the former.

It is well known that it is possible to recast quadratic modifications to GR in the form of a Brans-Dicke theory, which is a sub class of scalar tensor theories, and this equivalence is easily extended to the special case of $f(R)$ gravity [65], [76]. While metric $f(R)$ gravity explicitly seems not to include extra fields in the action, and Palatini gravity, though containing an independent connection is also fundamentally a metric theory, they both may be represented by various forms of a Brans-Dicke theory. Below the equivalence is discussed considering the equivalence of the actions.

Beginning with the action for metric $f(R)$ gravity as given at (3.13), we may introduce, for the sake of seeing the equivalence, an auxiliary field, χ, to the action, which becomes,

$$S_{met} = \frac{1}{2\kappa}\int d^4x\sqrt{-g}\left[f(\chi) + f'(\chi)(R-\chi)\right] + S_M(g_{\mu\nu},\psi), \tag{3.50}$$

where $f(R) = f(\chi) + f'(\chi)(R-\chi)$ is an expansion around the Ricci scalar. Varying with respect to χ reveals the following equation:

$$f''(\chi)(R-\chi) = 0. \tag{3.51}$$

Clearly, under the condition that $f''(\chi) \neq 0$, we obtain that $R = \chi$, which of course reproduces the original action. If we identify $f'(\chi)$ as a scalar degree of freedom, and set $f'(\chi) = \phi$ to be a scalar field, we can then define its effective potential:

$$V(\phi) = \chi(\phi)\phi - f(\chi(\phi)). \tag{3.52}$$

And this allows us to rewrite the action at (3.13) in terms of the scalar field ϕ and its potential;

$$S_{met} = \frac{1}{2\kappa}\int d^4x\sqrt{-g}\left[\phi R - V(\phi)\right] + S_M(g_{\mu\nu},\psi), \tag{3.53}$$

which is simply the action of a Brans-Dicke theory, in the Jordan frame, with the Brans-Dicke parameter $\omega_0 = 0$, known as "massive dilaton gravity" [77]. Note that this scalar field, ϕ, is unlike a matter field, and it can violate all the energy conditions[2] [58]. The field equations which result from metric variation of (3.53) are

$$G_{\mu\nu} = \frac{\kappa}{\phi}T_{\mu\nu} - \frac{1}{2}\frac{1}{\phi}g_{\mu\nu}V(\phi) + \frac{1}{\phi}(\nabla_\mu\nabla_\nu\phi - g_{\mu\nu}\Box\phi), \tag{3.54}$$

$$R = V'(\phi). \tag{3.55}$$

To guarantee that an $f(R)$ theory is dynamically equivalent to a scalar tensor theory the condition $f'' \neq 0$ must be satisfied. Following a similar approach as above for the Palatini formalism of $f(R)$

[2]The energy conditions will be specified in Section (3.4.1).

gravity reveals that in this framework, the Palatini $f(R)$ theory is dynamically equivalent to the Brans-Dicke theory, for which $\omega_0 = -\frac{3}{2}$ [65], [78], [79].

The trace of (3.54) may be used to eliminate R, resulting in an equation of motion for the scalar field in terms of its potential in the presence of matter:

$$(2\omega_0 + 3)\Box\phi + 2V(\phi) - \phi\frac{dV}{d\phi} = \kappa T. \tag{3.56}$$

The above equation highlights the difference between metric and Palatini $f(R)$ theories, and the dynamics which result. It is clear to see that in the Palatini formalism the emergent scalar field, or scalaron, is not a dynamic variable, where as in metric $f(R)$ theory the derivatives of the scalar field are non zero, therefore resulting in an extra scalar degree of freedom [65].

3.2.4 Viability

In this section I lay out the viability constraints on the general $f(R)$ Lagrangians which come from (1) reproducing the required behaviour in the weak field limit, (2) the cosmological and (3) primordial regimes of investigation, (4) theoretical instabilities and ghost fields, and (5) sudden singularities.

Given the apparent freedom on the form of f, it has become common practice to construct a theory which produces the desired results in the required energy level or time scale. It has been an interesting exercise for many years, given the $f(R)$ modified cosmological field equations, to find forms for f which are consistent with data [6], [80], [81], [82], [7]. Even the reverse has been done, where given sets of data, a function, which best suits the data, has been reconstructed (in fact it was found that in this situation no function of R does better than R+Constant [83]. Below we discuss the various considerations which must be made before an $f(R)$ theory is accepted as potentially viable.

Cosmological dynamics

It is not difficult to find a function, which, in principle, is consistent with the background observations, in that it can produce the late time acceleration. The point of interest is making sure that other aspects of gravitational and cosmological theory are also respected, especially Big Bang Nucleosynthesis, the temperature anisotropies of the CMB and the expected growth of large scale structure. The theory must provide an inflationary period, which can solve the horizon, flatness and monopole problems. After which a radiation domination phase of the universe, leading to a matter domination phase must be present. Finally evolving toward a stable de Sitter type expansion, such that the theory agrees with observations. Furthermore, there should be smooth transitions between the various phases.

Correct Weak-field limit

It took some time before consistent results regarding the weak field limit in $f(R)$ theories of gravity were derived and understood. In 2003, Chiba [84] concluded that, by virtue of the fact that observa-

tions required Brans-Dicke theories with $\omega_0 \geq 40000$, $f(R)$ theories must be ruled out, having $\omega_0 = 0$. However, the Parametrized Post Newtonian parameter, $\gamma = -\Psi/\Phi$, defined by the ratio of the Newtonian potentials, is determined by both the mass of the scalar field in these theories, as well as the Brans-Dicke parameter, ω_0. When the mass is small, constraints on ω_0 are equivalent to constraints on γ. However, if the mass of the scalar field is endowed with the *Chameleon mechanism* , and is able to acquire a large mass locally depending on the environment, then in this regime the mass of the scalar field will dominate over ω_0, allowing a select class of $f(R)$ theories to survive [61], [85]. Once the scalar is massive, and the range is short, it will effectively be invisible to experiments performed within the Newtonian limit, as well as the post Newtonian limit.

Regarding the existence of a Newtonian limit, it was shown in [86] that the existence of a stable Newtonian limit may be ascertained by the existence of a stable ground state of the theory, whether the ground state solution is Minkowski, de Sitter or anti-de Sitter. For a function to provide a theory with a stable Newtonian limit; that is in the regime for R where Newtonian gravity can be applied, compact objects, low velocities and relevant curvatures [3], the following conditions on $f(R)$ must be met [87]:

$$|f(R) - R| \ll R, \tag{3.57}$$

$$|f'(R) - 1| \ll 1, \tag{3.58}$$

$$RF''(R) \ll 1, \tag{3.59}$$

for $R \gg R_0$, which guarantee that any deviations from GR to the metric of a general space time are kept small. Also the Compton wavelength of the scalar field is much smaller than the radius of curvature of the background [87].

These are essential considerations regarding the form of f, and failing the weak field limit renders a theory worthless.

Instabilities

Another issue which is considered as a problem for most higher - order theories of gravity is the appearance of ghost fields. These are massive states of negative norm and, in this context, result in the Hamiltonian for a given theory to be unbounded from below.

Classical and quantum stability

If the modified Lagrangian includes higher order curvature invariants and derivatives, it has been shown that a new spin-2 ghost field appears [33], [32], resulting in issues with the quantum stability of the theory [88] as well as on a classical level.

[3] Curvatures much larger than the present background value in an FRLW universe, but smaller than those interior to very compact bodies, eg. neutrons stars/ black holes.

To ensure the classical and quantum stability of a theory in the physically relevant domain, $R > 0$, the following requirements on the derivatives of f are crucial:

$$f'(R) > 0, \tag{3.60}$$

$$f''(R) > 0. \tag{3.61}$$

(3.60) guarantees that gravity is attractive and that the effective gravitational constant is positive. It also ensures that the graviton is not a ghost [87], and a violation of this requirement has been shown to result in the loss of homogeneity and isotropy in regular FLRW models, and the formation of a strong space like anisotropy curvature singularity [89], [90].

The requirement (3.61) is to protect against the problem detailed in [91], known as the Dolgov-Kawasaki instability, which is a dangerous instability that occurs on very short time scales. Furthermore, a weak sudden singularity can also form if $f''(R) = 0$ for a finite value of the scalar curvature.

The Dolgov-Kawasaki Instability

To summarize its importance, following [91], let us parametrize the correction to general relativity as $f(R) = R + \epsilon g(R)$, such that ϵ is a small positive constant, containing the dimensions of mass squared, leaving the function $g(R)$ dimensionless. Substituting this into the modified trace equation (3.48), we obtain

$$\Box R + \frac{g'''}{g''}\nabla^\mu R \nabla_\mu R + \left(\frac{\epsilon g' - 1}{3\epsilon g''}\right) R = \frac{\kappa T}{3\epsilon g''} + \frac{2g}{3g''}, \tag{3.62}$$

assuming $g'' \neq 0$.
We may approximate the local metric as

$$g_{\mu\nu} = \eta_{\mu\nu} + h_{\mu\nu}, \tag{3.63}$$

in a weak field region, where we can expand the scalar curvature R as

$$R = -\kappa T + R_1, \tag{3.64}$$

where R_1 is a small perturbation around the GR approximation. η is the usual Minkowski metric We may then consider the trace equation to study the dynamics of R_1, which to a first order gives:

$$\ddot{R_1} - \nabla^2 R_1 - \frac{2\kappa g'''}{g''}\dot{T}\dot{R}_1 + \frac{2\kappa g'''}{g''}\vec{\nabla}T \cdot \vec{\nabla}R_1 + \frac{1}{3g''}\left(\frac{1}{\epsilon} - g'\right) R_1 = \kappa\ddot{T} - \kappa\nabla^2 T - \frac{(\kappa T g^2 + 2g)}{3g''} \tag{3.65}$$

The coefficient of the last term on the left hand side is effectively the square of the mass of R_1

$$m^2 \simeq \frac{1}{3\epsilon g''}, \tag{3.66}$$

and is dominated by the term $(\frac{1}{3\epsilon g''})$, since the value of ϵ is very small [91], [92].

The theory will be fine if $g'' = f'' > 0$ is satisfied, and unstable if the sign of the effective mass is negative [92]. To protect against the Dolgov-Kawasaki instability, we require that $f''(R) > 0$. To include the case of general relativity, where $f''(R) = 0$, we require that $f''(R) \geq 0$. Interestingly, because the scalar field in the Palatini formalism is non dynamical, it does not suffer any Dolgov-Kawasaki instability. Of course, the above considerations only hold in a small neighbourhood confined to local expansion. However, we may derive a condition for the stability of the de Sitter space in $f(R)$ theories of gravity, by assuming a de Sitter background, and considering a very general action which includes $f(R)$ gravity, scalar tensor gravity, and mixtures of the two [66]. Considering, as we shall do in general in this work, an FLRW metric to describe the background, the following conditions for the existence of a stable de Sitter space solution is obtained

$$\frac{(f_0')^2 - 2f_0 f_0''}{f_0' f_0''} \geq 0, \tag{3.67}$$

which is consistent with the stability condition for homogeneous perturbations [65], [93], [94].

Sudden Singularities

There exists another instability issue which plagues $f(R)$ gravity even at a background level, due to non linearities. Many, if not all, of the functions which are constructed to effectively produce GR dynamics in the high curvature regime result in scalar fields for which the potentials $V(\phi)$ contain an unprotected singularity [8].

Some of the first considerations of such singularities, in $f(R)$ gravity, were those which occur as density increases interior to compact objects [citations.] These were found, largely to be curable by adding UV corrections to the action, specifically of the form R^2 [87], which are in fact the exact forms for f which were considered as inflationary theories.

It was discovered that oscillations in the Ricci scalar in $f(R)$ theories evolving with increasing redshift, or going back in time, are common in all viable theories of gravity [87]. The oscillations, occurring about the GR limit, were found to increase in frequency and amplitude, and eventually result in a singularity. Interestingly, in the high energy regime when considering an inflationary period driven by $f(R)$ theory, such oscillations are actually useful in driving gravitational particle production, enabling phases of reheating, the creation of ordinary matter and the transition to the radiation dominated FRW stage [37]. However, in the classical context these oscillations are problematic;

1. The frequency[4] grows rapidly with redshift to exceed the Planck value, rendering the classical description no longer valid [95], [96], [97].

2. The amplitude of the linear oscillations also grow quickly with redshift, resulting in an "over-abundance" of scalarons at early times, while we require its number density to be appropriately small during BBN [96].

[4]The frequency of oscillations of R, correspond to the rest mass of the scalarons.

Perturbative approaches such that the Ricci scalar is defined by its value in GR plus a perturbation, $R = R_{GR} + \delta R$, isolated an analytic expression for the oscillating part of the Ricci scalar [96]. It was found that the oscillations become asymmetric and eventually evolve toward a singularity, and that an analysis neglecting nonlinear effects will be blind to pathological behaviour.

These singularities have been widely considered in the scalar tensor framework, where the scalar field $f'(R)$ or $1 - f'(R)$ is identified and examined using the trace of the modified field equations (3.80), as an oscillator equation of motion [8],

$$\Box f_R = \frac{1}{3}(2f - f_R R) + \frac{8\pi G}{3}T, \tag{3.68}$$

where f_R is the first derivative of $f(R)$ with respect to R, and thus, the additional degree of freedom, which we write as the scalar field ϕ, is given by:

$$\phi = f_R - 1. \tag{3.69}$$

Considering the above, Equation (3.68) in terms of ϕ is

$$\Box\phi = V'(\phi) - \mathcal{F}, \tag{3.70}$$

where the effective scalar field potential can be determined by

$$V'(\phi) = \frac{dV}{d\phi} = \frac{1}{3}(2f - f_R R), \tag{3.71}$$

and the force $\mathcal{F}$ driving the scalar field ϕ is the trace of the stress energy momentum tensor T. Recall, for a perfect fluid this is

$$\mathcal{F} = \frac{8\pi G}{3}(\rho - 3p). \tag{3.72}$$

The dynamics of the scalar field is determined by its potential, which is obtained by integrating the following equation

$$\frac{dV}{dR} = \frac{dV}{d\phi}\frac{d\phi}{dR} = \frac{1}{3}(2f - f_R R)f_{RR}, \tag{3.73}$$

so that the potential as a function of the scalar field is a function depending on ϕ and R. The minimum of this potential, which we will identify to be located at ϕ_{min}, is the point which is relevant to Cosmology, and corresponds to the de Sitter solution. There also exists, in most, if not all [8] viable cosmological $f(R)$ theories, a point ϕ_{sing}, where the Ricci scalar diverges to infinity resulting in a curvature singularity. It has been shown that these two points are often easily separated by a finite value of the potential, thus it is possible (and usually highly likely) that the scalar field, in its oscillation about the potential minimum, may verge on the point leading to singularity. Theories which do not protect against this type of eventuality would be disqualified.

This is a useful approach, and has lead to an intuition with understanding the occurrence of these singularities, and insight into how to possibly avoid them, however it has also been argued recently that this approach is not reliable, and should be performed with caution [98].

Cosmological Perturbations in $f(R)$ gravity

Arranging a function to mimic a desirable background is straight forward. In principle there is an infinite number of such functions, and finding them is not a problem. In fact the bigger problem is finding ways to discriminate between them, and studying perturbations around their background cosmology is one of the strongest methods we have toward this. Changing the underlying theory of gravity affects the way perturbations in the density of the matter components and curvature evolve, leaving an impression in the cosmic microwave background and its fluctuation spectrum, and the large scale structure of galaxies and galaxy clusters. It is important that the perturbation spectrum produced is consistent with the cosmological perturbation observables and the ΛCDM Concordance model.

In $f(R)$ theory, only scalar perturbation modes are affected by the modification to the Einstein-Hilbert action, for which $f''(R)$ must be greater than zero. Other consequences include a difference in the correlation between the CMB and the large scale structure, as well as a decrease in the large angle anisotropy of the CMB [43]. The gravitational coupling in $f(R)$ gravity is stronger, resulting in less large scale structure than in ΛCDM. Most studies of perturbations in the $f(R)$ gravity context are performed with respect to a quasi-static limit, and while this approximation may be valid in certain regimes, for specific functions, it must be used with caution, especially in the context of perturbation theory. It cannot be taken for granted that the evolution of perturbations in this approximation is a reliable description of the perturbations in general for a given function. Although studying the evolution of the full fourth order perturbation equations (which will be discussed in Section 4.2) may be lengthy, it is worth the exercise to check that the results of both the approximation and the full equations are consistent with each other.

The Initial Value Problem

In order for any physical theory to be viable it must have the ability to predict the future of a system given the details of an instance of its past (an initial vector specifying all the quantities present in the theory), including a description of all interactions at play in the system. Technically speaking, it must have a *well formulated* and *well posed* initial value problem. Beginning with a vector describing the initial state of a physical system with N finite degrees of freedom such that the interactions between them are known, the problem is *well-formulated* if its future dynamical evolution is completely and uniquely determined. In addition to this feature, we must be sure that small perturbations around the initial conditions produce only small perturbations in the subsequent dynamics of the theory; so that the evolution equations show a reliable dependence on the initial data, ensuring predictability and that the problem is *well posed*. Any changes in the initial values must produce results that maintain the causal structure of the equations.

This issue has been studied in the scalar tensor framework and in metric $f(R)$ gravity, and it has

been discovered that this type of ETG is a well formulated initial value problem in the presence of "reasonable" matter, and well posed in a vacuum [99], [92].

3.3 Background Cosmology in the Metric Formulation

In the late 60's Ehlers, Geren and Sachs provided a compelling argument that if an observer measured the relic background radiation of the universe to be isotropic, assuming that the isotropy holds around every point in the universe, then such a universe must be isotropic and homogeneous, and thus may be described completely as an FLRW space time [100]. While the measurements of the CMB from our observer perspective reveal striking isotropy, our modern ability to resolve tiny anisotropies, indicate that in fact the real universe exhibits perturbations about what appears to be a "nearly isotropic" background radiation. The Ehlers-Geren-Sachs theorem was shown to hold for a "nearly" isotropic measurement of the CMB as well [101]. The "almost EGS" theorem is also valid for $f(R)$ gravity, proven for both metric $f(R)$ and scalar tensor theory [102], [103], when the matter content is described by a barotropic equation of state.

We thus, comfortably, for the moment, choose to work in an FLRW space time, which according to the above considerations is a reasonable place to begin. Recall, the FLRW line element is given by

$$ds^2 = -dt^2 + a(t)^2 \left[\frac{dr^2}{1 - Kr^2} + r^2(d\theta^2 + \sin^2\theta d\phi^2) \right], \tag{3.74}$$

indicating the isotropy and homogeneity of the space time, where (t, r, θ, ϕ) are comoving coordinates. We choose $K = 0$, as justified in Chapter 2.

The standard stress - energy tensor for a time-like observer, having four velocity u^μ is given by,

$$T_{\mu\nu} = \rho u_\mu u_\nu + q_{(\mu} u_{\nu)} + q_{(\nu} u_{\mu)} + p h_{\mu\nu} + \pi_{\mu\nu}, \tag{3.75}$$

where $h_{\mu\nu}$ is the projection tensor, ρ is the density, p is the pressure, q is the heat flux and $\pi_{\mu\nu}$ gives the anisotropic stress. We have the following :

$$q_\mu u^\mu = 0, \quad \pi_{\mu\nu} u^\nu = 0, \quad \pi_\mu{}^\mu = 0, \quad \pi_{\mu\nu} = \pi_{\nu\mu}.$$

For simplicity we consider a fluid consisting of a single energy density form. This simplification is intuitive and close to the truth, in practice, in most senses, since we often study the Universe in intervals of time which are dominated singly by a specific form of energy density. Furthermore, we assume that the form of energy density pervading the Universe is described by a perfect fluid, with density ρ, pressure p and barotropic equation of state, $p = p(\rho)$, reducing the stress - energy tensor to that of a perfect fluid, having the form

$$T_{\mu\nu} = (p + \rho) u_\mu u_\nu + p g_{\mu\nu}, \tag{3.76}$$

with a barotropic equation of state usually given by

$$p = w\rho \tag{3.77}$$

Once the metric at (3.74) and stress- energy tensor at (3.76) are substituted in to the modified field equations at (3.44), we recover the following modified cosmological evolution equations, where the dot indicates derivatives with respect to time:
The modified Friedmann equation:

$$H^2 = \frac{1}{3f'}\left(\rho + \frac{1}{2}(Rf' - f) - 3H\dot{R}f''\right), \tag{3.78}$$

The modified Raychaudhuri equation:

$$2\dot{H} + 3H^2 = -\frac{1}{f'}\left(P + 2H\dot{R}f'' + \frac{1}{2}\left(f - Rf'\right) + \dot{R}^2 f''' + \ddot{R}f''\right). \tag{3.79}$$

We can also calculate the trace of the field equations in this space-time :
The modified trace equation:

$$3\ddot{R}f'' = \rho(1 - 3w) + f'R - 2f - 9Hf''\dot{R} - 3f'''\dot{R}^2. \tag{3.80}$$

The cosmological field equations in $f(R)$ gravity are fourth order in metric derivative, and since $K = 0$, we may in fact eliminate the scale factor altogether, in favour of the Hubble parameter being the only dynamical quantity, reducing the order of the equations by one.

In the spirit of the fact that we may identify all the extra terms in the field equations associated with the function $f(R)$ and its derivatives as an effective *curvature fluid*, we may define its effective equation of state, by using the modified Friedmann and Raychaudhuri equations to define its effective density and pressure:

$$\rho_{curv} = \frac{1}{2f'}\left[Rf' - f - 6H\dot{R}f''\right], \tag{3.81}$$

$$P_{curv} = \frac{1}{f'}\left[\dot{R}^2 f''' + 2H\dot{R}f'' + \ddot{R}f'' + \frac{1}{2}(f - Rf')\right], \tag{3.82}$$

such that $\rho_{curv} \geq 0$ in spatially flat FLRW space time. In this interpretation, in a vacuum, the curvature correction is viewed as effective fluid, which may be useful for gaining certain intuition, but certainly should not be taken too far. Even considering energy conditions for this effective geometric fluid is meaningless, since it is well known that such fluids violate all energy conditions in general [58]. The equation of state for this effective fluid may then be written:

$$w_{curv} = \frac{P_{curv}}{\rho_{curv}} = \frac{\left[\dot{R}^2 f''' + 2H\dot{R}f'' + \ddot{R}f'' + \frac{1}{2}(f - Rf')\right]}{\frac{1}{2}\left[Rf' - f - 6H\dot{R}f''\right]}. \tag{3.83}$$

Since we require that the energy density ρ_{eff} is positive, the sign of the effective equation of state is controlled by the numerator, the effective pressure. For our purposes, in the late time regime, we

require negative pressure to the end of generating accelerated expansion; and from this constraint $w_{curv} = -1$, we obtain the following relationship between the derivatives of the function f, and the Ricci scalar:

$$\frac{f'''}{f''} = \frac{\dot{R}H - \ddot{R}}{\dot{R}^2}. \tag{3.84}$$

3.4 1+3 Formalism

In Section 3.3 the metric approach to the derivation of the cosmological field equations in $f(R)$ gravity was presented. As the field of modified theories matured, it became clear that their added complexity, the benefits of which we sought to investigate all the issues with the standard model, leads to practical trouble with analysis. Thus, other frameworks from which a space time can be studied have been considered, such as decomposing the space time into a set of 1+3 covariant variables, as has been set out for GR in Chapter 2 [11], [104], [105], [106].

The advantage of using the 1+3 covariant formalism to study FRW universes is twofold; the first advantage is that this formalism lends to the process of conveniently extending the GR 1+3 formalism [11] to modified theories, which must be a major consideration when the task of modifying gravity can come with significant complications, and the second is that in this formalism it is clear to track the physical meaning underlying calculations, which is another important consideration since it is easy to lose intuition at the expense of complexity in modified theories. Below, the 1+3 formalism is extended for use in the $f(R)$ gravity framework [42],[52],[53],[54], by discussing the kinematical approach from the perspective of a fundamental observer having 4 velocity u_α. We present the constraint and propagation equations which may be derived using the Bianchi identities and conservation equations for momentum and energy.

The kinematic set up is identical to that in GR, the extension to $f(R)$ gravity is performed simply by adding the curvature fluid, as described in section 3.2.2, as an additional fluid component in the stress energy momentum tensor.

In this context, it is most natural and intuitive to choose what is known as the matter frame, u^M_α, which is comoving with standard matter, representing motion of galaxies and galaxy clusters. The choice is also preferred for the obvious reason that this frame happens to coincide with the one we are in.

3.4.1 Fluid Sources

The first step is to write down the covariant decomposition of the stress energy momentum tensor relative to the 4-velocity. The critical argument which allows this decomposition analysis in fourth order theories of gravity is the ability to express the modification to GR in $f(R)$ gravity as an additional source term arising from the extra terms involving curvature and the correction f, where the purely matter part is influenced by a factor of $(\frac{1}{f'})$, such that the field equations resemble the

Einstein field equations including a curvature fluid:

$$\left(R_{\alpha\beta} - \frac{1}{2}g_{\alpha\beta}R\right) = \tilde{T}^M_{\alpha\beta} + T^R_{\alpha\beta} = T_{\alpha\beta}, \tag{3.85}$$

where $\tilde{T}^M_{\alpha\beta} = \frac{1}{f'}T^M_{\alpha\beta}$, and

$$T^R_{\alpha\beta} = \frac{1}{f'}\left[\frac{1}{2}g_{\alpha\beta}(R - Rf') + \nabla_\beta\nabla_\alpha f - g_{\alpha\beta}\nabla_\sigma\nabla^\sigma f\right], \tag{3.86}$$

give the expressions for the effective matter fluid and the effective curvature fluid. The stress energy momentum tensor is given by (3.75) where, in terms of the individual contributing sources, the total effective energy density for the combined matter and curvature fluid is

$$\rho = \tilde{\rho}^M + \rho^R = T_{\alpha\beta}u^\alpha u^\beta, \tag{3.87}$$

the total effective isotropic pressure is

$$p = \tilde{p}^M + p^R = \frac{1}{3}T_{\alpha\beta}h^{\alpha\beta}, \tag{3.88}$$

the total effective momentum density, or energy flux relative to u^α, is

$$q_\alpha = \tilde{q}^M_\alpha + q^R_\alpha = -T_{\beta\mu}u^\mu h^\beta{}_\alpha, \tag{3.89}$$

and the total effective projected symmetric trace free anisotropic stress tensor is

$$\pi_{\alpha\beta} = \tilde{\pi}^M_{\alpha\beta} + \pi^R_{\alpha\beta} = T_{\mu\nu}h^\mu{}_{\langle\alpha}h^\nu_{\beta\rangle}. \tag{3.90}$$

Here the tilde denotes the coupling to the $f'(R)$ field:

$$\tilde{\rho}^M = \frac{\rho^M}{f'}, \quad \tilde{p}^M = \frac{p^M}{f'}, \quad \tilde{q}^M_\alpha = \frac{q^M_\alpha}{f'}, \quad \tilde{\pi}^M_{\alpha\beta} = \frac{\pi^M_{\alpha\beta}}{f'}. \tag{3.91}$$

And the following properties are true of q_α and $\pi_{\alpha\beta}$:

$$q_\alpha u^\alpha = 0, \quad \pi^\alpha{}_\alpha = 0, \quad \pi_{\alpha\beta} = \pi_{(\alpha\beta)}, \tag{3.92}$$

$$\pi_{\alpha\beta}u^\beta = 0, q_\alpha = q_{\langle\alpha\rangle}, \pi_{\alpha\beta} = \pi_{\langle\alpha\beta\rangle}. \tag{3.93}$$

The physics will be contained in the specification of an equation of state which relates the quantities above. Widely used is the example of a perfect fluid which is characterised by the following constraint:

$$q^\alpha = \pi_{\alpha\beta} = 0 \implies T_{\alpha\beta} = \rho u_\alpha u_\beta + p h_{\alpha\beta}. \tag{3.94}$$

Applying the twice contracted Bianchi identities to the *total* stress energy tensor, $\nabla^\beta T_{\alpha\beta} = 0$, reveal the conservation properties of the effective fluids. The effective matter fluid is not conserved,

$$\nabla^\beta\tilde{T}^M_{\alpha\beta} = \frac{\nabla^\beta T^M_{\alpha\beta}}{f'} - \frac{f''}{f'^2}T^M_{\alpha\beta}\nabla^\beta R. \tag{3.95}$$

And the conservation of *total* energy-momentum implies

$$\nabla^\beta T^R_{\alpha\beta} = \frac{f''}{f'^2}\tilde{T}^M_{\alpha\beta}\nabla^\beta R. \tag{3.96}$$

While the standard matter component is still subject to the energy conditions discussed previously, the effective matter and curvature fluids are free to, and in general do, violate the weak energy condition, leaving the natural choice of frame as the energy frame of the standard matter u^α_M, since the thermodynamical properties of standard matter are always preserved.

The Bianchi identities, as applied to the total stress energy momentum tensor, show that as long as the stress energy momentum tensor for standard matter is conserved; $\nabla^\beta T^M_{\alpha\beta} = 0$, then the total stress energy momentum tensor will satisfy conservation of energy.

3.4.2 Geometry

In the covariant formalism for general relativity it is more useful to use the reverse representation of the Einstein field equations,

$$R_{\alpha\beta} = T_{\alpha\beta} - \frac{1}{2}Tg_{\alpha\beta}. \tag{3.97}$$

The Curvature Fluid

To discuss the "thermodynamical" properties of the curvature fluid, consider the right hand side of Equation (3.42), where the *curvature fluid* in $f(R)$ gravity is defined to be

$$T^R_{\alpha\beta} = \frac{1}{f'(R)}\left[\left(\nabla_\alpha\nabla_\beta - g_{\alpha\beta}\Box\right)f' + \frac{1}{2}g_{\alpha\beta}(f - f'R)\right]. \tag{3.98}$$

Decomposing the terms of (3.98) containing derivative operators into their space and time parts we have,

$$T^R_{\alpha\beta} = \frac{1}{f'}\left[\frac{1}{2}g_{\alpha\beta}(f - Rf') - \dot{f}'\left(\frac{1}{3}h_{\alpha\beta}\Theta + \sigma_{\alpha\beta} + \omega_{\alpha\beta}\right) + \frac{1}{3}h_{\alpha\beta}\tilde{\nabla}^2 f'\right. \tag{3.99}$$

Now, using Equations (3.87) – (3.91) and the above decomposition, we may rewrite the thermodynamical quantities associated with the curvature fluid in terms of the $1+3$ variables:

$$\rho^R = \frac{1}{f'}\left[\frac{1}{2}(Rf' - f) + f'''\tilde{\nabla}^\alpha R\tilde{\nabla}_\alpha R + f''\tilde{\nabla}^2 R - \Theta f''\dot{R}\right], \tag{3.100}$$

$$p^R = \frac{1}{f'}\left[\frac{1}{2}(f - Rf') - \frac{2}{3}f''\tilde{\nabla}^2 R - \frac{2}{3}f'''\tilde{\nabla}^\alpha R\tilde{\nabla}_\alpha R + \frac{2}{3}\Theta f''\dot{R} + f'''\dot{R}^2 + f''\ddot{R} - \dot{u}_\mu f''\tilde{\nabla}^\mu R\right], \tag{3.101}$$

$$q^R_\alpha = -\frac{1}{f'}\left[f'''\dot{R}\tilde{\nabla}_\alpha R + f''\tilde{\nabla}_\alpha\dot{R} - \frac{1}{3}\Theta f''\tilde{\nabla}_\alpha R - \sigma_{\alpha\mu}f''\tilde{\nabla}^\mu R - \omega_{\alpha\mu}f''\tilde{\nabla}^\mu R\right], \tag{3.102}$$

$$\pi^R_{\alpha\beta} = \frac{1}{f'}\left[f'''\tilde{\nabla}_{\langle\alpha}R\tilde{\nabla}_{\beta\rangle}R + f''\tilde{\nabla}_{\langle\alpha}\tilde{\nabla}_{\beta\rangle}R - \sigma_{\alpha\beta}f''\dot{R}\right]. \tag{3.103}$$

The twice contracted Bianchi identities at (2.11) are used to obtain evolution equations for ρ^M, ρ^R and q^R_α:

$$\dot{\rho}^M = -\Theta(\rho^M + p^M), \tag{3.104}$$

$$\dot{\rho}^R + \tilde{\nabla}^\alpha q^R_\alpha = -\Theta(\rho^R + p^R) - 2\dot{u}^\alpha q^R_\alpha - \sigma^{\alpha\beta}\pi^R_{\beta\alpha} + \rho^M \frac{f''\dot{R}}{f'^2}, \tag{3.105}$$

$$\dot{q}^R_{\langle\alpha\rangle} + \tilde{\nabla}_\alpha p^R + \tilde{\nabla}^\beta \pi^R_{\alpha\beta} = -\frac{4}{3}\Theta q^R_\alpha - \sigma_\alpha{}^\beta q^R_\beta - (\rho^R + p^R)\dot{u}_\alpha - \dot{u}^\beta \pi^R_{\alpha\beta} - \eta^{\beta\mu}_\alpha \omega_\beta q^R_\mu + \rho^M \frac{f''\tilde{\nabla}_\alpha R}{f'^2}. \tag{3.106}$$

We also have the following relationship between the acceleration and the energy density and pressure of the standard matter,

$$\tilde{\nabla} p^M = -(\rho^M + p^M)\dot{u}^\alpha, \tag{3.107}$$

coming from the conservation of momentum for standard matter.

Substituting into (3.97) for the total effective energy momentum tensor, we may write the Ricci tensor and Ricci scalar in terms of the thermodynamic quantities of the total effective fluid as

$$R_{\alpha\beta} = \frac{1}{2}(\rho^T + 3p^T)u_\alpha u_\beta + \frac{1}{2}(\rho^T - p^T)h_{\alpha\beta} + 2u_{(\alpha}q^T_{\beta)} + \pi^T_{\alpha\beta}, \tag{3.108}$$

$$R = \rho^T - 3p^T. \tag{3.109}$$

We can also construct the trace equation of the curvature fluid by considering $\tilde{T}^M$ and T^R, the traces of the effective matter and curvature fluids respectively:

$$\tilde{T}^M = \frac{1}{f'} g^{\alpha\beta} T^M_{\alpha\beta} = \frac{1}{f'}\left(3p^M - \rho^M\right), \tag{3.110}$$

$$T^R = g^{\alpha\beta} T^R_{\alpha\beta} = \frac{1}{f'}\Big[2(f - Rf') - 3\Big(f''\tilde{\nabla}^2 R + f'''\tilde{\nabla}^\alpha R\tilde{\nabla}_\alpha R - f'''\dot{R}^2 - f''\ddot{R} + \dot{u}_\mu f''\tilde{\nabla}^\mu R - f''\theta\dot{R}\Big)\Big], \tag{3.111}$$

by taking the trace of (3.99). If we substitute (3.110) and (3.111) into the equation for the Ricci scalar, (3.109), and considering only the curvature terms, we obtain the trace equation corresponding to the curvature fluid:

$$Rf' - 2f = -3\left(f''\tilde{\nabla}^2 R + f'''\tilde{\nabla}^\alpha R\tilde{\nabla}_\alpha R - f'''\dot{R}^2 - f''\ddot{R} + \dot{u}_\mu f''\tilde{\nabla}^\mu R - f''\theta\dot{R}\right). \tag{3.112}$$

3.4.3 Propagation and constraint equations

Using equations for the decomposition of the Riemann tensor (2.49) - (2.53), we can obtain three sets of propagation and constraint equations, coming from the Einstein equations, and its integrability conditions in the 1+3 covariant decomposition.

1. Ricci identities

From the Ricci identities for the velocity vector field u^α,

1. The Raychaudhuri propagation equation is given by

$$\dot{\Theta} - \tilde{\nabla}_\alpha \dot{u}^\alpha + \frac{1}{3}\Theta^2 - (\dot{u}_\alpha \dot{u}^\alpha) + \sigma_{\alpha\beta}\sigma^{\alpha\beta} - 2\omega_\alpha\omega^\alpha + \frac{1}{2}(\tilde{\rho}^M + 3\tilde{p}^M) = -\frac{1}{2}(\rho^R - 3p^R), \tag{3.113}$$

2. The vorticity propagation equation is as before,

$$\dot{\omega}^{\langle\alpha\rangle} - \frac{1}{2}\eta^{\alpha\beta\mu}\tilde{\nabla}_\beta \dot{u}_\mu = -\frac{2}{3}\Theta\omega^\alpha + \sigma^\alpha{}_\beta\omega^\beta. \tag{3.114}$$

3. The shear propagation equation

$$\dot{\sigma}^{\langle\alpha\beta\rangle} - \tilde{\nabla}^{\langle\alpha}\dot{u}^{\beta\rangle} + \frac{2}{3}\Theta\sigma^{\alpha\beta} - \dot{u}^{\langle\alpha}\dot{u}^{\beta\rangle} + \sigma^{\langle\alpha}{}_\mu\sigma^{\beta\rangle\mu} + \omega^{\langle\alpha}w^{\beta\rangle} + E^{\alpha\beta} = \frac{1}{2}\pi_R^{\alpha\beta}, \tag{3.115}$$

4. The (0α) *shear divergence constraint*,

$$0 = (C_1)^\alpha = \tilde{\nabla}_\beta\sigma^{\alpha\beta} - \frac{2}{3}\tilde{\nabla}^\alpha\Theta + \eta^{\alpha\beta\nu}\left[\tilde{\nabla}_\beta\omega_\nu + 2\dot{u}_\beta\omega_\mu\right] + q_R^\alpha, \tag{3.116}$$

5. The vorticity divergence constraint

$$0 = (C_2) = \tilde{\nabla}_\alpha\omega^\alpha - \dot{u}_\alpha\omega^\alpha. \tag{3.117}$$

6. The gravito-magnetic $H_{\alpha\beta}$ *constraint*,

$$0 = (C_3)^{\alpha\beta} = H^{\alpha\beta} + 2\dot{u}^{\langle\alpha}\omega^{\beta\rangle} - \eta^{\mu\nu\langle\alpha}\tilde{\nabla}_\mu\sigma^{\beta\rangle}{}_\nu + \tilde{\nabla}^{\langle\alpha}\omega^{\beta\rangle}. \tag{3.118}$$

2. Twice-contracted Bianchi identities

The constraint obtained by projecting parallel to u^α yields

7. The energy conservation equation:

$$\dot{\rho} + \tilde{\nabla}_\alpha q^\alpha = -\Theta(\rho + p) - 2\dot{u_\alpha}q^\alpha - \sigma_{\alpha\beta}\pi^{\alpha\beta}, \tag{3.119}$$

and by projecting orthogonally to u^α yields

8. The conservation of momentum equation:

$$\dot{q}^{\langle\alpha\rangle} + \tilde{\nabla}^\alpha p + \tilde{\nabla}_\beta\pi^{\alpha\beta} = -\frac{4}{3}\Theta q^\alpha - \sigma^\alpha{}_\beta q^\beta - (\rho + p)\dot{u}^\alpha - \dot{u}_\beta\pi^{\alpha\beta} - \eta^{\alpha\beta\mu}\omega_\beta q_\nu. \tag{3.120}$$

For a perfect fluid,

$$\dot{\rho}^M = -\Theta(\rho^M + p^M), \tag{3.121}$$

$$\tilde{\nabla}_\alpha p^M = -(\rho^M + p^M)\dot{u}_\alpha. \tag{3.122}$$

3. Once contracted Bianchi identities

9. The gravito-electric $\dot{E}$ propagation equation:

$$\begin{aligned}(\dot{E}^{\langle\alpha\beta\rangle}+\frac{1}{2}\dot{\pi}^{\langle\alpha\beta\rangle})-\eta^{\mu\nu\langle\alpha}\tilde{\nabla}_\mu H^{\beta\rangle}{}_\nu+\frac{1}{2}\tilde{\nabla}^{\langle\alpha}q^{\beta\rangle}\\ =-\frac{1}{2}(\rho+p)\sigma^{\alpha\beta}-\Theta\left(E^{\alpha\beta}+\frac{1}{6}\pi^{\alpha\beta}\right)+3\sigma^{\langle\alpha}{}_\mu\left(E^{\beta\rangle\mu}-\frac{1}{6}\pi^{\beta\rangle\mu}\right)\\ -\dot{u}^{\langle\alpha}q^{\beta\rangle}+\eta^{\mu\nu\langle\alpha}\left[2\dot{u}_\mu H^{\beta\rangle}{}_\nu+\omega_\mu\left(E^{\beta\rangle}{}_\nu+\frac{1}{2}\pi^{\beta\rangle}{}_\nu\right)\right].\end{aligned}\tag{3.123}$$

10. The gravito-magnetic $\dot{H}$ propagation equation:

$$\begin{aligned}\dot{H}^{\langle\alpha\beta\rangle}+\eta^{\mu\nu\langle\alpha}\tilde{\nabla}_\mu\left(E^{\beta\rangle}{}_\nu-\frac{1}{2}\pi^{\beta\rangle}{}_\nu\right)=&-\Theta H^{\alpha\beta}+3\sigma^{\langle\alpha}{}_\mu H^{\beta\rangle\mu}+\frac{3}{2}\omega^{\langle\alpha}q^{\beta\rangle}\\ &-\eta^{\mu\nu\langle\alpha}\left[2\dot{u}_\mu E^{\beta\rangle}{}_\nu-\frac{1}{2}\sigma^{\beta\rangle}{}_\mu q_\nu-\omega_\mu H^{\beta\rangle}{}_\nu\right].\end{aligned}\tag{3.124}$$

11. The gravito-electric divergence constraint:

$$\begin{aligned}0=(C_4)^\alpha=&\tilde{\nabla}_\beta\left(E^{\alpha\beta}+\frac{1}{2}\pi^{\alpha\beta}\right)-\frac{1}{3}\tilde{\nabla}^\alpha\rho+\frac{1}{3}\Theta q^\alpha-\frac{1}{2}\sigma^\alpha{}_\beta q^\beta-3\omega_\beta H^{\alpha\beta}\\ &-\eta^{\alpha\beta\mu}\left[\sigma_{\beta\nu}H^\nu{}_\mu-\frac{3}{2}\omega_\beta q_\mu\right].\end{aligned}\tag{3.125}$$

12. The gravito-magnetic divergence (div H) constraint:

$$0=(C_5)^\alpha=\tilde{\nabla}_\beta H^{\alpha\beta}+(\rho+p)\omega^\alpha+3\omega_\beta\left(E^{\alpha\beta}-\frac{1}{6}\pi^{\alpha\beta}\right)\tag{3.126}$$

$$+\eta^{\alpha\beta\mu}\left[\frac{1}{2}\tilde{\nabla}_\beta q_\mu+\sigma_{\beta\nu}(E^\nu{}_\mu+\frac{1}{2}\pi^\nu{}_\mu)\right].\tag{3.127}$$

We will recover the GR versions of these equations simply by setting $f(R)=R$, resulting in the matter parts being identical to standard matter, and all curvature fluid terms vanishing. In general, we can close the system by specifying the equation of state of the fluid sources, which amounts to choosing restrictions on the thermodynamic quantities. Very relevant for late time considerations is that of pressureless non relativistic matter, dust, with $p=q_\alpha=\pi_{\alpha\beta}=0\implies\dot{u}_\alpha=0$.

Applying the decomposition to $f(R)$ modified gravity theories, for general spacetimes we get

$$\nabla_\alpha\nabla_\beta f'=-\dot{f}'\left(\frac{1}{3}h_{\alpha\beta}\Theta+\sigma_{\alpha\beta}+\omega_{\alpha\beta}\right)+u_\beta u_\alpha\ddot{f}'+u_\alpha\dot{f}'\dot{u}_\beta.\tag{3.128}$$

Furthermore, we obtain

$$\Box f'=-\Theta\dot{f}'-\ddot{f}',\tag{3.129}$$

where, any terms containing orthogonally projected derivatives have been neglected, since we are only considering isotropic and homogeneous space times.

The kinematics and thermodynamics above, prescribed by equations (3.113)-(3.126), along with (3.104) - (3.106) formalize the physical interaction and evolution of the matter and gravitational fields in $f(R)$ gravity, and completely specify a cosmological model. This approach is invaluable in the investigations into alternative theories to GR, as it sets out a scheme which is both mathematically rigorous and intuitive. It has also been extremely useful in constructing and studying cosmological perturbations [107], [11], [108], and in the following chapter, we spend some time on the 1+3 covariant gauge invariant treatment of perturbations in $f(R)$ gravity.

3.5 Geodesic Deviation in $f(R)$ gravity

The geodesic deviation equation was considered in the $f(R)$ scenario in [109]. This paper commented on the importance of a full extension of the geodesic deviation equation in the $f(R)$ context. In particular, the derivation of the dynamic equation for η, the geodesic deviation, was presented. Through this equation we know the relative deviation between two neighbouring geodesics, which is pertinent to deriving important results for cosmologies.

Furthermore, we recast this equation in terms of the set of expansion normalised dynamical variables, which are used through out the rest of this thesis. Using this equation, we were able to apply the result to the Hu-Sawicki model and gain some insight into how it differs from general relativity. In this section, I present a summary of those results, and the accompanying plots. This is a useful point of analysis, elegantly revealing the way $f(R)$ gravity behaves in cosmology, and is widely relevant.

The general geodesic deviation equation is given by

$$\frac{\delta^2\eta^\alpha}{\delta v^2} = -R^\alpha{}_{\beta\sigma\gamma}V^\beta V^\gamma\eta^\sigma, \tag{3.130}$$

where η is the deviation vector, V^α is the normalised tangent vector field, and v is an affine parameter. It is useful to be able to express this deviation in terms of the density, by substituting the expressions for the Riemann and Ricci tensors and the Ricci scalar.

Using the Riemann tensor:

$$R_{\alpha\beta\sigma\gamma} = C_{\alpha\beta\sigma\gamma} + \frac{1}{2}\left(g_{\alpha\sigma}R_{\beta\gamma} - g_{\alpha\gamma}R_{\beta\sigma} + g_{\beta\gamma}R_{\alpha\sigma} - g_{\beta\sigma}R_{\alpha\gamma}\right) - \frac{R}{6}\left(g_{\alpha\sigma}g_{\beta\gamma} - g_{\alpha\gamma}g_{\beta\sigma}\right), \tag{3.131}$$

and the fact that in FLRW space times $C_{\alpha\beta\sigma\gamma}$, the Weyl tensor, vanishes, upon contracting (3.131) with $V^\beta\eta^\sigma V^\gamma$, we obtain

$$R^\alpha{}_{\beta\sigma\gamma}V^\beta\eta^\sigma V^\gamma = \frac{1}{2}\left(\eta^\alpha V^\beta V^\gamma R_{\beta\gamma} - V^\alpha V^\beta\eta^\sigma R_{\beta\sigma} + \epsilon R^\alpha{}_\sigma\eta^\sigma\right) - \frac{R}{6}\eta^\alpha\epsilon. \tag{3.132}$$

By writing $E = -V_\alpha u^\alpha$, $\eta_\alpha u^\alpha = \eta_\alpha V^\alpha = 0$, and $\epsilon = V^\alpha_\alpha$, we can simplify the terms of Equation (3.132) as follows:

$$R^{\alpha}{}_{\beta\sigma\gamma}\eta^{\sigma} = \frac{1}{f'}\left[\eta^{\alpha}\left(p_m + \frac{f}{2} - \Box f'\right) + (\nabla^{\alpha}\nabla_{\sigma}f')\eta^{\sigma}\right], \tag{3.133}$$

$$R_{\beta\sigma}V^{\alpha}V^{\beta}\eta^{\sigma} = \frac{1}{f'}\left[(\nabla_{\beta}\nabla_{\sigma}f')V^{\alpha}V^{\beta}\eta^{\sigma}\right], \tag{3.134}$$

$$R_{\beta\gamma}V^{\beta}V^{\gamma}\eta^{\alpha} = \frac{1}{f'}\left[(\rho_m + p_m)E^2 + \epsilon\left(p_m + \frac{f}{2} - \Box f'\right) + V^{\beta}V^{\gamma}\nabla_{\beta}\nabla_{\gamma}f'\right]\eta^{\alpha}. \tag{3.135}$$

Using Equation (3.128) and that for FLRW spacetimes, $\omega_{\alpha\beta} = \sigma_{\alpha\beta} = 0$, we can arrive at the following expressions:

$$V^{\beta}V^{\gamma}\nabla_{\beta}\nabla_{\gamma}f' = -\frac{1}{3}\dot{f}'\Theta(\epsilon + E^2) + E^2\ddot{f}', \tag{3.136}$$

$$(\nabla_{\beta}\nabla_{\sigma}f')V^{\alpha}V^{\beta}\eta^{\sigma} = 0, \tag{3.137}$$

$$(\nabla^{\alpha}\nabla_{\sigma}f')\eta^{\sigma} = -\frac{1}{3}\dot{f}'\Theta\eta^{\alpha}. \tag{3.138}$$

Substituting the above results into Equation (3.132) gives

$$R^{\alpha}{}_{\beta\sigma\gamma}V^{\beta}V^{\gamma}\eta^{\sigma} = \frac{1}{2f'}\left[\frac{f + \rho_m - 2\dot{f}'\Theta}{3} - \Box f' + p_m\right]\eta^{\alpha}\epsilon + \frac{1}{2f'}\left[\rho_m + p_m - \frac{1}{3}\dot{f}'\Theta + \ddot{f}'\right]\eta^{\alpha}E^2. \tag{3.139}$$

We can then identify terms in Equation (3.139) to be combinations of the curvature fluid density and pressure, from

$$\rho^R + p^R = \frac{1}{f'}\left[-\frac{1}{3}\dot{f}'\Theta + \ddot{f}'\right], \tag{3.140}$$

$$\rho^R + 3p^R = \frac{1}{f'}\left[f + \Theta\dot{f}' + 3\ddot{f}'\right] - R, \tag{3.141}$$

such that, we may obtain the final result for the geodesic deviation equation in metric $f(R)$ gravity [109]:

$$R^{\alpha}{}_{\beta\gamma\sigma}V^{\beta}V^{\gamma}\eta^{\sigma} = \frac{1}{2}\left(\rho^T + p^T\right)E^2\eta^{\alpha} + \left[\frac{R}{6} + \frac{1}{6}\left(\rho^T + 3p^T\right)\right]\epsilon\eta^{\alpha}. \tag{3.142}$$

The result is consistent with what is expected in a homogeneous and isotropic geometry. The tidal force produced will only depend on η^{α} and thus according to [110] only the magnitude of the deviation vector η will change along the geodesic, while its direction is preserved.

Considering only the paths of photons, where $V^{\alpha} = k^{\alpha}$, and $k_{\alpha}k^{\alpha} = 0$, so $\epsilon = 0$, Equation (3.142) becomes

$$R^{\alpha}_{\beta\sigma\gamma}k^{\beta}k^{\gamma}\eta^{\sigma} = \frac{1}{2}(\rho_{total} + p_{total})E^2\eta^{\alpha}, \tag{3.143}$$

showing the focusing of all families of past directed null geodesics as long as

$$(\rho_{total} + p_{total}) > 0. \tag{3.144}$$

Both Equations (3.142) and (3.143) will reduce to the GR result when $f(R) = R$.

Past-directed null geodesics and area distance in $f(R)$ gravity

We now consider how the case $V^\alpha = k^\alpha, k_\alpha k^\alpha = 0, k^0 < 0$ affects Equation (3.143). Let $\eta^\alpha = \eta e^\alpha$ and $e^\alpha e_\alpha = 1$, and $e_\alpha u^\alpha = e_\alpha k^\alpha = 0$, with a basis e that is parallel propagated and aligned, such that, $\delta e^\alpha/\delta v = 0 = k^\beta \nabla_\beta e^\alpha$. Equation (3.143) may thus be written as

$$\frac{\mathrm{d}^2\eta}{\mathrm{d}v^2} = -\frac{1}{2}(\rho_{total} + p_{total})E^2\eta. \tag{3.145}$$

Once again, all families of past directed null geodesics will be focused so long that $(\rho_{total}+p_{total}) > 0$. When the RHS of (3.145) is zero (de Sitter universe in GR), the solution to this equations is the same as that in a flat Minkowski space time: $\eta(v) = C_1(v) + C_2$. The chain rule gives

$$\frac{\mathrm{d}^2}{\mathrm{d}v^2} = \left(\frac{\mathrm{d}z}{\mathrm{d}v}\right)^2 \left[\frac{\mathrm{d}^2}{\mathrm{d}z^2} - \frac{\mathrm{d}z}{\mathrm{d}v}\frac{\mathrm{d}^2 v}{\mathrm{d}z^2}\frac{\mathrm{d}}{\mathrm{d}z}\right], \tag{3.146}$$

$$\frac{\mathrm{d}z}{\mathrm{d}v} = E_0 H(1+z). \tag{3.147}$$

Using this and the modified Friedmann and Raychaudhuri expressions, we obtain the following evolution equation for η with redshift, which depends only on the total equation of state:

$$\frac{\mathrm{d}^2\eta}{\mathrm{d}z^2} + \frac{(7+3w_{total})}{2(1+z)}\frac{\mathrm{d}\eta}{\mathrm{d}z} + \frac{3(1+w_{total})}{2(1+z)^2}\eta = 0. \tag{3.148}$$

We may then infer an expression for the observer area distance $r_0(z)$

$$r_0(z) = \sqrt{\left|\frac{\mathrm{d}A_0(z)}{\mathrm{d}\Omega}\right|} = \left|\frac{\eta(z')|_{z'=0}}{\mathrm{d}\eta(z')/\mathrm{d}\ell|_{z'=0}}\right|, \tag{3.149}$$

where A_0 is the area of the object, and Ω is the solid angle in the sky. Using the fact that $\mathrm{d}/\mathrm{d}\ell = E_0^{-1}(1+z)^{-1}\mathrm{d}/\mathrm{d}v = H(z+1)\mathrm{d}/\mathrm{d}z$, we can express r_0 in terms of redshift derivatives as

$$r_0(z) = \left|\frac{\eta(z)}{H(0)\mathrm{d}\eta(z')}/\mathrm{d}z'|_{z'=0}\right|. \tag{3.150}$$

In general to find the observer distance relation, we need to resort to numerical integration.

In [109], we expressed the GDE in terms of a set of dynamical systems variables, which I define in Chapter 5, so I will come back to this point later.

3.6 The attractive character of gravity

In this section we study the positive contributions of the Raychaudhuri equation for time-like geodesics which guarantee the attractive character of the gravitational interaction in $f(R)$ theories [111]. Following [112], we write the Raychaudhuri equation as

$$\frac{d\theta}{d\tau} = -\frac{1}{3}\theta^2 - \sigma_{\mu\nu}\sigma^{\mu\nu} + \omega_{\mu\nu}\omega^{\mu\nu} - R_{\mu\nu}\xi^\mu\xi^\nu, \tag{3.151}$$

where θ is the expansion, $\sigma_{\mu\nu}$ is the shear, and $\omega_{\mu\nu}$ is the rotation of a congruence of timelike geodesics, generated by the tangent vector field ξ^μ, and τ is an affine parameter.

In GR, assuming the strong energy condition (2.41);

$$T_{\mu\nu}\xi^\mu\xi^\nu \geq -\frac{1}{2}T, \tag{3.152}$$

implies that $R_{\mu\nu}\xi^\mu\xi^\nu \geq 0$. This is an important statement and results in the attractive nature of the gravitational interaction. It follows that the mean curvature [113], defined by $\mathcal{M}_\xi = -R_{\mu\nu}\xi^\mu\xi^\nu$, in every timelike direction must be negative or zero in GR, for fluids for which (3.152) holds. Following [113], [112], the mean curvature in every timelike direction,

$$\mathcal{M}_\xi \equiv -R_{\mu\nu}\xi^\mu\xi^\nu \tag{3.153}$$

is negative or zero in GR, provided that the strong energy condition holds. If one chooses a congruence of timelike geodesics whose tangent vector field is locally hypersurface-orthogonal, then $\omega_{\mu\nu} = 0$ for all the congruences. This result enables the use of the Raychaudhuri equation in the singularity theorems. Since the term $\sigma_{\mu\nu}\sigma^{\mu\nu}$ is non-negative, assuming $R_{\mu\nu}\xi^\mu\xi^\nu \geq 0$, then

$$\frac{\mathrm{d}\theta}{\mathrm{d}\tau} + \frac{1}{3}\theta^2 \leq 0 \rightarrow \theta^{-1}(\tau) \geq \theta_0^{-1} + \frac{1}{3}\tau. \tag{3.154}$$

Inequality (3.154) indicates that a congruence which is initially converging ($\theta_0 \leq 0$) will converge to zero in a finite time. For this reasoning to be true, we require that $R_{\mu\nu}\xi^\mu\xi^\nu \geq 0$ for every non space like vector. In particular, for timelike geodesics, we consider this inequality in the late time cosmological scenario, assuming a de Sitter phase of expansion, and negligible contributions from radiation and dust. In order to have accelerated expansion of timelike geodesics, the Ricci scalar, $R = R_0$ will be approximately constant.

We followed the results [113], it can be proved that

$$R_{\mu\nu}\xi^\mu\xi^\nu \geq \frac{f(R_0 - R_0 f'(R_0))}{2(1 + f'(R_0))}, \tag{3.155}$$

where we require that the field equations (3.44) with constant scalar curvature and standard matter sources satisfies the SEC. Thus, the RHS of (3.155) must be negative in order to have $R_{\mu\nu}\xi^\mu\xi^\nu < 0$. Equivalently, $\mathcal{M}_\xi > 0$, and this means we need $\mathcal{M}_\xi$ to be bounded from above. Thus the condition for timelike geodesics to diverge at late times becomes:

$$\frac{f(R_0 - R_0 f'(R_0))}{2(1 + f'(R_0))} < 0. \tag{3.156}$$

If $1 + f'(R_0) > 0$, we obtain

$$f(R_0) - R_0 f'(R_0) < 0. \tag{3.157}$$

If we take Equation (3.44) in a vacuum ($T = 0$) for constant scalar curvature solutions, the value of R_0 satisfies

$$R_0 = \frac{-2f(R_0)}{1 - f'(R_0)}. \tag{3.158}$$

Although, in general this can not be solved analytically, some $f(R)$ models exist, depending on their parameters, for which a closed solution can be found. Rearranging the terms in Equation (3.157), we can find for a given model whether (3.158) implies that $R_0 > 0$. A positive contribution to the Raychaudhuri equation from the space-time geometry $\mathcal{M}_\xi$ for every time like direction is obtained, when this is true. This is an important theoretical consideration which may be used to constrain the parameter space of $f(R)$ models. We investigated this for the HS model, and show in Figures 5.11 and 5.12 regions of the parameter space, due to a negative contribution of the space time geometry to the Raychaudhuri equation, where gravity is not attractive.

Chapter 4

Cosmological Perturbations

Perturbation theory is arguably one of the cornerstones of modern cosmology. To forward the study of cosmology we rely on fundamental assumptions that manage to avoid major suspicion on very large scales. However, in order to obtain a universe that resembles the one we reside in we know that *something* triggered the time evolution of gravitational potentials and the collapse of ordinary matter. Making the reasonable leap that tiny fluctuations in the density of the universe are the root of the observable structure today, there are in principle two ways to imagine the scenario playing out. We could assume that the seeds of the density perturbations occurred as a result of dynamic processes during the evolution of the universe, which at the initial moment was indeed in complete equilibrium leading to a class of models known as isocurvature theories. However, this initial fluctuation spectrum would have had to have been present at the time of recombination at least, in order for us to observe the structure we see today. For this reason it is the second interpretation, the so called adiabatic model, which is more widely accepted, in which the seeds of structure were a feature of the initial state of the universe. There must have been some *tiny* fluctuations of the gravitational potential which initiated the growth of structure. The best way forward would be to perturb our simple universe by perturbing the metric;

$$g_{\mu\nu} = \bar{g_{\mu\nu}} + \delta g_{\mu\nu}, \tag{4.1}$$

and track the evolution of perturbations throughout time where as is usual, barred quantities represent the background value, and those containing a prefix of δ represent the perturbation on that background, with the perturbed Einstein equations appearing as

$$\delta G_{\mu\nu} = 8\pi\delta T_{\mu\nu}. \tag{4.2}$$

This gives the exercise of effectively reconstructing the growth of structure in our Universe, and moreover, model universes, whose validity needs checking against the large scale structure observations we have available.

Studying the growth of structure ultimately reduces to :

1. Choosing a set of initial conditions for the universe and its *initial fluctuation spectrum*; whether adiabatic or iso-curvature models are being considered.

2. Identifying what components of the *dark sector* we consider important for study, and the space-time evolution of the stresses of this component. The nature of dark matter chosen to feature in the model will determine the evolution of the gravitational potential, playing a significant role in observable effects of the large scale structure of the universe - thus the large scale structure (LSS) provides strict constraints on the properties of the dark matter content. For example, non clustering components of dark matter will contribute nothing to the growth of gravitational potentials, and will instead add to the effects of expansion, leading to more diluted large scale structure. Models with higher neutrino densities lead to less large scale structure and more large angle anisotropies.

3. The *type of perturbation* which will be considered to be evolving. Specifically, any perturbation can be decomposed into scalar, vector and tensor modes, each perturbation giving rise to different physical effects. Scalar perturbations occur as a result of fluctuations in the energy density content of the universe and in general grow with sufficient gravitational instability. Vector perturbation modes are associated with vorticity perturbations and require a source in order to be generated, these modes will always decay in a smoothly expanding universe. Tensor perturbations are a phenomenon of the early universe, generated by transverse-traceless stresses in the matter, predicted by inflation and in general result in the generation of gravitational waves. There are models which predict both scalar and tensor fluctuations initially, however the simplest inflationary models usually contain only scalar modes, where tensor fluctuations are negligibly small at Planck scales. At scales for which linear perturbation theory is relevant, these three types of perturbations are decoupled from each other dynamically and may be studied separately. For this work, we limit our investigation to the linear regime.

4.1 The Gauge Problem

The problem associated with computing perturbations to solutions is one associated to a user defined ambiguity in the process. Consider a general cosmologically relevant quantity, $Q(x,t)$, we may assign it a background value of $Q^{(0)}(t)$ (of zero order), which is determined by the evolution of the background cosmological equations, for example those corresponding to the FRW metric discussed in the previous section. Investigating the evolution of a generic linear perturbation to the background quantity, we may assign this perturbation $Q^{(1)}(x)$, of first order. The linearization is performed by strictly neglecting products of two first order quantities in the equations. However, solutions to the linearized

Einstein equations do not determine the perturbations uniquely. For a solution $Q^{(1)}(x)$, there exists solutions like $\hat{Q}^{(1)}$, such that,

$$\hat{Q}^{(1)}(x) = Q^{(1)}(x) + \phi(x)\partial_0 Q^{(0)}(t), \tag{4.3}$$

which also are able to satisfy the linearized Einstein equations. Therefore, the perturbation $Q^{(1)}$ is really only fixed by the linearized Einstein equations up to a small arbitrary function $\phi(x)$, known as the gauge function. This implies a perturbation calculated in this way is not consistent with the physical perturbation itself, since it depends on some arbitrary function, and the actual notion of what the physical perturbation is becomes blurry. This is the heart of the gauge problem, and in the quest to solve the perturbations around a suitable background cosmology, and reproduce the current observables, like the distribution of anisotropies in the cosmic microwave background, and the distribution of baryonic and cold dark matter in the sky, many gauge choices have been defined, based on various case justified choices. The choice of gauge will ultimately change the appearance of the metric and therefore produce results specific to that choice.

Some popular gauge choices are the synchronous, spatially flat, comoving, uniform density and Newtonian conformal gauges, each having advantages in their own right, either simplifying equations or producing well behaved solutions in a specific situation.

A classical description of cosmological perturbations was treated by Lifshitz [114], in which the physical interpretation of the evolution of perturbations could not be established until a gauge was chosen. Later Lifshitz and Kalatnikov [115] further developed the theory, in which they discarded the gauge modes. The cleverest approach would be to find those variables which have the property that they are *gauge invariant*; vanishing in the background, such that these gauge invariant variables maintain their values regardless of the coordinate system or gauge chosen. Bardeen [116] formulated the first gauge invariant framework through which cosmological perturbations could be studied, by using specific linear combinations of naturally gauge invariant quantities occurring in the perturbed Einstein equations and emergent conservation laws [117]. However, while his variables are gauge invariant, they lack geometrical intuitive power, since they are defined with respect to some coordinate base in the first place, as gauge invariant linear combinations of gauge dependent perturbations [118] - a mathematical tool to get the job done.

Following work on this problem by Hawking (1966), Ellis et al developed a covariant gauge invariant framework in which the physical meaning of the gauge invariant variables are clear. Specifically, the density contrast itself is treated gauge invariantly. This is done by defining a covariant set of exact variables which vanish in an FLRW space time, such that the variables themselves *are* the perturbations in a perturbed FLRW universe [118]. In the next section we give a brief overview before presenting the perturbation evolution equations in this framework.

4.2 Covariant Gauge Invariant Approach to Cosmological Perturbations

Once we have the equations governing the background evolution for a cosmology, given a specific metric, we can examine the evolution of perturbations around said background, as long as the metric of choice is verified to be a solution of the background cosmology. This section aims to present the covariant gauge invariant (CoGI) description of the evolution of perturbations, through a set of covariant equations expressed in terms of variables which are naturally gauge invariant, and that have a direct physical meaning [107], [11].

To begin the process, we split all the "real" quantities in (3.113) to (3.126) into a theoretical background part (zero order) and a small perturbation (first order). In a FLRW space time, background quantities are exclusively time dependent, however, the perturbations will not in general obey isotropy, and are functions of space as well. Once the sum of the zero and first order parts are substituted into the propagation and constraint equations, neglecting products of quantities with order higher than one leads to the linearized propagation and constraint equations of the 1+3 cosmological system,

$$\dot{\Theta} + \frac{1}{3}\Theta^2 - \tilde{\nabla} A_\alpha + \frac{1}{2}(\tilde{\rho}^M + 3\tilde{p}^M) = -\frac{1}{2}(\rho^R + 3p^R), \tag{4.4}$$

$$\dot{\omega}_\alpha + \frac{2}{3}\Theta\omega_\alpha + \frac{1}{2}\text{curl } A_\alpha = 0, \tag{4.5}$$

$$\sigma_{\alpha\beta} + \frac{2}{3}\Theta\sigma_{\alpha\beta} + E_{\alpha\beta} - \tilde{\nabla}_{\langle\alpha} A_{\beta\rangle} = -q^R_\alpha, \tag{4.6}$$

$$\begin{aligned}\dot{E}_{\alpha\beta} + \Theta E_{\alpha\beta} - \text{curl}H_{\alpha\beta} + \frac{1}{2}(\tilde{\rho}^M + \tilde{p}^M)\sigma_{\alpha\beta} \\ = -\frac{1}{2}(\rho^R + p^R)\sigma_{\alpha\beta} - \frac{1}{2}\dot{\pi}^R_{\langle\alpha\beta\rangle} - \frac{1}{2}\tilde{\nabla}_{\langle\alpha} q^R_{\beta\rangle} - \frac{1}{6}\Theta\pi^R_{\alpha\beta},\end{aligned} \tag{4.7}$$

$$\dot{H}_{\alpha\beta} + \Theta H_{\alpha\beta} + \text{curl } E_{\alpha\beta} = \frac{1}{2}\text{curl } \pi^R_{\alpha\beta}, \tag{4.8}$$

$$\tilde{\nabla}^\beta\sigma_{\alpha\beta} - \text{curl } \omega_\alpha - \frac{2}{3}\tilde{\nabla}_\alpha\Theta = -q^R_\alpha, \tag{4.9}$$

$$\text{curl } \sigma_{\alpha\beta} + \tilde{\nabla}_{\langle\alpha}\omega_{\beta\rangle} - H_{\alpha\beta} = 0, \tag{4.10}$$

$$\tilde{\nabla}^\beta E_{\alpha\beta} - \frac{1}{3}\tilde{\nabla}_\alpha\tilde{\rho}^M = -\frac{1}{2}\tilde{\nabla}^\beta\pi^R_{\alpha\beta} + \frac{1}{3}\tilde{\nabla}_\alpha\rho^R - \frac{1}{3}\Theta q^R_\alpha, \tag{4.11}$$

$$\tilde{\nabla}^\beta H_{\alpha\beta} - (\tilde{\rho}^M + \tilde{p}^M)\omega_\alpha = -\frac{1}{2}\text{curl } q - \alpha^R + (\rho^R + p^R)\omega_\alpha, \tag{4.12}$$

$$\tilde{\nabla}^\alpha\omega_\alpha = 0. \tag{4.13}$$

where, $A_\alpha = \dot{u}_\alpha$. Notice that at first order the vorticity decouples and is spatially homogeneous. The linearized conservation equations are

$$\dot{\rho}^M = -\Theta(\rho^M + p^M), \tag{4.14}$$

$$\tilde{\nabla}^\alpha p^M = -(\rho^M + p^M)\dot{u}^\alpha, \tag{4.15}$$

$$\dot{\rho}^R + \tilde{\nabla}^\alpha q^R_\alpha = -\Theta(\rho^R + p^R) + \rho^M \frac{f''\dot{R}}{f'^2}, \tag{4.16}$$

$$\dot{q}^R_{\langle\alpha\rangle} + \tilde{\nabla}_\alpha p^R + \tilde{\nabla}^\beta \pi^R_{\alpha\beta} = -\frac{4}{3}\Theta q^R_\alpha - (\rho^R + p^R)\dot{u}_\alpha + \rho^M \frac{f''\tilde{\nabla}_\alpha R}{f'^2}. \tag{4.17}$$

These equations set up the system to describe the cosmological perturbations in $f(R)$ gravity in a covariant and gauge-invariant framework.

4.2.1 Perturbation variables

Fixing the background, in such a covariant gauge-invariant approach, is done by deciding which of the background quantities may be turned off, or on, as the case may be. In this thesis, we will only consider expanding ($\Theta \neq 0$), homogeneous and isotropic ($\pi_{\alpha\beta} = 0, \omega_\alpha = 0$) backgrounds. As discussed in Chapter 1, there is no unique correspondence between the real world, which we could represent by a spectrum of perturbations, and the chosen theoretical background. The problem will always come down to selecting a gauge, or better yet, eliminating the appearance of the gauge function in the equations all together. So in this section we will present a set of gauge invariant perturbation variables, which do in fact facilitate the elimination of the gauge functions [107], [11], [119].

The key quantities in a perturbation study for cosmology would be the energy density contrast and the perturbation associated with the Ricci scalar, indeed it is these two perturbations which we are most interested in. The following two gauge invariant quantities provide the basis for the discussion of the time evolution of energy density perturbations:
the orthogonal projection of the energy density gradient

$$X_\alpha \equiv \tilde{\nabla}\rho^M, \tag{4.18}$$

which can be obtained in a number of ways; by using the observations of large scale structure paired with estimates derived from the virial theorem, by measuring the way the number of sources change and taking an estimate of the mass to light ratio, and by gravitational lensing observations [11], and *the orthogonal projection of the expansion gradient*

$$Z_\alpha \equiv \tilde{\nabla}_\alpha \Theta. \tag{4.19}$$

Because these variables are not directly related to the measurable quantities, the following more suitable variables are used, defined in terms of the above projections, scaled by the scale factor, $a(t)$:

$$\mathcal{D}_\alpha \equiv a\frac{X_\alpha}{\rho^M}. \tag{4.20}$$

$\mathcal{D}_\alpha$ is the matter - comoving fractional energy density gradient , and is gauge invariant and dimensionless, giving the spatial variation of energy density for a fixed comoving scale [11] . The ratio X_α/ρ is a measure of the difference in magnitude between the density perturbations and the background energy density, and the appearance of the scale factor ensures $\mathcal{D}_\alpha$ is dimensionless. Its magnitude is given as usual by $\mathcal{D} = \sqrt{\mathcal{D}_\alpha \mathcal{D}^\alpha}$, and is the preferred variable; $\mathcal{D}$ is the gauge invariant covariant version of $\delta\rho/\rho$, but it represents an actual spatial fluctuation in the energy density, instead of a fictitious time fluctuation [11] . The Bardeen variable $\epsilon \propto \delta\rho/\rho$ is in fact the scalar harmonic component of $\mathcal{D}_\alpha$ [120], [121]. The variable involving Θ is also scaled by the scale factor:

$$Z_\alpha \equiv a\tilde{\nabla}_\alpha \Theta, \tag{4.21}$$

known as the matter - comoving spatial expansion gradient. And another important variable, not independent of (4.20), is the spatial gradient of the Ricci scalar,

$$C_\alpha \equiv a\tilde{\nabla}_\alpha \tilde{R}, \tag{4.22}$$

where $\tilde{R} = 6K/a^2$ is the 3-Ricci curvature. In $f(R)$ gravity, the above variables do not complete the story, we also require a perturbation variable which can characterise the inhomogeneity in the Ricci scalar. As in the previous section, the Ricci scalar curvature is treated as an effective field, and thus we define the variables in terms of the following gradients:

$$\mathcal{R}_\alpha = a\tilde{\nabla}_\alpha R, \quad \mathfrak{R}_\alpha = a\tilde{\nabla}\dot{R}, \tag{4.23}$$

where, $\mathcal{R}_\alpha$ is the spatial perturbation in the Ricci scalar itself, and $\mathfrak{R}_a$ is the perturbation in its momentum, $\dot{R}$. These quantities vanish in the background which render them gauge invariant. The variables defined above will characterise all of scalar, vector and tensor perturbations, including those involving the evolution of non-spherically symmetric and rotational modes of motion, which, in the context of a linear analysis in FLRW backgrounds, are independent from each other, allowing the dynamics of each to be studied separately. Given that we are only for the moment interested in the matter density perturbations, it is in our interest to extract the scalar part, relevant for this purpose, simplifying the equations significantly. We do this by using the local splitting:

$$\tilde{\nabla}_\alpha X_\beta = X_{\alpha\beta} = \frac{1}{3}h_{\alpha\beta}X + \Sigma^X_{\alpha\beta} + X_{[\alpha\beta]}, \tag{4.24}$$

where,

$$X = \tilde{\nabla}_\alpha X^\alpha, \quad \Sigma^X_{\alpha\beta} = X_{(\alpha\beta)} - \frac{1}{3}h_{\alpha\beta}X, \tag{4.25}$$

from which, geometrically, it is clear that really the only the scalar part X can describe spherically symmetric collapse, thus the analysis will now only be concerned with the scalar part of the perturbations. The scalar part is extracted by applying the comoving differential operator $a\tilde{\nabla}_\alpha$ to (4.20) -

(4.23), resulting in the following *Scalar Perturbation Variables*:

$$\Delta_M = \frac{a^2}{\rho^M}\tilde{\nabla}^2\rho^M, \tag{4.26}$$

$$Z = a^2\tilde{\nabla}^2\Theta, \tag{4.27}$$

$$C = a^4\tilde{\nabla}^2 R_3, \tag{4.28}$$

$$\mathcal{R} = a\tilde{\nabla}^2 R, \tag{4.29}$$

$$\mathfrak{R} = a^2\tilde{\nabla}^2\dot{R}. \tag{4.30}$$

and these new variables are also gauge invariant.

The Newtonian potential is constructed using the divergence of the electric component of the Weyl curvature tensor:

$$\begin{aligned}\Phi^N_\alpha =& a^2\rho^{total}\mathcal{D}^{total}_\alpha \\ =& \frac{1}{2\Theta f' + 3\dot{R}f''}\left[2a^2\rho\Theta\mathcal{D}^M_a + \frac{3}{2}\dot{R}f''C_\alpha - 2a^2 f''\Theta^2\mathfrak{R}_\alpha\right. \\ &\left. + \frac{a^2}{f'}\left(f''(f - 2\rho + 2\dot{R}\Theta f'') - 2\dot{R}\Theta f' f^{(3)}\right)\Theta\mathcal{R}_\alpha\right],\end{aligned} \tag{4.31}$$

where $\mathcal{D}_\alpha$ represents the total energy density fluctuation, and its corresponding scalar gauge invariant perturbation is defined as

$$\Phi^N = a\tilde{\nabla}^\alpha\Phi^N_\alpha. \tag{4.32}$$

Thus, once a background is specified, the set of variables $\{\Delta_M, Z, C, \mathcal{R}, \mathfrak{R}, \Phi^N\}$ will completely describe the evolution of the spherically symmetric component of the gradients defined by (4.20)-(4.23) in $f(R)$ gravity. And the Stewart Walker lemma guarantees that the new perturbation variables are gauge invariant in accordance with the fact that the quantities by which they are defined are gauge invariant.

4.2.2 Evolution Equations

Standard FLRW cosmology is provided by the following background equations, where the curvature fluid is also a source in $f(R)$ gravity, for an observer with velocity u^M_α in the matter energy density frame, where the sources are described by perfect fluids, such that $p^M = w\rho^M$:

$$\Theta^2 = 3\frac{\rho^M}{f'} + 3\rho^R - \frac{3}{2}R_3, \tag{4.33}$$

$$\dot{\Theta} + \frac{1}{3}\Theta^2 + \frac{1}{2f'}(\rho^M + 3p^M) + \frac{1}{2}(\rho^R + 3p^R) = 0, \tag{4.34}$$

$$\dot{\rho}^M + \Theta(\rho^M + p^M) = 0, \tag{4.35}$$

$$\dot{\rho}^R + \Theta(\rho^R + p^R) - \rho^M\frac{f''}{f'^2}\dot{R} = 0, \tag{4.36}$$

and ρ^R and p^R are provided by Equations (3.100) and (3.101), and are the zero order energy density and pressure of the curvature fluid. Using equations (4.33) - (4.36), the following evolution and constraint equations for the variables (4.26) to (4.30) may be derived [107], [119] comprising a set of first order partial differential equations:

$$\dot{\Delta} = w\Theta\Delta_M - (1+w)Z, \tag{4.37}$$

$$\begin{aligned}\dot{Z} = &\left(\frac{\dot{R}f''}{f'} - \frac{2\Theta}{3}\right)Z + \left[\frac{(w-1)(3w+2)}{2(w+1)}\frac{\rho^M}{f'} + \frac{2w\Theta^2 + 3w(\rho^R+3p^R)}{6(w+1)}\right]\Delta_M + \frac{\Theta f''}{f'}\mathfrak{R} \\ &+ \left[\frac{1}{2} - \frac{1}{2}\frac{ff''}{f'} - \frac{\rho^M f''}{f'} + \dot{R}\Theta\left(\frac{f''}{f'}\right)^2 + \dot{R}\Theta\frac{f^{(3)}}{f'}\right]\mathcal{R} - \frac{w}{w+1}\tilde{\nabla}^2\Delta_M - \frac{f''}{f'}\tilde{\nabla}^2\mathcal{R}\end{aligned} \tag{4.38}$$

$$\dot{\mathcal{R}} = \mathfrak{R} - \frac{w}{w+1}\dot{R}\Delta_M, \tag{4.39}$$

$$\tag{4.40}$$

$$\begin{aligned}\dot{\mathfrak{R}} = &-\left(\Theta + 2\dot{R}\frac{f^{(3)}}{f''}\right)\mathfrak{R} - \dot{R}Z - \left[\frac{(3w-1)}{3}\frac{\rho^M}{f''} + 3\frac{w}{w+1}(p^R+\rho^R)\frac{f'}{f''}\right. \\ &+\frac{w}{3(w+1)}\dot{R}\left(\Theta - 3\dot{R}\frac{f^{(3)}}{f''}\right)\Bigg]\Delta_M + \left[2\frac{K}{a^2} - \left(\frac{1}{3}\frac{f'}{f''} + \frac{f^{(4)}}{f'}\dot{R}^2 + \Theta\frac{f^{(3)}}{f'}\dot{R} - \frac{2}{9}\Theta^2\right.\right. \\ &\left.\left.+\frac{1}{3}(\rho^R+3p^R) + \ddot{R}\frac{f^{(3)}}{f''} - \frac{1}{6}\frac{f}{f'} + \frac{1}{2}(w+1)\frac{\rho^M}{f'} - \frac{1}{3}\dot{R}\Theta\frac{f''}{f'}\right)\right]\mathcal{R} + \tilde{\nabla}^2\mathcal{R},\end{aligned} \tag{4.41}$$

$$\begin{aligned}\dot{C} = &K^2\left[\frac{18f''\mathcal{R}}{a^2\Theta f'} - \frac{18\Delta_M}{a^2\Theta}\right] + K\left[\frac{3}{a^2\Theta}C + \Delta_M\left(\frac{2(w-1)\Theta}{1+w} + \frac{6\rho^R}{\Theta}\right) - \frac{6f''}{\Theta f''}\tilde{\nabla}^2\mathcal{R}\right. \\ &\left.+\frac{6f''}{f'}\mathfrak{R} + \frac{6\dot{R}\Theta f' f^{(3)} - f''(3f - 2(\Theta^2 - 3\rho^R)f' + 6\dot{R}\Theta f'')}{\Theta f'^2}\mathcal{R}\right] \\ &+\tilde{\nabla}^2\left[\frac{4wa^2\Theta}{3(w+1)}\Delta_M + \frac{2a^2 f''}{f'}\mathfrak{R} - \frac{2a^2(\Theta f'' - 3\dot{R}f^{(3)})}{3f'}\mathcal{R}\right],\end{aligned} \tag{4.42}$$

and the following constraint on the system:

$$\begin{aligned}\frac{C}{a^2} + \left(\frac{4}{3}\Theta + \frac{2\dot{R}f''}{f'}\right)Z - 2\frac{\rho^M}{f'}\Delta_M + \left[2\dot{R}\Theta\frac{f^{(3)}}{f'} - \frac{f''}{f'^2}(f - 2\rho^M + 2\dot{R}\Theta f'')\right]\mathcal{R} \\ + \frac{2\Theta f''}{f'}\mathfrak{R} - \frac{2f''}{f'}\tilde{\nabla}^2\mathcal{R} = 0.\end{aligned} \tag{4.43}$$

The perturbations determined by this system of four equations, or a single fourth order differential equation, result in solutions which, in general, contain four modes. This differs from GR, where in general the density perturbations only have solutions containing adiabatic growing and decaying

modes, determined by a second order differential equation. It is also clear to see that the dependence on the scale factor is far more prominent than that of GR, implying that the evolution of perturbations are significantly more sensitive to background behaviour and scale.

4.2.3 Harmonic Decomposition

To make the equations (4.37) – (4.42) more palatable, a harmonic analysis can be employed to reduce them to a set of ordinary differential equations, which effectively separates out the time variation from the space variation of density perturbations. In doing so, the differential equation describing the time variation is converted to a set of separate time variation equations corresponding to each component of spatial variation, characterised by a matter comoving wavenumber, k [11], [118], resulting in a set of equations which are easier to solve. Using the eigenfunctions of the spatial Laplace-Beltrami operator, defined by

$$\tilde{\nabla}^2 Q = -\frac{k^2}{a^2} Q, \tag{4.44}$$

where $k = 2\pi a/\lambda$ is the wavenumber and $\dot{Q} = 0$, each first order quantity in the above equations can be expanded via

$$X(t, \mathbf{x}) = \sum X^{(k)}(t) Q^{(k)}(\mathbf{x}), \tag{4.45}$$

where $\sum$ represents both summation and integration for discrete and continuous indices respectively. Applying (4.45) to (4.26) – (4.32), we obtain equations describing the k^{th} mode for scalar perturbations in $f(R)$ gravity:

$$\dot{\Delta}_M^{(k)} = w\Theta\Delta_M^{(k)} - (1+w)Z^{(k)}, \tag{4.46}$$

$$\dot{Z}^{(k)} = \left(\frac{\dot{R}f''}{f'} - \frac{2\Theta}{3}\right) Z^{(k)} + \left[\frac{(w-1)(3w+2)}{2(w+1)}\frac{\rho^M}{f'} + \frac{2w\Theta^2 + 3w(\rho^R + 3p^R)}{6(w+1)}\right] \Delta_M^{(k)} \tag{4.47}$$

$$+ \frac{\Theta f''}{f'}\mathfrak{R}^{(k)} + \left[\frac{1}{2} - \frac{f''}{f'}\frac{k^2}{a^2} - \frac{1}{2}\frac{f}{f'}\frac{f''}{f'} - \frac{f''}{f'}\frac{\rho^M}{f'} + \dot{R}\Theta\left(\frac{f''}{f'}\right)^2 + \dot{R}\Theta\frac{f^{(3)}}{f'}\right]\mathcal{R}^{(k)}, \tag{4.48}$$

$$\dot{\mathcal{R}}^{(k)} = \mathfrak{R}^{(k)} - \frac{w}{w+1}\dot{R}\Delta_M^{(k)}, \tag{4.49}$$

$$\dot{\mathfrak{R}}^{(k)} = -\left(\Theta + 2\dot{R}\frac{f^{(3)}}{f''}\right)\mathfrak{R}^{(k)} - \dot{R}Z^{(k)} - \left[\frac{(3w-1)}{3}\frac{\rho^M}{f''} + \frac{w}{3(w+1)}\ddot{R}\right]\Delta_M^{(k)} \tag{4.50}$$

$$+ \left[\frac{k^2}{a^2} - \left(\frac{1}{3}\frac{f'}{f''} + \frac{f^{(4)}}{f'}\dot{R}^2 + \frac{f^{(3)}}{f''}(\Theta\dot{R} + \ddot{R}) - \frac{R}{3}\right)\right]\mathcal{R}^{(k)},$$

$$\begin{aligned}\dot{C}^{(k)} =&\frac{36K^2}{a^2(2\Theta f' + 3\dot{R}f'')}\left(f''\mathcal{R} - f'\Delta_M\right) + K\left[\frac{1}{a^2(2\Theta f' + 3\dot{R}f'')}\left(6f'C\right.\right.\\ &-12f''\tilde{\nabla}^2\mathcal{R} + 12\Theta f''\mathfrak{R} + 12\dot{R}\Theta f' f^{(3)} - 2f''\left(3f - 2(\Theta^2 - 3\rho^R)f' + 6\dot{R}\Theta f''\right)\frac{\mathcal{R}}{f'}\Big)\\ &\left.+\Delta\left(\frac{4w\Theta}{w+1} - \frac{4f'\Theta^2 - 12f'\rho^R}{2\Theta f' + 3\dot{R}f''}\right)\right] \qquad (4.51)\\ &+\tilde{\nabla}^2\left[\frac{4wa^2\Theta}{3(w+1)}\Delta_M^{(k)} + \frac{2a^2 f''}{f'}\mathfrak{R} - \frac{2a^2(\Theta f'' - 3\dot{R}f^{(3)})}{3f'}\right]\mathcal{R}_M^{(k)},\end{aligned}$$

together, with the constraint,

$$\begin{aligned}0 =&\frac{C^{(k)}}{a^2} + \left(\frac{4}{3}\Theta + \frac{2\dot{R}f''}{f'}\right)Z^{(k)} - 2\frac{\rho}{f'}\Delta_M^{(k)} + \frac{2\Theta f''}{f'}\mathfrak{R}^{(k)} \qquad (4.52)\\ &+\left[2\dot{R}\Theta\frac{f^{(3)}}{f'} - \frac{f''}{f'^2}\left(f - 2\rho + 2\dot{R}\Theta f''\right) + 2\frac{f''}{f'}\frac{k^2}{a^2}\right]\mathcal{R}^{(k)} = 0.\end{aligned}$$

Changing variables, we can further simplify the appearance of the above equations, reducing to a pair of second order ordinary differential equations:

$$\ddot{\Delta}_M^{(k)} + \mathcal{A}\dot{\Delta}_M^{(k)} + \mathcal{B}\Delta_M^{(k)} = \mathcal{C}\mathcal{R}^{(k)} + \mathcal{D}\dot{R}^{(k)}, \qquad (4.53)$$

$$f''\ddot{R}^{(k)} + \mathcal{E}\dot{\mathcal{R}}^{(k)} + \mathcal{F}\mathcal{R}^{(k)} = \mathcal{G}\Delta_M^{(k)} + \mathcal{H}\dot{\Delta}_M^{(k)}, \qquad (4.54)$$

where,

$$\mathcal{A} = \left(\frac{2}{3} - w\right)\Theta - \frac{\dot{R}f''}{f'}, \qquad (4.55)$$

$$\mathcal{B} = -\left[w\frac{k^2}{a^2} - w(3p^R + \rho^R) - \frac{2w\dot{R}\Theta f''}{f'} - \frac{(3w^2-1)\rho^M}{f'}\right], \qquad (4.56)$$

$$\mathcal{C} = \frac{1}{2}(w+1)\left[-2\frac{k^2}{a^2}\frac{f''}{f'} - 1 + (f - 2\rho^M + 2\dot{R}\Theta f'')\frac{f''}{f'^2} - 2\dot{R}\Theta\frac{f^{(3)}}{f'}\right], \qquad (4.57)$$

$$\mathcal{D} = -\frac{(w+1)\Theta f''}{f'}, \qquad (4.58)$$

$$\mathcal{E} = (\Theta f'' + 2\dot{R}f^{(3)}), \qquad (4.59)$$

$$\begin{aligned}\mathcal{F} =& -\left[\frac{k^2}{a^2}f'' + 2\frac{K}{a^2}f'' + \frac{2}{9}\Theta^2 f'' - (w+1)\frac{\rho^M}{2f'}f'' - \frac{1}{6}(\rho^R + 3p^R)f'' - \frac{f'}{3}\right.\\ &\left.+\frac{f}{6f'}f'' + \dot{R}\Theta\frac{f''^2}{f'} - \ddot{R}f^{(3)} - \Theta f^{(3)}\dot{R} - f^{(4)}\dot{R}^2\right], \qquad (4.60)\end{aligned}$$

$$\mathcal{G} = -\left[\frac{1}{3}(3w-1)\rho^M + \frac{w}{w+1}\left(f^{(3)}\dot{R}^2 + (p^R + \rho^R)f' + \frac{7}{3}\dot{R}\Theta f'' + \ddot{R}f''\right)\right], \qquad (4.61)$$

$$\mathcal{H} = -\frac{(w-1)\dot{R}f''}{w+1}. \qquad (4.62)$$

If we set $f(R) = R$, the above equations reduce to the evolution equations for density and curvature perturbations in GR:

$$\ddot{\Delta}_M^{(k)} - (w - \frac{2}{3})\Theta\dot{\Delta}_M^{(k)} - \left[w\frac{k^2}{a^2} - \left(\frac{1}{2} + w - \frac{3}{2}\right)\rho^M\right]\Delta_M^{(k)} = 0, \tag{4.63}$$

$$\mathcal{R}^{(k)} = (3w - 1)\rho^M\Delta_M^{(k)}. \tag{4.64}$$

In this section I presented the equations of motion for scalar perturbations in the $1 + 3$ covariant gauge invariant formalism. We use the solution of these equations to form quantities which are inferred from cosmological data. In the Section 5.3.3 I will define this observable quantity, and its relation to the theoretical solution of equations (4.53) and (4.54).

Chapter 5

A general class of viable broken power law models for $f(R)$ gravity

In Chapter 1 we discussed the first questions which lead to the development of the research in this thesis. In Chapter 2, 3 and 4 we presented the relevant background required to address these questions. And we are now at the stage to begin answering some of these.

The model which represents a general class of viable $f(R)$ theories is given in [7], and has the form

$$f(R) = R - R_s\beta\left\{1 - \left[1 + \left(\frac{R}{R_*}\right)^n\right]^{-\frac{1}{\beta}}\right\}. \tag{5.1}$$

In Figure 5.3, the correction of this function is plotted with the curvature, to illustrate the dependence of its behaviour on the free parameter n.

For $n = 2$, we obtain the models examined in [] ;

$$f(R)_S = R + \lambda R_S\left\{\left[1 + \left(\frac{R}{R_S}\right)^2\right]^{-q} - 1\right\}, \tag{5.2}$$

with $\lambda > 0$ and $R_S \sim \Lambda$ in the ΛCDM model. In [7], an example of the model (5.1) was considered for which $\beta \to \infty$, resulting in the form for f :

$$f(R)_{MJW} = R - \alpha R_* \ln\left(1 + \frac{R}{R_*}\right). \tag{5.3}$$

For $\beta = 1$ we have the models studied in [6], which was the first model we considered in 2015,

$$f(R)_{HS} = R - m^2\frac{c_1\left(\frac{R}{m^2}\right)^n}{c_2\left(\frac{R}{m^2}\right)^n + 1}, \tag{5.4}$$

model parameters c_1, c_2, n are positive dimensionless constants, and m^2 which in [6] is defined in terms of the average density as

$$m^2 \equiv \frac{\kappa^2\bar{\rho}_0}{3}, \tag{5.5}$$

gives the mass of the scalar field, which we relate to the Hubble constant through the parameter c;

$$m_f^2 = \sqrt{3f''(R)} = cH_0^2. \tag{5.6}$$

The HS broken power law form for $f(R)$ at (5.4) is probably one of the earliest models constructed to evade local tests of gravity. In order for the scalar field to have a smooth transition from high to low curvature regimes, such that in environments of high density there are no deviations from GR (like the solar system), the mass of the scalar field must be large [122], [123]. Both the HS model and the more general form given by (5.1) have a mass dependent on the curvature of the environment, satisfying the following limits [96], [6] :

$$\begin{aligned} \lim_{cH_0^2/R\to 0} g(R) &= const, \\ \lim_{cH_0^2/R\to \infty} g(R) &= 0. \end{aligned} \tag{5.7}$$

the correction to the Ricci scalar, $g(R)$ is chosen such that as it can produce an effective cosmological constant at late times, while also avoiding violations of local gravity tests. A viable model for $f(R)$ would be one that firstly had GR as a limiting case, and the second limit, which sends the corrective term $g(R)$ to zero when spatial curvature is zero corresponds to this. These limits are a set of essential considerations when picking out a form for $f(R)$ that can at very least produce the correct expansion history for its resulting universe.

That observed expansion, which is quite well described by the ΛCDM parameterisation of the BBT must be produced at high redshifts - we would like if the $f(R)$ function could essentially behave like the ΛCDM model at high redshifts, especially because high precision data is available from the cosmic microwave background. Since radiation dominates in this regime, the theory describing the background need only be as good as GR, and having a correction which disappears in this regime is suitable.

In order to show how these models can mimic cosmological constant behaviour at late times by satisfying the limits (5.7), Figure 5.2 gives the corrections in the Hu-Sawicki, Starobinsky, MJW model as a function of curvature. It is clear to see how these functional forms for $f(R)$ satisfy the limits stated previously. The correction $g(R)$ goes to zero as the curvature goes to zero, reducing to GR gravity, and as the curvature increases compared to the local density, the correction evolves to a constant valued plateau; and it is this plateau which mimics the cosmological constant behaviour.

A comparison of the resultant expansion histories, represented by a redshift evolution of the Hubble parameter and the deceleration parameter, for the models stated above is shown in Figure 5.1a. The broken power law functions with more parameters can match the behaviour of the ΛCDM model, far better than that of R^n, alone. As is discussed below, depending on the initial conditions chosen, these $f(R)$ models cannot obtain the exact values for $H(z)$ and $q(z)$ at the present epoch - this is highlighted in Figure 5.1 below.

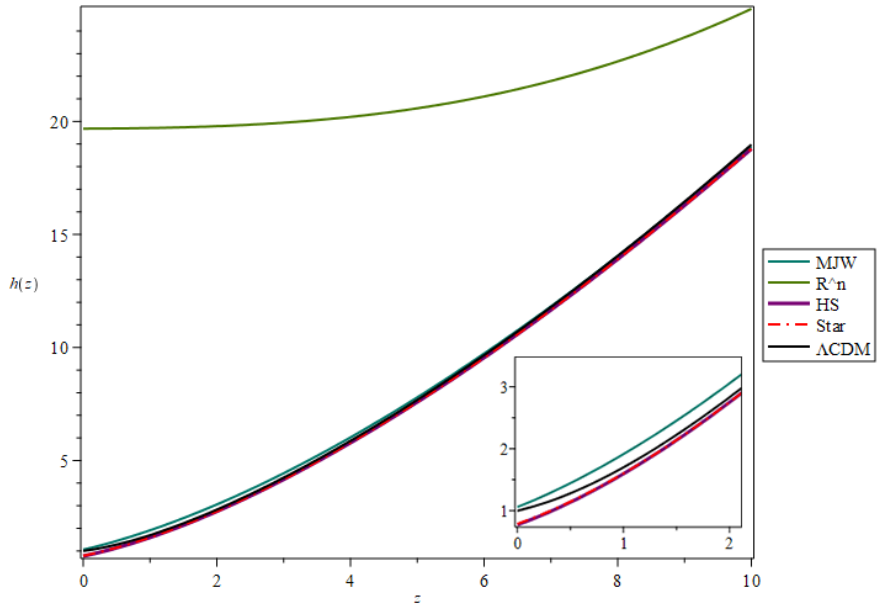

(a) The Hubble rate, $H = \frac{\dot{a}}{a}$ is shown for four $f(R)$ models, along with the ΛCDM model.

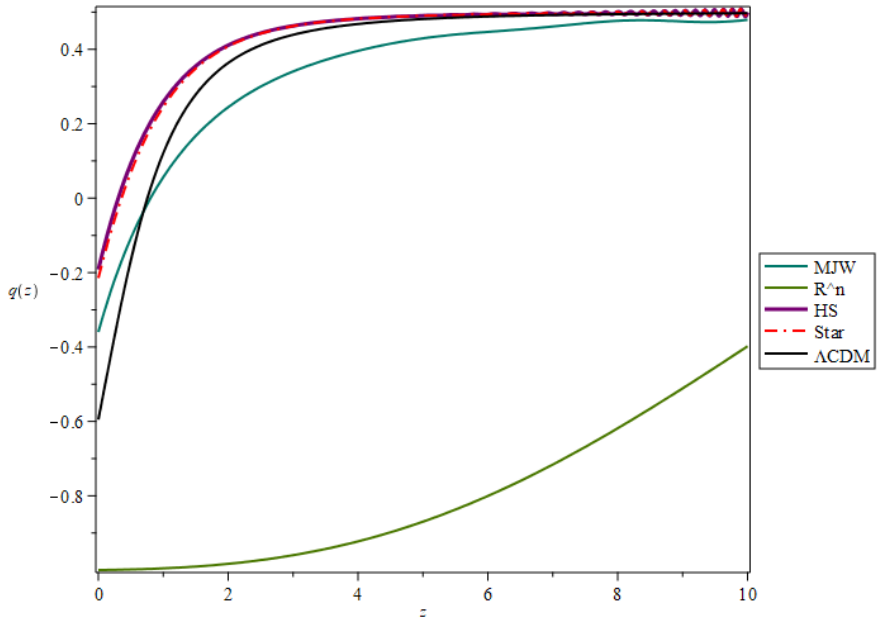

(b) The deceleration parameter corresponding to the four $f(R)$ models, is plotted along with the ΛCDM model. The HS and Starobinsky models asymptote to ΛCDM like behaviour, while the MJW model does not do as well.

Figure 5.1

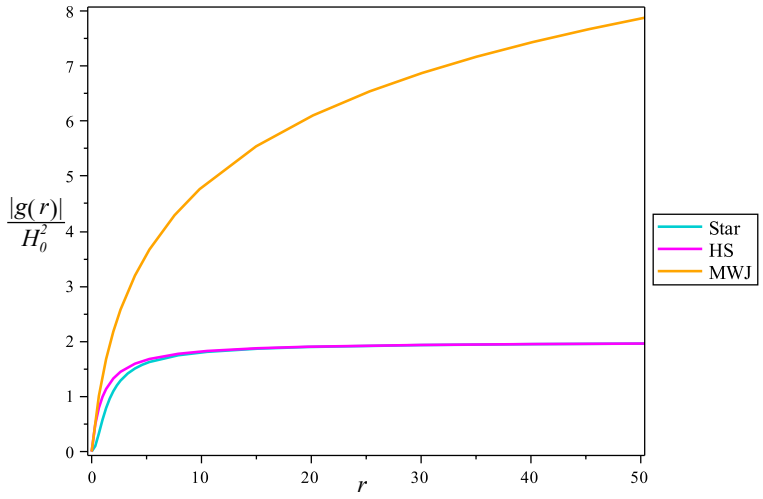

Figure 5.2: A plot of the correction (second term) of Equation (5.1), showing the change in the amplitude of the correction with curvature, for various values of key parameters which define the literature's most popular viable theories. STAR indicates a form of the Starobinsky model which is set by $(n, \alpha, \beta, \sigma) = (2, 1, 2, 1)$, HS indicates a form of the Hu-Sawicki model set by $(n, \alpha, \beta, \sigma) = (1, 2, 1, 1)$, MJW indicates a form of the MJW model [7] set by $(n, \alpha, \beta, \sigma) = (1, 2, \to \infty, 1)$. The correction goes to zero for low values of R/cH_0^2 and tends to a constant valued plateau as the curvature increases in relation to the local density.

The parameter n controls how quickly the correction transitions from zero to the constant plateau, and the amplitude of the correction is determined by the mass scale, or β in the GV model (5.1), or c in the HS model (5.6). Specifically regarding the HS model now, in the high curvature limit we obtain:

$$\lim_{cH_0^2/R \to 0} f^{HS}(R) \approx -\frac{c_1}{c_2} m^2, \tag{5.8}$$

and, following the idea in [6] of initially considering models which look like ΛCDM by setting the height of the plateau to 2Λ, we obtain a relation between the free parameters:

$$c = 6(1 - \Omega_m)\frac{c_2}{c_1}. \tag{5.9}$$

Thus the height of the plateau is controlled by the free parameters $\{c_1, c_2\}$ and the matter density today $\Omega_m \equiv \rho_{m,0}/3H_0^2$.

Even in the GV model, as can be seen from the curves in Figure 5.4, the exact behaviour of the correction we desire - that is a height approximately equal to 2Λ, and a transition which is rapid enough that initial conditions[1] may be set not too far back in the past (for efficiency of numeric integration, which we will get to later) - is fixed by a combination/relation of the model parameters.

[1]The choice of suitable initial conditions depend on the correction as I will discuss in Section 5.1.1.

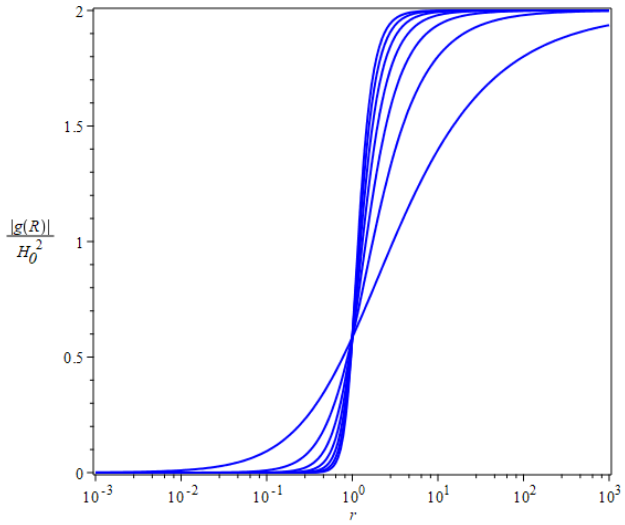

Figure 5.3: The correction of (5.1), plotted for integer values of n ranging from $n = 1$ to 7, while all of β, α and σ are fixed to be 1. The larger the value of n, the more rapid the transition from the GR limit ($g(R) = 0$) to the constant valued plateau, the effective cosmological constant limit ($g(R)$ =constant).

Simply by inspecting the curves it looks like it would be most suitable to choose β positive and small, with $n > 1$, but the final say will have to be made by a data analysis.

For convenience, the function (5.1) is rewritten in terms of the following

$$r = \frac{R}{H_0^2}, \tag{5.10}$$

$$h = \frac{H(z)}{H_0}, \tag{5.11}$$

giving dimensionless versions of the Ricci scalar and the Hubble rate, and,

$$R_s = R_* = \sigma H_0^2, \tag{5.12}$$

$$\tag{5.13}$$

such that (5.1) is now

$$f(R) = rH_0^2 - \beta\sigma H_0^2 \left\{ 1 - \left[1 + \left(\frac{r}{\sigma} \right)^n \right]^{-\frac{1}{\beta}} \right\}. \tag{5.14}$$

Similarly as in the HS model, both β and σ will affect the behaviour of the model, and here σ is related to the mass of the scalaron. In this broken power law class of prospective viable functions for $f(R)$, it would be expected there would be a preferred class, associated with one or a range of values of specific model parameters. The physical meaning of these parameters is a notion we must come back to, however, in our quest for a theory which can, without an explicit cosmological constant term,

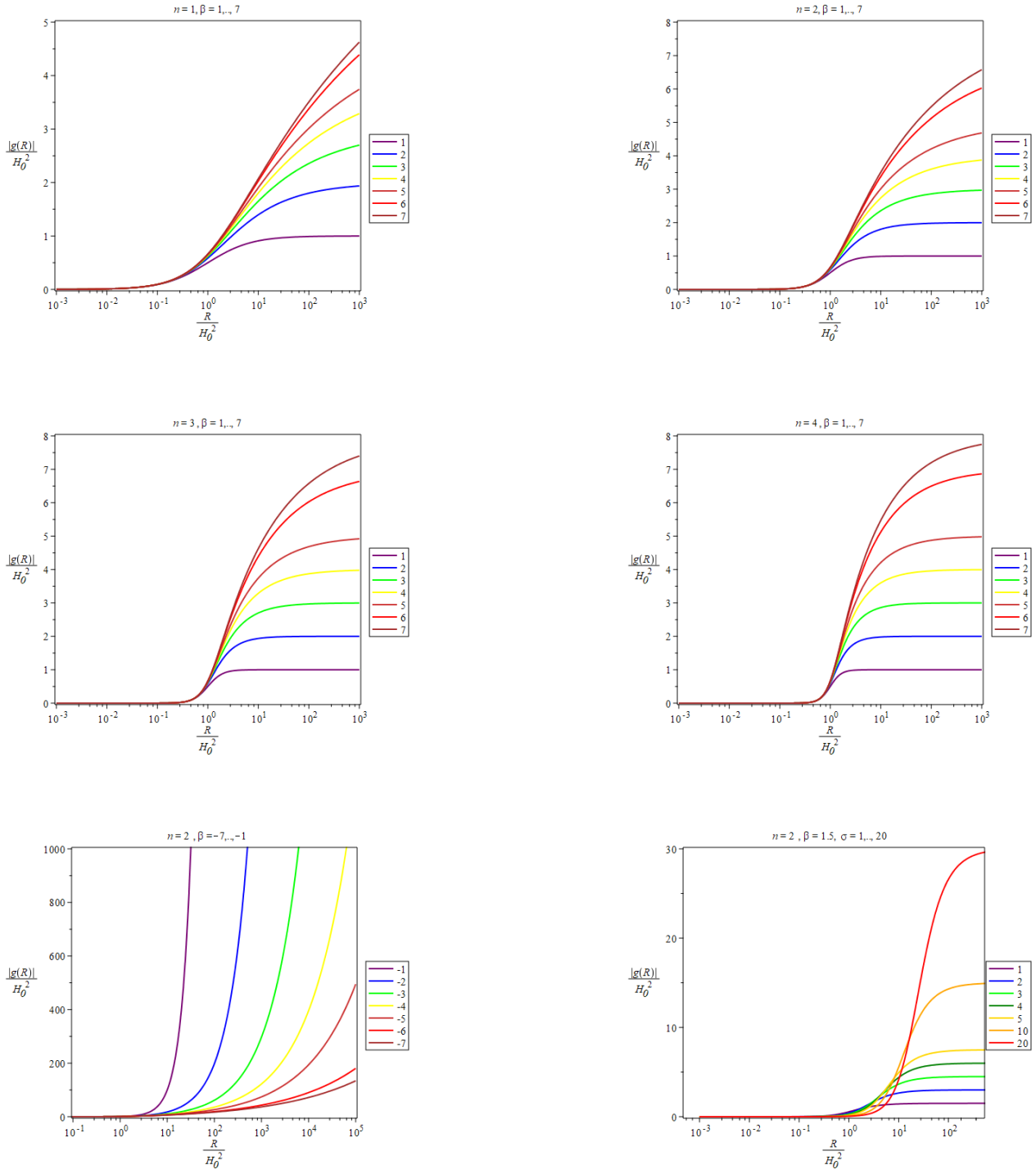

Figure 5.4: Examples of the correction term for the GV model at (5.1) are plotted in four panels for different values of the parameter β, n, to illustrate its change in behaviour. Larger values for β increases the height of the plateau, and also works to slow the transition from effective "GR" to effective"cosmological constant". Where $n = 1$, $\beta \geq 1$, the plateau is only reached at very high values for curvature, however larger values of n afford reaching the constant valued plateau for smaller values of the Ricci scalar, enabling the required behaviour. The first panel of the third row shows how negative values of β affect the behaviour of the correction; reaching its cosmological behaviour at only very high redshifts, while the second panel of the third row shows how changing σ affects both the amplitude and the slope of the correction.

produce the observed late time acceleration, we investigate what numeric values of these functions are preferred.

5.1 Dynamical Systems Approach to $f(R)$ gravity

One of the main problems in making quick progress in laying out the results of an $f(R)$ cosmology is related to the complexity of the field equations due to the inclusion of higher order curvature terms in the gravitational action. This makes the problem of deriving the dynamics of the cosmological quantities, and finding exact solutions extremely difficult if not impossible.

The dynamical systems approach to study cosmological models has become a popular method amongst authors in the field, starting with [124], [125], where cosmological models deriving from GR were investigated, extending to many papers using a DS method to study modified gravity models see for example [2], [126], [127], [128], where the dynamical systems approach was very clearly laid out for $f(R)$ and scalar tensor theories, and see [1], [3], [5], [129], [130], for example, where it was implemented to study the asymptotic solutions in $f(R)$ theories.

The technique requires expressing the differential equations of motion of a given physical quantity, for example the scale factor in cosmology, in terms of a set of newly defined variables, which convert the system into ordinary first order autonomous differential equations. This framework was developed to study the asymptotic solutions of a system, and the stability of the various solutions based on a study of eigenvalues.

The compact system was obtained by defining variables, normalised by a positive definite quantity, which constructed a finite phase space, pulling asymptotic fixed points into the normalised phase space. Using the same tactic we use a non compact dynamical system, defined by a set of *expansion normalised* variables, comprising terms of the modified Friedmann equation.

Results coming from such analyses showed that in the general class of $f(R)$ theories, at least those examinable within the specific framework - definition of variables, normalisations and independent variable - contain "radiation-like" repeller and "de Sitter-like" attractor asymptotic solutions. Certain $f(R)$ theories are even found to reveal an unstable, saddle "matter-like" fixed point solution [4]. These results testify to the fact that suitably chosen functions for $f(R)$ have the ability to produce universes which chronologically mimic that of our own.

For completion of the section we rewrite the modified cosmological equations below. From the general modified field equations as given by Equation (3.44) we obtain the following modified evolution equations for the scale factor

$$2\dot{H} + 3H^2 = -\frac{1}{f'}\left(p_m + 2H\dot{f'} + \frac{1}{2}(f - Rf') + \dot{R}^2 f''' + \ddot{R}f''\right), \tag{5.15}$$

$$H^2 = \frac{1}{3f'}\left(\rho_m + \frac{1}{2}(Rf' - f) - 3H\dot{f'}\right). \tag{5.16}$$

The dependence of f on the Ricci scalar is implicit, and primes, as usual, denote derivatives with respect to R.

We also make use of the continuity equation, where w is the equation of state;

$$\dot{\rho} = -3H(1+w)\rho. \tag{5.17}$$

We have chosen to perform the entirety of our analysis within this dynamical systems framework, as it lends to substantial simplification of the cosmological system, and the variables defined in terms of physical quantities allow direct tracking of the dynamics of these quantities. The dynamical variables are defined from the terms of the modified Friedmann equation (3.78) as

$$x = \frac{\dot{f}'}{f'}\frac{1}{hH_0}, \qquad v = \frac{1}{6}\frac{R}{h^2H_0^2}, \tag{5.18}$$

$$y = \frac{1}{6}\frac{f}{f'}\frac{1}{h^2H_0^2}, \qquad \Omega = \frac{1}{3}\frac{\rho_m}{f'}\frac{1}{h^2H_0^2}. \tag{5.19}$$

The variable v represents the Ricci scalar, Ω, not to be confused with the matter density fraction Ω_m represents the matter density field modified by the scalar field f', x and y are variables related only to the model function, $f(R)$, and $h \equiv H/H_0$, is the dimensionless Hubble parameter.

The Friedmann equation is a constraint on this system, and in terms of the above variables, is written:

$$1 = \Omega + v - x - y, \tag{5.20}$$

and the Raychaudhuri equation provides a dynamic equation for the dimensionless Hubble parameter;

$$\frac{dh}{dz} = \frac{h}{z+1}\left(2 - v\right). \tag{5.21}$$

Since we are interested in integrating the system with respect to redshift, the differential equations corresponding to the non-compact (see [1] for details on the compact version of these variables) dynamical system can be obtained by differentiating the variables at (5.18) and (5.19) with respect to redshift, z, and rewriting all cosmological quantities in terms of these variables:

$$\frac{dx}{dz} = \frac{1}{(z+1)}\left[(-1+3\,w)\,\Omega + x^2 + (1+v)\,x - 2v + 4y\right], \tag{5.22}$$

$$\frac{dy}{dz} = -\frac{1}{(z+1)}\left[vx\Gamma - xy + 4\,y - 2\,yv\right], \tag{5.23}$$

$$\frac{dv}{dz} = -\frac{v}{(z+1)}\left[(x\Gamma + 4 - 2\,v)\right], \tag{5.24}$$

$$\frac{d\Omega}{dz} = \frac{1}{(z+1)}\left[\Omega\ (-1+3\,w + x + 2\,v)\right], \tag{5.25}$$

where Γ is given by $\Gamma = f'/f''R$. The first order autonomous differential equations written at (5.21) - (5.25) represent a cosmological dynamical system for any $f(R)$ theory, which can be inverted for the Ricci scalar such that Γ can be expressed in terms of the dynamical system variables (5.18) - (5.19) [4]. The only model dependent term is Γ. For the HS model (5.4), Γ takes the following form, in terms of the model parameters

$$\Gamma_{HS} = -\frac{(c_2 r^n + 1)\left[r(c_1 r^n + 1)^2 - c_1 n c r^n\right]}{c_1 n c\left[r^n(n-1) - c_2 r^{2n}(n+1)\right]}, \tag{5.26}$$

and for the general viable model at (5.1), in terms of its model parameters

$$\Gamma_{GV} = \frac{\beta}{n\sigma}\frac{\left(-\left(1+\left(\frac{r}{\sigma}\right)^n\right)^{\frac{1+2\beta}{\beta}}\left(\frac{r}{\sigma}\right)^{-n} r + n\sigma\left(1+\left(\frac{r}{\sigma}\right)^n\right)\right)}{\left((-\beta-n)\left(\frac{r}{\sigma}\right)^n + \beta\,(n-1)\right)^{-1}}. \tag{5.27}$$

In both of Equations (5.26) and (5.27), $r = 6vh^2$, as given by the dynamical variables. To solve for the background of the $f(R)$ models we consider, the system (5.21)-(5.25) is integrated from initial conditions fixed to ΛCDM values at a time in the past, we will elaborate on the choice of initial conditions in the next section.

As a quick aside, we show the expression of the GDE, as described in Section (3.5), in terms of the DS variables we defined at (5.18) - (5.19). In terms of these variables, $w_{total} = (1 - 2v(z))/3$. Therefore, using the Friedmann constraint (5.20), the geodesic deviation equation for $f(R)$ models, for which the DS variables are suitable, may be written as

$$\frac{\mathrm{d}^2\eta}{\mathrm{d}z^2} + \frac{4 - v(z)}{(z+1)}\frac{\mathrm{d}\eta}{\mathrm{d}z} + \frac{2 - v(z)}{(z+1)^2}\eta = 0, \tag{5.28}$$

which is a result valid for all $f(R)$ theories.

5.1.1 Initial Conditions

It was previously found that requiring an $h_{f(R),0}$ and $q_{f(R),0}$ equal to those of ΛCDM as an initial condition for such early analyses came at the expense of large deviations from the ΛCDM model, and the observed Universe for much of the rest of the expansion history [82], [1]. In fact, in the HS model, a dark energy phase of expansion is preceded by a "radiation-like" expansion era, with no matter dominated period [1].

This can be understood by considering the correction $g(R)$ in an $f(R) = R + g(R)$ scenario, as discussed previously. Specifically, consider the correction corresponding to viable theories; for instance the HS model as shown in Figure 5.5, where, as curvature increases the function asymptotes to a constant value. Such models allow high curvatures to be re-associated with high density, as it is in GR + Λ.

Counterintuitively, if initial conditions are set too low, before the constant limit, the evolution of the Ricci scalar is not guaranteed to be monotonically increasing with redshift (see Figure 5.6).

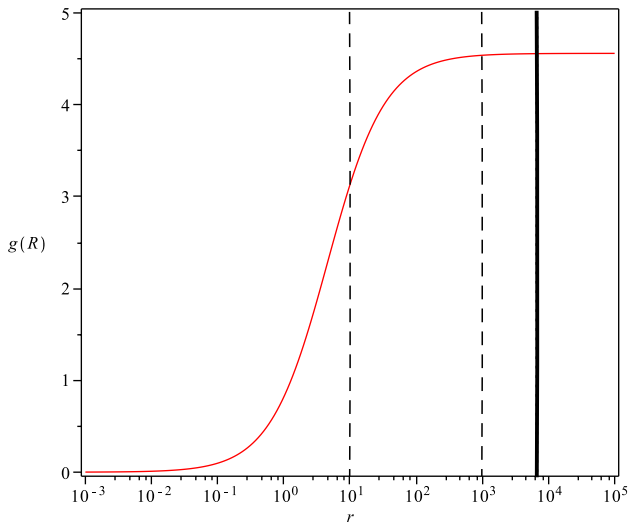

Figure 5.5: To show the effects of initial condition, I plot an example of the correction of the HS model with dimensionless curvature. The black lines represent the initial values of the Ricci scalar, $r_0 = r(z_0)$, when computed at three separate initial conditions, from left to right, $z = 0, 10, 20$, respectively. The value for the r_0 for $z_0 = 0$ is too small and does not enable the correct cosmological behaviour since the integration actually will force it away from the plateau. Increasing z_0 places the initial value of the correction already on the plateau, by increase the value of r_0.

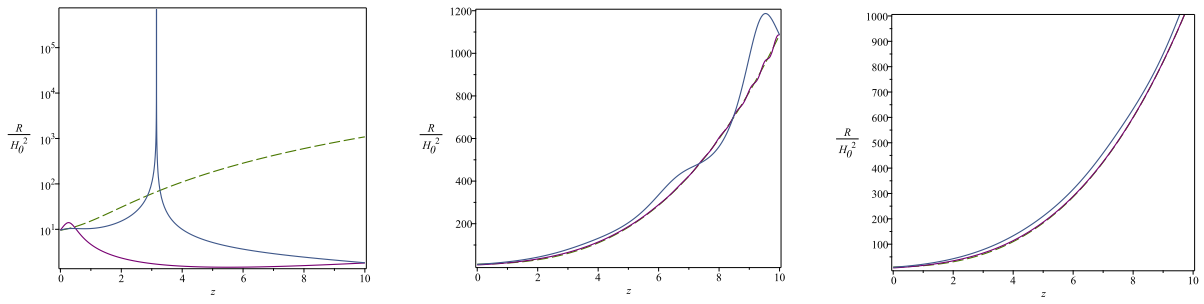

Figure 5.6: We show the effects of initial conditions on the dynamics of the cosmological models by considering the R/H_0^2. Each panel from left to right shows the evolution of Ricci scalar when initial conditions are chosen to equal the values of ΛCDM, at $z_0 = 0, 10, 20$ respectively, for the HS model(purple), GV model (blue) and the ΛCDM model (green dash). The first panel requires a logscale for clarity, and both the $f(R)$ models reveal non monotonic behaviour. As we increase the redshift at which we require the models to mimic ΛCDM, the behaviour improves, with oscillations, small in the HS model, and larger in the GV. This is evidence for the fact that the closer to infinity we place our initial conditions equal to the ΛCDM model, the better the behaviour we can expect. Models considered here were : $HS(n, c_1, c_2, \Omega_m) = (1, 1, 1, 0.27)$ and $\mathrm{GV}(n, \beta) = (2, 180)$.

By setting initial conditions at a high redshift, we can set the initial condition of the Ricci scalar, R at a sufficiently large value, to force the initial value for the correction to assume its "cosmological constant" limit. In this way we are able to ensure that the system contains the ΛCDM model as a high curvature limit. This in a sense is a way to state that we want this $f(R)$ theory to behave in the way the observed Universe appears to do, and let's see how close it can get, for how long to our favourite model.

An additional concern related to initial conditions is dealing with the occurrence of singularities at, at least for now, unpredictable finite redshifts. Depending on initial conditions, some classes of models exhibit numeric oscillations, others just have asymptotic discontinuities. It turns out, for the two models most closely studied, one a subclass of the other, that the higher the initial conditions, the farther away from the present epoch oscillations and/or singularities can occur. This points to the obvious advantage of selecting an initial condition to at least numerically represent infinity, for which the main drawback is compute time.

These notes, taken during numeric experimentation, hint toward the fact that initial conditions must be chosen carefully and the limitations of an initial condition which is not set to infinity must be acknowledged in the proceeding analysis of any $f(R)$ theory of gravity.

For our analysis we chose the initial redshift to be $z_0 = 20$, and we fixed the initial conditions for the integration of the dynamical system, in both the GV and HS models, to be equal to the ΛCDM models, therefore the initial conditions for the dynamical quantities are set as follows:

$$h_0 = h(z_0) = \left[\Omega_{m,0}(1+z)^3 + \Omega_\Lambda\right]^{1/2}, \tag{5.29}$$

$$q_0 = q(z_0) = \frac{1}{2h_0^2}\left[\Omega_{m,0}(1+z)^3 - 2\Omega_\Lambda\right], \tag{5.30}$$

$$r_0 = r(z_0) = 6(1-q_0)h_0^2, \tag{5.31}$$

$$v_0 = v(z_0) = 1 - q_0, \tag{5.32}$$

$$\Omega_0 = \Omega(z_0) = \frac{\Omega_{m,0}(1+z_0)^3}{h_0^2 f'(r_0)}, \tag{5.33}$$

$$y_0 = y(z_0) = \frac{f(r_0)}{6h_0^2 f'}, \tag{5.34}$$

$$x_0 = x(z_0) = \Omega_0 + v_0 - y_0 - 1. \tag{5.35}$$

The redshift z_0 was chosen as a compromise between efficiency and the model being satisfactorily similar to ΛCDM at and beyond $z_0 = 20$. Note that $\Omega_{m,0}$ and Ω_Λ are the ΛCDM values.

5.2 Numerical Method

A set of Python based scripts were developed to minimise the residuals between three sets of data , representing distinct redshift eras, and the theoretical predictions for the observables. However due

to the occurrence of singularities we found performing the MCMC was not as simple as randomly walking through the phase space.

In this situation, simply searching through the parameter space using a Markov Chain Monte Carlo method requires synthetic ways to avoid or reject points that have a singularity in the expansion history. This appears to compromise the statistics of the free parameters in that certain points in the parameter space which would otherwise not be important in the posterior distribution are "over-saturated" due to the algorithm finding too many singularities and not getting a chance to move away from these points in the usual random way. In the next section, I discuss how we dealt with this problem by generating a kind of numerical prior on the parameter space, using a grid and the singularity detection condition. Once this "prior" was obtained, we implemented a Metropolis Hastings (M-H) algorithm to generate the posterior distributions of the model parameters.

As a first exercise and foundation for the frame work of the rest of the analysis, we used Union2.1 SNIa data in an MCMC routine to find constraints on the parameters of the HS and GV models. We then supplemented these constraints, which were found to be weak, with an MCMC analysis using BAO data. Finally, we considered the perturbations of the $f(R)$ models, by constructing the matter density power spectrum from linear perturbation theory, and comparing it to data obtained with the Sloan Digital Sky Survey of clustering of luminous red galaxies. The last part of the analysis, that pertaining to comparing power spectra predictions to data, the χ^2 surface was obtained using a grid of the parameter space, instead of an MCMC parameter estimation.

Below, I describe the M-H algorithm:
In a loop, a point in the parameter space (of the model in question), which for reference we denote as X^f, is chosen[2]. The background expansion history is obtained as a function of redshift by integrating the system at (5.21)-(5.25). In the case of computing perturbations around this background, we pass this solution to the perturbation equations (7.3)-(7.6), and obtain the solutions for the (linear) density and curvature perturbations. The theoretical prediction for the observable is formed, and the $\chi^2(X^f)$ parameter is computed. This $\chi^2(X^f)$ is compared with that of the previous point, X^i; $\chi^2(X^i)$.

If $\chi^2(X^f) < \chi^2(X^i)$ then, we update the value of X^i to be equal to X^f - we *accept* this new point is better than the previous one- , and repeat the procedure, resulting in a convergence to the smallest value for χ^2 and thus pointing to the direction of the best fit model. The routine will only store one value of parameters at a time, and only has memory of the behaviour of the previous point.

If $\chi^2(X^f) > \chi^2(X^i)$ then we will accept X^f with a probability, $R = \frac{\chi^2_i}{\chi^2_f}$. When X^f is a better point, i.e. it has a smaller χ^2, then $R > 1$ and the chain will always accept X^f to be the new X^i. But when $R < 1$, while it is not immediately apparent that X^f is a better point than X^i, it may still be a step in the right direction. And in this case we accept the new point X^f with a probability equal to R; this acts as an assessment of how bad X^f actually is. Points for which the ratio R is closer to one

[2] X denotes a point in the parameter space, its superscript "f" or "i" indicates a new and old point respectively.

will be accepted with higher probability: A random number, w, is drawn from a uniform distribution in the range $[0, 1)$. If w is smaller than R, then the new point X^f is accepted, stored in the chain, and is saved as X^i. If it is larger then X^f is rejected, and the chain keeps X^i as its original value.

Accepting a point, results in taking a step in the parameter space, while rejecting a point means the chain stays where it is, and tries out a different X^f.

The new coordinates of the point, X^f are decided by imposing a gaussian distribution on each model parameter, centred about its current location at X^i,

$$X \sim \mathcal{N}(X^i, \sigma_X). \tag{5.36}$$

where the standard deviation σ_X regulates the sizes of the steps taken. X^f is computed from X^i by

$$X^f = X^i + \Delta, \tag{5.37}$$

where Δ is a random number drawn from the distribution (5.36). The σ_X's are different for each model and for each parameter and is chosen based on how quickly we want to move through the space, how finely resolved we would like the parameter optimisation to be, and the parameters themselves.

In this problem, where the parameters have no physical significance, and the only constraint is that the height of the plateau of the model is desired to be approximately Λ, which is a constraint on a *combination or ratio* of the parameters. The values for σ_X were fixed after a period of trial and inspection.

5.3 Data

5.3.1 Supernovae Ia

Supernovae are violent astrophysical phenomena that are so bright that they can outshine their host galaxies, making them observable at several hundreds of Mpc. There are two main classes of SNIa depending on whether their spectra reveal hydrogen lines or not. And these classes are further broken down into categories, based on their progenitor mechanism for explosion. The data we use is of the category type Ia. These supernova occur in binary star systems consisting of a white dwarf (WD) and a main sequence star, where the WD is accreting matter from its companion, which has exceeded its Roche lobe. This mass accretion eventually leads to the WD reaching the Chandresakher limit (1.4 solar masses), collapsing in on itself due to gravitational instability, and an explosion of material in the form of one of the brightest transient objects known to exist.

Studying the luminosity curves of close supernovae, it has been shown that there is an empirical relation between the peak and the width of the luminosity curve, allowing the SNIa to become a standard candle after an appropriate standardisation method is employed. Assuming distant supernova follow the same relation as close ones, SNIa have been taken to be very reliable distance

indicators [131]. Their reliability has been confirmed by testing the consistency of their distance predictions with those of the BAO [132]. Finding them in agreement is a powerful consistency check of the SNIa data. Such a check is important because SNIa are secondary distance indicators; we require a very large number of these objects of known distance to allow the calibration of standardisation of the luminosity curves. Several other factors affect the accuracy of results such as intergalactic absorption, change in metallicity with redshift of the progenitors, and even incorrect classification could be a source of error. However, once correctly calibrated, the set of SNIa are able to provide stringent constraints on the expansion of the universe.

Since the first studies revealed the accelerated expansion [133], [134], [22], the size and quality of SNIa data sets have increased considerably. The data set we consider is compiled by Suzuki *et al.* [135], consisting of samples drawn from 19 data sets (including old and newer data sets observed from HST, large surveys from SNLS [136], ESSENCE [137], SDSS [138] and SCP [139], totalling 830 SNe, of which 580 passed usability tests.

We used the combined data set, known as the *Union2.1* SNIa catalogue to place constraints on the parameter space of the HS and GV models.

Observable Quantities

The observable to be compared with the catalog of Union2.1 is the distance modulus of the object, defined by the difference of its apparent and absolute magnitudes. The apparent magnitude is given by

$$m^{th}(z;\Omega_m^0,z_0,x_i) = \bar{M}(M,H_0) + 5\log_{10}\left[D_L(z;\Omega_m^0,z_0,x_i)\right] \tag{5.38}$$

where x_i are the free parameters of the model, D_L is the luminosity distance (Mpc), and $\bar{M}$ is the magnitude zero point offset, which is given by

$$\bar{M} = M + 5\log 10\left[\frac{cH_0^{-1}}{Mpc}\right] + 25. \tag{5.39}$$

Here, M is the absolute magnitude and H_0 is the Hubble parameter evaluated today, and $D_L(z;\Omega_m^0,z_0,x_i)$ is obtained by:

$$D_L(z;\Omega_m^0,z_0,x_i) = (1+z)\int_0^z dz' \frac{H_0}{H(z';\Omega_m^0,z_0,x_i)}. \tag{5.40}$$

For a particular set of the free parameters $\{\Omega_m^0; xi\}$,the Hubble parameter $H(z;\Omega_m^0;z_0;x_i)$ is obtained by solving the differential equations which represent the cosmological model at (5.21) - (5.25). The theoretical value of the apparent magnitude (5.38), can be determined, and compared with the observational data from [135], which provides the observed apparent magnitudes m^{obs} of the SNIa with the corresponding redshifts z and errors $\sigma_{m(z)}$.

We can then compute the best fit model by studying the probability distribution

$$P(\bar{M},\Omega_m^0,w_0,z_0) = \mathcal{N}\mathrm{e}^{-\chi^2/2}, \tag{5.41}$$

where $\mathcal{N}$ is a normalisation factor and $\chi^2 \equiv \chi^2(\bar{M}, \Omega_m^0, z_0, x_i)$ as

$$\chi^2 = \Sigma_{i=1}^{N} \frac{(m^{obs}(z_i) - m^{th}(z_i; \bar{M}, \Omega_m^0, x_i))^2}{\sigma^2_{m^{obs}(z_i)}}. \tag{5.42}$$

Here $\sigma_{m^{obs}(z_i)}$ is the uncertainty associated with each distance modulus data point, and $N = 580$. Those free parameters $\{\Omega_m^0, \bar{z_0}, \bar{x_i}\}$ minimising the χ^2 expression (5.42) will correspond to what we call the *best fit*. On the other hand the $\bar{M}$ can be minimised and dropped out of the χ^2 expression, by expanding (5.42) in terms of $\bar{M}$ as

$$\chi^2(\Omega_m^0, z_0, x_i) = A - 2\bar{M}B + \bar{M}^2 C, \tag{5.43}$$

where

$$A(\Omega_m^0, z_0, x_i) = \sum_{i=1}^{n_{SNIa}} \frac{(m^{obs}(z_i) - m^{th}(z_i; \bar{M}, \Omega_m^0, x_i))|^2_{\bar{M}=0}}{\sum^2_{m^{obs}(z_i)}}, \tag{5.44}$$

$$B(\Omega_m^0, z_0, x_i) = \sum_{i=1}^{n_{SNIa}} \frac{(m^{obs}(z_i) - m^{th}(z_i; \bar{M}, \Omega_m^0, x_i))|_{\bar{M}=0}}{\sum^2_{m^{obs}(z_i)}}, \tag{5.45}$$

$$C = \sum_{i=1}^{n_{SNIa}} \frac{1}{\sigma^2_{m^{obs}(z_i)}}. \tag{5.46}$$

The minimum of equation (5.43) is located at $\bar{M} = B/C$, such that χ^2 turns out to be

$$\tilde{\chi}^2(\Omega_m^0, z_0, x_i) = A(\Omega_m^0, z_0, x_i) - \frac{B(\Omega_m^0, z_0, x_i)^2}{C}. \tag{5.47}$$

Thus, minimising $\tilde{\chi}^2(\Omega_m^0, z_0, x_i)$, independently of $\bar{M}$ is enough to find the best fit since $\chi^2_{\rm min} = \tilde{\chi}^2_{\rm min}$, which is how we proceed. Figure 5.7 shows examples of the theoretical curves for the HS and GV models against the SNIa Union2.1 data. Both models are reasonable representations of the data, lying within the data errors.

5.3.2 Baryon Acoustic Oscillations

Baryonic Acoustic Oscillations are an essential advancement for data collection in cosmology and represent a unique method to measure the expansion of the universe through distance measurements along and perpendicular to the line of sight.

It is widely accepted that in the beginning, the matter content (as far as we know) consisted of Cold Dark Matter and neutrinos, interacting only weakly, and radiation and ionised baryons - which are coupled electromagnetically. An initially over-dense region of this primordial plasma, experiencing gravitational instability due to its size, will also experience an excess of radiation pressure, leading to a back and forth between the two dominating forces. Thus, any fluctuation in the density of the universe at this time would experience acoustic oscillations driven by the forward and backward forces

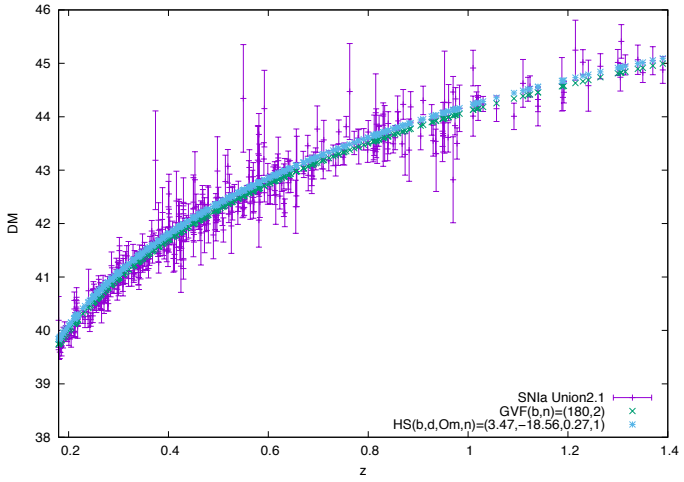

Figure 5.7: Here we present a plot of the SNIa Union2.1 data versus the theoretical predictions from HS and GV models for reference, for example sets of model parameters.

of radiation pressure and gravity, and these oscillations interfere and propagate throughout the fluid as space expands [140] [132].

The distance these acoustic waves can travel before the matter and radiation fluids decouple becomes a characteristic scale in the evolution of the universe, corresponding to the sound horizon at that time. This scale is detectable in the anisotropies of the CMB e.g. [141], as well as in the large scale clustering of galactic structures, e.g. [142], [143]. The imprint of these oscillations will appear as a peak in the matter correlation function at the scale of the sound horizon. The CMB can provide the scale of the sound horizon, and this scale can be mapped to an angular diameter distance, and the Hubble parameter. One of the main advantages of the BAO as an observable is the fact that linear physics is sufficient to study the phenomena, and therefore is not expected to suffer from errors accumulated due to the neglecting of nonlinear effects [144]. Moreover, the imprint of BAO in the large scale structure will not appear in the dark matter.

BAO are known as standard rulers, as objects of known comoving size, and the angular diameter distance is computed using Equation (2.85). The data used, shown in Table 5.1, is the following ratio

$$\frac{r_s(z_{CMB})}{D_V(z)}, \tag{5.48}$$

of the comoving sound horizon, given by

$$r_s(z_{CMB}) = \frac{1}{H_0}\int_{\infty}^{z_{CMB}} \frac{c_s(z)}{h(z)} dz. \tag{5.49}$$

Survey	z	$\frac{r_s(z_{CMB})}{D_V(z)}$	Ref
6dF	0.106	0.3360	[145]
SDSS DR7	0.2	0.1905	[146]
SDSS DR7	0.35	0.1097	[146], [147]
WiggleZ	0.44	0.0916	[141]
WiggleZ	0.6	0.0726	[141]
WiggleZ	0.73	0.0592	[141]

Table 5.1: We use data from several different surveys.

and the dilation scale, given by

$$D_V(z_{BAO}) = \left[\left(\int_0^{z_{BAO}} \frac{dz}{H(z)}\right)^2 \frac{z_{BAO}}{H(z_{BAO})}\right]^{1/3}. \tag{5.50}$$

The c_s in (5.49) is the speed of sound in the photon-baryon plasma,

$$c_s(z) = \frac{1}{\sqrt{3(1+\frac{\bar{R}_b}{z+1})}}, \text{ where } \bar{R}_b = \frac{3}{4}\frac{\Omega_b \tilde{h}^2}{\Omega_\gamma \tilde{h}^2}, \tag{5.51}$$

where $\tilde{h}$ is the uncertainty in the Hubble parameter, $H_0 = 100\tilde{h}$, and we have used $\tilde{h} = 0.6711$ and $z_{CMB} = 1021.44$.

The χ^2 parameter is defined as follows

$$\chi^2_{BAO} = (\mathbf{d}_z^{obs} - \mathbf{d}_z^{th})^T \mathbf{C_{BAO}}^{-1} (\mathbf{d}_z^{obs} - \mathbf{d}_z^{th}), \tag{5.52}$$

where the inverse covariance matrix used corresponding to the correlated uncertainties in the data points is [148] , [141],

$$\mathbf{C^{-1}} = \begin{bmatrix} 4444.0 & 0. & 0. & 0. & 0. & 0. \\ 0. & 30318. & -17312. & 0.0 & 0. & 0. \\ 0. & -17312. & 87046. & 0. & 0. & 0. \\ 0. & 0. & 0. & 23857. & -22747. & 10586.0 \\ 0. & 0. & 0. & -22747. & 128729. & -59907. \\ 0. & 0. & 0. & 10586. & -59907. & 125536. \end{bmatrix}. \tag{5.53}$$

5.3.3 Matter Power Spectrum, $P(k)$

One of the most powerful probes of our physical universe is the spatial distribution of luminous bodies across the sky. It has been the intuition of physicists for many decades that the distribution of galaxies on sufficiently large scales is uniform. It is also expected that when smoothed over large scales the galaxy density distribution should have a simple relationship to the matter density of the

primordial universe. If this is true, then the clustering of galaxies will be directly related to the clustering of the underlying matter density. This argument suggests that the clustering of galaxies in the universe gives information about the initial conditions of the universe as well as its subsequent evolution [149].

Large scale clustering of any mass tracer, typically characterised by its power spectrum, has three features which are of particular interest to modern cosmologists: (i) Oscillations in the power spectrum caused by acoustic waves in the photon baryon plasma before hydrogen recombination at $z \sim 1000$, (ii) The largest scales of the power spectrum can be used to constrain the primordial potential of the universe (testing inflation), (iii) The power spectrum turns over at $k \sim 0.01h\mathrm{Mpc}^{-1}$. The power spectrum turns over from a slope $\propto k$ (the initial fluctuations are scale invariant) to k^{-3}, caused by modes that entered the horizon during radiation dominated era, and were suppressed. The position of this turn over is determined by the size of the horizon at matter-radiation equality, and corresponds to a physical scale determined by the matter and radiation densities [149].

In order to use the theoretical predictions of cosmological perturbation theory to analyse the snapshot data we currently have of the universe, we need to exploit the statistical nature of the perturbations. While Equations (4.53) - (4.54) will give the evolution of a single wave mode of perturbations, we need to make use of Fourier analysis to study the evolution of a superposition of growing and decaying wave modes in an expanding universe. The standard approach to this is assuming that the density fluctuation $\Delta(\vec{x})$ can be interpreted as a Gaussian random field.

If Δ_k is the spatial Fourier transform of $\Delta(\vec{x})$;

$$\tilde{\Delta}(\vec{k}) = \frac{1}{(2\pi)^3} \int \mathrm{d}^3\vec{x} e^{-i\vec{k}\cdot\vec{x}} \Delta(\vec{x}), \tag{5.54}$$

we can define the power spectrum of these perturbations as

$$\langle \Delta(\vec{x}_1)\Delta(\vec{x}_2)\rangle = P(k_1)\Delta^D(\vec{k}_1 + \vec{k}_2). \tag{5.55}$$

The power spectrum gives a measure of the average squared amplitude of the k^{th} mode of any perturbation in Fourier space.

The real space version of the power spectrum is the 2-point correlation function; a measure of the correlation between the densities at two points separated by a *distance* $\vec{r}$:

$$\xi(\vec{r}, t) = \langle \Delta(\vec{x}, t)\Delta(\vec{x} + \vec{r}, t)\rangle = \frac{1}{(2\pi)^3} \int \mathrm{d}^3 k P_m(k, t) e^{i\vec{k}\cdot\vec{x}}, \tag{5.56}$$

integrated over Fourier space.

The power spectrum of fluctuations is an invaluable tool spanning all of cosmology. Its shape gives insight into how the matter fluid we consider clusters as a function of scale, in Fourier space, how its clustering depends on redshift, giving information about its temporal evolution as well as its particle nature. We are able to extract information regarding propagation speed features which were imprinted onto the spectrum via the baryonic acoustic oscillations occurring at a time before recombination.

Investigations into redshift-space distortions, a popular line of data-modelling research, is driven by studying the shape of the power spectrum on small scales, and the effect small scale velocities have on it. The power spectrum of matter densities is usually measured using large galaxy surveys to obtain the amplitude of fluctuations on a range of scales.

The matter power spectrum is defined as:

$$P_m(k,t) = \frac{2\pi^2}{k^3} \left\langle \Delta_m(k,t)\Delta_m^*(k,t) \right\rangle , \tag{5.57}$$

The shape of the matter power spectrum is fixed by the cosmological model under investigation, and several inflationary scenarios (see for example [150]) result in a power-law shape

$$P(k) = Ak^n. \tag{5.58}$$

Features of the primordial power spectrum are expected to be imprinted onto the cosmic structure observable today. However, it is also expected that, via a number of physical processes occurring through out the expansion of space-time arising from the interplay of pressure and gravity, these features will undergo a sort of "processing", such that the growth of perturbations of certain scales will be suppressed relative to others. The manner of coupling between baryonic matter and radiation and the type of dark matter are both factors which will contribute to suppressing of the growth of perturbations having scales smaller than, for example, the distance an acoustic wave can travel in the time it would take for an over dense region to collapse.

These effects are encapsulated in the so called transfer function, $T(k)$, which relates the power spectrum of large scale density contrasts to the initial fluctuation spectrum, supposedly prior to inflation. The transfer function is related to the correlation function as follows:

$$\left\langle \Delta_m(\vec{k}_1)\Delta_m(\vec{k}_2) \right\rangle = T(k_1)\Delta(\vec{k}_1 + \vec{k}_2), \tag{5.59}$$

where $T(\vec{k}) = T(k)$ is a result of the isotropy in the distribution of perturbations. The transfer function, which is essentially proportional to $\Delta^2(k)$, gives a measure of the density fluctuations at a scale of k^{-1}.

We use SDSS DR7 LRG matter power spectrum data in the range $k = [0.018, 0.29]$ [151], [152], which consists of spectroscopic redshifts of 400 000 galaxies, spread over 3275 deg^2 of the sky, in the redshift range $0.45 < \mathrm{z} < 0.65$.

The LRG matter power spectrum represents an observable which is derived by considering the evolution of scalar density perturbations with the expansion of the universe. It is a good supplement to the analysis as it gives a method to test the theory beyond its construction to mimic the background of the ΛCDM model. We can gain insight into how scalar perturbations evolve in this theory and how this evolution, considering its dependence on scale, k, compares to real data.

5.4 Sudden Cosmological Singularities

$f(R)$ gravity has been studied in detail both with regards to UV corrections of GR, in black holes and the early universe, as well as producing the late time acceleration of the Universe. Modified theories have been found to contain several types of singularities, some due to violation of conditions, which can be resolved fairly easily by careful selection of the form of the theory, and others which seem to exist as a consequence of the modification to GR, and are much more complicated to avoid. Moreover, the presence of singularities have very bad consequences, may prevent the formation of compact relativistic astrophysical objects [153].

5.4.1 Hu-Sawicki Model

We have followed previous works, eg. [8], which use this approach, to assist in an analysis of the HS model in 2015 [111], where we calculated the potential for the HS model in this class, and observed its behaviour with scalar field, ϕ, to understand how to proceed with a numeric analysis. The HS model may be written as:

$$f_{HS}(r) = rH_0^2 - \frac{H_0^2 c_1 r}{\frac{1}{6}\frac{rc_1}{1-\Omega_m} + 1}, \tag{5.60}$$

where we rewrite the Ricci scalar in a dimensionless form by introducing the Hubble constant; $r = R/H_0^2$, and we rewrite the scalar mass in terms of the matter density fraction as in the ΛCDM model; For this form, the scalar field is expressed as

$$\phi_{HS} = \frac{6dn(\Omega_m - 1)\left(-\frac{1}{6}\frac{c_1 r}{(\Omega_m - 1)c_2}\right)^n}{r\left[c_2\left(-\frac{1}{6}\frac{c_1 r}{c_2(\Omega_m - 1)}\right)^n + 1\right]^2}. \tag{5.61}$$

For $n = 1$, with

$$\phi_{HS,n=1} = -\frac{c_1}{\left(1 - \frac{1}{6}\frac{c_1 r}{\Omega_m - 1}\right)^2}, \tag{5.62}$$

it is clear to see that as $r \to \infty$, $\phi \to 0$, demonstrating that the Ricci scalar actually diverges at a finite value of the scalar field; $\phi_{sing} = 0$. Solve for the dimensionless Ricci scalar:

$$r(\phi) = \pm 6\,\frac{\left(\phi + \sqrt{-c_1\phi}\right)(-1 + \Omega m)}{c_1\phi}, \tag{5.63}$$

giving the following expressions for the potential $V(\phi)$

$$V(r, \phi) = -\frac{(-1 + \Omega_m)\left(\phi \pm 2\sqrt{-b\phi} - 2\right)\left(2\sqrt{-b\phi} + \phi\right)}{b}. \tag{5.64}$$

This potential is as depicted in Figure 5.8, for fixed values of n and Ω_m, and varying values of c_1.

The effects of matter, following [8], are included by considering an effective potential, where the force term related to the presence of matter is modelled by a linear potential proportional to the present curvature scalar, R_0:

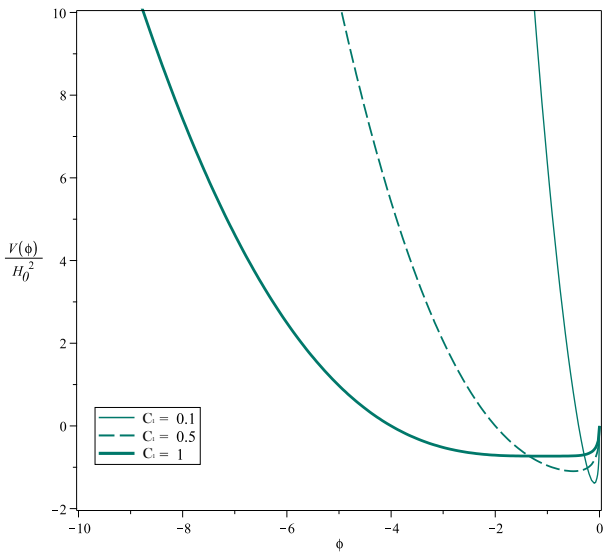

Figure 5.8: Plotting the potential at (5.64) for $n = 1, \Omega_m = 0.27$ and $b = (0.1, 0.5, 1.0)$.

$$\Box\phi = V'_{eff}(\phi), \tag{5.65}$$

$$V'_{eff}(\phi) = V'(\phi) + R_0(\phi_\star - \phi), \tag{5.66}$$

where $V'(\phi)$ is given by Equation (3.71), and $\phi_\star$ is the de Sitter minimum of the vacuum potential, $V(\phi)$.

Examining the effective potential for the scalar field ϕ gives useful information about the viability of the models we consider, and provide a rough idea of ranges of the free parameters which can be excluded from the statistical parameter optimisation analysis. In general it is not possible to express the potential, $V(\phi, R)$ given by solution to Equation (3.73) analytically, however, below for simple enough cases, usually where some free parameters are set to unity, we are able to show an analytic expression for the scalar fields and potentials for both of the HS and GV model.

Specifically for the HS model we found that decreasing c_1 resulted in safer potential minima, however after a point, smaller values for c_1 result in the minimum moving closer to the singularity again. Including matter appears to increase the depth of the potential.

From this short study, I had concluded that moving forward I could suggest the following weak but surely useful prior on c_1: $c_1 \in (0, 1]$, as an attempt to study what appear to be the safest models in the HS class, at least for $n = 1$, to avoid the sigularity at $\phi_{sing} = 0$.

However upon doing a statistical analysis, we found that $c_1 > 1$ such that $\phi = -\frac{b}{+\sqrt{b^2-b}}$, result in significantly smaller values of the χ^2 parameter. The computations which lead to this result will be detailed in the following sections, but for example,

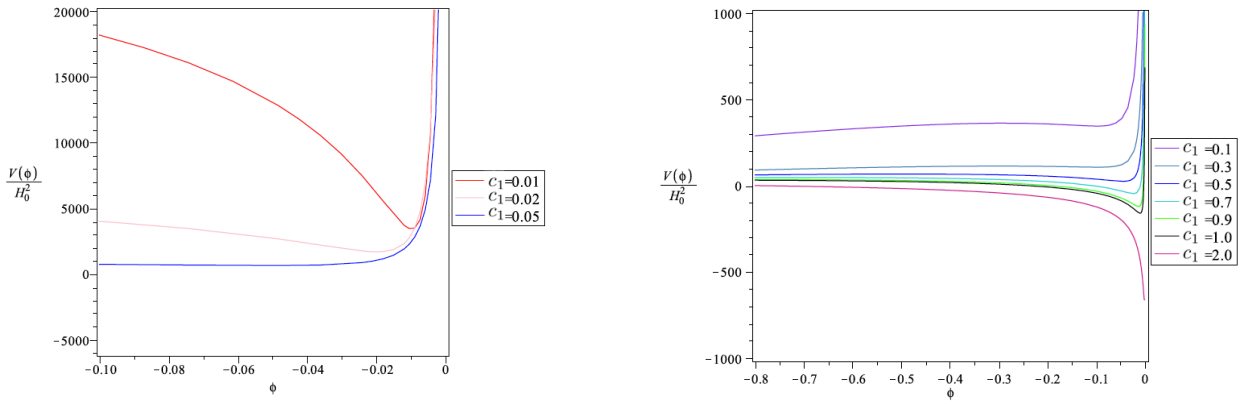

Figure 5.9: The effects of matter, approximated by including a linear addition to the potential, are plotted here. These panels illustrate how the potential depends on the value of c_1. For several values of c_1, we plot the potential for the HS model. In the left panel it can be seen that as c_1 increases, the minimum of the potential shifts to the left, *away* from the singularity. However, as can be seen in the panel on the right, after a certain point $c_1 \sim 0.5$, increasing c_1 works to move the minimum back towards the singularity.

$$\chi^2 \approx 602 \text{ for } c_1 = 0.8, \Omega_m = 0.27 \tag{5.67}$$

$$\chi^2 \approx 542 \text{ for } c_1 = 80., \Omega_m = 0.27 \tag{5.68}$$

This renders confining a search of the parameter space to the range $c_1 \in (0, 1]$ to be quite unfruitful, since the best cosmologies will be produced outside this range. The range of reduced χ^2 values for $c_1 \in [0.1, 1.0]$ is $[1039.6, 593.8]$, with the previously found minimum in [111] being ≈ 542.3. Therefore the constraint coming from the rough analysis of the scalar potential is neglected, leaving the parameter space open to search, although models outside this region will necessarily contain unprotected singularities, which can only be avoided by careful choice of initial conditions[3] .

In [111], an unrestricted survey of the parameter space for the HS model revealed that SNIa data place weak constraints on the HS model, however an interesting result was obtained on analysing the clustering of singular models in the phase space. This clustering was observed in data alternative to an MCMC chain, where we stored points which were classified as singular during the chain[4].

In Figures 5.11 and 5.12 we show these regions of the HS parameter space for $n = 2, 3$, to illustrate that there exist regions of the parameter space which are completely singular.

[3] As discussed in Section 5.1.1.

[4] The details of the analysis, initial conditions and models analysed will be discussed in Section 6.1 pertaining to [111].

5.4.2 GV Model

The scalar field for the GV model, in general, is given by:

$$\phi = -\frac{\sigma\, n}{r}\left(1+\left(\frac{r}{\sigma}\right)^{n}\right)^{\frac{-1-\beta}{\beta}}\left(\frac{r}{\sigma}\right)^{n}. \tag{5.69}$$

With its model parameters set to $(\beta,\sigma,n)_q = (1,1,1)$, we have

$$\phi_q = -\left(1+r\right)^{-2}, \tag{5.70}$$

such that the minimum of the potential occurs at $\phi = -1$. Solving (5.70) for the dimensionless Ricci scalar, we obtain:

$$r = \left(-\frac{\sqrt{-\phi}+1}{\sqrt{-\phi}}, -\frac{\sqrt{-\phi}-1}{\sqrt{-\phi}}\right). \tag{5.71}$$

Solving (3.73) and substituting in for the Ricci scalar, we obtain the following expressions for the potential for the domains of positive and negative Ricci scalar respectively.

$$V_{q+}\left(r\right) = 1/6\,\left(\left(-\phi\right)^{3/2} - 4\,\phi + 6\,\sqrt{-\phi} + 4\right)\sqrt{-\phi}, \tag{5.72}$$

$$V_{q-}\left(r\right) = 1/6\,\left(\left(-\phi\right)^{3/2} + 4\,\phi + 6\,\sqrt{-\phi} - 4\right)\sqrt{-\phi}. \tag{5.73}$$

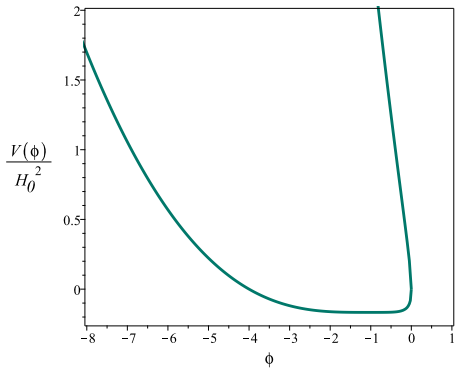

Figure 5.10: GV Potential, for parameter values $(\beta,\sigma,n) = (1,1,1)$, for $R < 0$ and $R > 0$. The potential minimum is at $\phi = -1$. We are only interested in $R > 0$.

5.4.3 Singular regions of the HS parameter space

To be clear, the singularities occur in the first derivative of the Hubble parameter, $h(z)$, and is reflected in the deceleration parameter, $q(z)$.

Given that singularities are expected within the parameter space, it is useful to determine the regions of parameter-space containing regular solutions, so that appropriate "priors" on the free parameters may be considered. To isolate a singular[5] set of parameters, once the background system

[5]To clarify, a "singular" parameter set would be one that results in a universe which contains a sudden curvature singularity as described in Section 3.2.4 in its expansion history.

(5.21) - (5.25) has been solved, the solution is scanned for any unexpected behaviour. In particular, if the Hubble parameter becomes too small, such that its reciprocal is numerically undefined, or the deceleration parameter switches sign, or grows suddenly too large, the set of parameters is recognised to be singular, and the theory not viable. To avoid the risk of generating unreliable posterior distributions, we generated a grid of the parameter space determining the regions in the space which are known to be completely regular, within a chosen redshift range[6] .

Searching the parameter space of the HS model revealed it was dotted with sets of parameters inevitably leading to singular behaviour. Interestingly, the singular models appeared to cluster into regions of the space in such a way that showed those regions containing *no viable models* appear to be bounded by neat, apparently "continuous" curves.

The case $n = 1$ is particularly simple as the appearance of singularities solely depends upon two free parameters $\{c_1; \Omega_m\}$, and the scalar potential is obtained exactly in (5.62). Consequently the region of parameter-space leading to regular solutions can easily be found [154]. As pointed out above, we need to stay initially on the lower branch of the scalar potential in order to avoid the singularity, which is located at $\phi = 0$ where $V(\phi = 0) = \frac{bc}{d} H_0^2$. This leads to the condition:

$$V_{\phi=0} < \frac{bc}{d} H_0^2 \ . \tag{5.74}$$

Then, by imposing the initial conditions to match the model with ΛCDM at a particular redshift and using the expression (5.64), we get the following constraint on c_1

$$c_1 < \frac{3(\Omega_m - 1)H_0^2}{R_{0,\Lambda\mathrm{CDM}}} = \frac{\Omega_m - 1}{\left[z_0\left(z_0^2 + 3z_0 + 3\right) - 3\right]\Omega_m + 4} \ , \tag{5.75}$$

where z_0 is the initial redshift. For $n > 1$, we resort to the numerical technique described above. We present two dimensional representations of this grid, showing the $c_1 - c_2$ plane, for fixed values of Ω_m in Figures 5.11 and 5.12 for $n = 2$ and $n = 3$, respectively. According to this, for higher values of n the singular regions in the phase space are more complicated. While the filled regions in the plot represent regions which contain the singularities in this range of parameter space, there may exist regular parameter sets for different values of Ω_m within those regions as well. Similarly, the white space gives singularity free regions that also depend on the value of Ω_m. This analysis ensures a smooth cosmological evolution for $z \leq 0$ but is unable to ensure a future cosmological evolution in absence of singularities. However, note that many other dark energy models allowed by the observations contain future cosmological singularities [14].

In [111] we presented Figures 5.11 and 5.12 to show the singular regions in the parameter space of the HS model for $n = 2, 3$.

[6]Due to the phenomenology of the background of models like the ones we consider, it is common and not unscientific to select a redshift range which is smaller than infinity, since the model becomes indistinguishable from ΛCDM at high redshifts. The statement to be made is then that these models represent no singular behaviour within the redshift range $z = [0, 20]$.

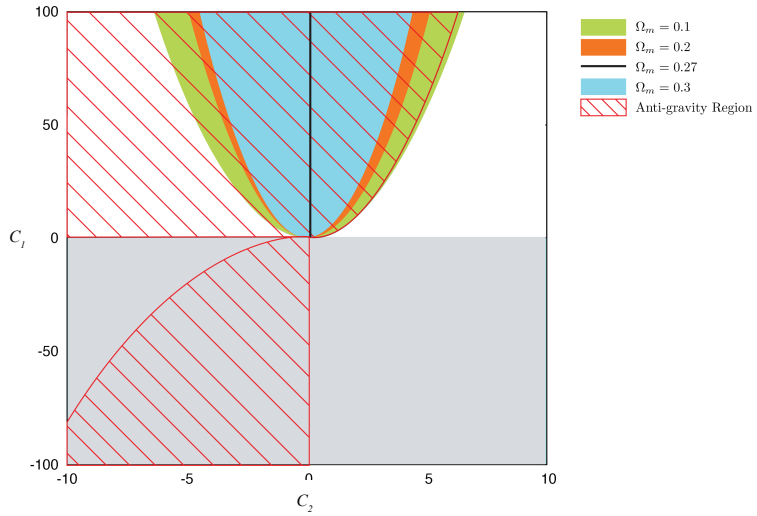

Figure 5.11: Regions in the $c_1 - c_2$ plane, for $n = 2$ containing singular sets of parameters for different values of Ω_m, and regions with different signs of r_0. We also show regions of the phase space in this model for which the gravitational force is repulsive, or $R_0 < 0$ (red hatch), in accordance with Section 3.6, for the sake of interest. Any zone clear of the hatch pattern represents $R_0 > 0$. The grey region, $c_2 < 0$, represent entirely and always singular regions (regardless of the value of Ω_m); for $n = 2$ this corresponds to $c_2 < 0$. Other singular regions in the $c_1 - c_2$ plane depend upon the value of Ω_m, since this is a 2D slice of the 3D parameter space. They have been represented in solid colours (see legends in the panels). Note that this analysis focuses on the past cosmological evolution $z \geq 0$, thus this does not ensure a whole regular condition for $n > 1$. For the case $n = 2$, the closer Ω_m gets to its best-fit value $\Omega_m m = 0.27$, the narrower the aforementioned upper singular quasi-parabolic region becomes. When $\Omega_m = 0.27$, the phase space is completely regular for all values of $c_2 > 0$ and all values of $c_1 \neq 0$. The best fit values found in Table 6.1 lie in the blank regions for both $n = 2, 3$.

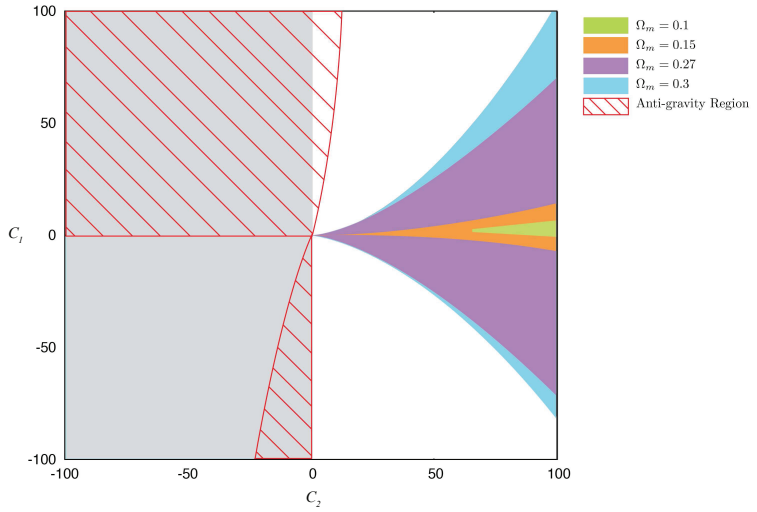

Figure 5.12: For the case $n = 3$, there appears not to be any improvement as we get closer to the Ω_m best-fit value but the singular region located at $c_1 > 0$ grows with Ω_m. and for $n = 3$ this corresponds to $c_1 < 0$.

Chapter 6

Determining Viable $f(R)$ Models from Background Data

In this chapter I will present the constraints obtained from background data and observables on the HS and GV models discussed in the previous chapter. Note that these models are constructed to produce a background behaviour which is identical (as far as possible) to the ΛCDM model, without an additional energy field. For this reason, we already know that background data will likely provide weak constraints, if any, on the parameters of the models we look at. However, this was an important exercise to develop the framework of further analysis, especially in terms of the dynamical systems approach described in Section 5.1. We also obtained a set of very interesting plots for the HS model showing that within the parameter space there are neatly bound regions containing only singular models.

For the more general power law model given by (5.1), and short hand dubbed GV, we obtain constraints on the exponent of the Ricci scalar, using BAO and SNIa data, significantly reducing the parameter space of the models.

6.1 SNIa Constraints on HS Model parameter space

In this section we present the results of a Markov Chain Monte Carlo method performed to fit for the free parameters of the Hu-Sawicki model subject to the theoretical and numerical constraints presented above. The results obtained in the previous section aid in the avoidance of highly dense singular regions, as well as the interpretation of the MCMC chains. The regions for which the cosmological evolution does not guarantee expansion are excluded *a priori* in the calculations here, although once the maximum likelihood is obtained, we are able to determine whether the corresponding points in the parameter-phase space lie in the allowed, i.e., singularity-free and late-time expansion, regions.

The MCMC analysis for the Hu-Sawicki model proceeded by fixing integer values of $n = 1, 2, 3$, sampling for the posterior distributions of the remaining free parameters c_1, c_2 and Ω_m.

For each of $n = 1, 2, 3$, several chains were generated, comprising 250 000 sampled points in the respective parameter space. The obvious prior on Ω_m, $\Omega_m \in (0, 1]$ was imposed. For the sake of simplicity, each parameter was sampled from a normal distribution centered at zero, with standard deviations set, by trial and inspection to $\sigma_{c_1} = 5$, $\sigma_{c_2} = 5$ and $\sigma_{\Omega_m} = 0.03$ [111]. Having initially little information about the scales of c_1 and c_2, the sampling distribution was chosen so as to scan the available phase space as efficiently as possibly. While the relatively large values of σ_{c_1} and σ_{c_2} were settled upon ultimately to optimise computing time, it is important to note that more conservative values for these quantities were tested and the results - while significantly scaled down - were not different to those presented here.

Each chain was initialised at unique points in the phase space, and for each Markov Chain, convergence of the matter density fraction of the universe today, i.e., Ω_m occurred fairly quickly. In fact, Ω_m is very well described by a Gaussian posterior distribution for all three values of n, with an error comparable to that of a similar analysis done for ΛCDM. Table 6.1 summarises the results for each value of n. We include the best fit values for each parameter corresponding to each value of the exponent n, as well as the mean and 1-σ standard deviation of their sample distribution. To compare the result to the ΛCDM model we compute the reduced χ^2 parameter, defined as

$$\chi^2_{red} = \frac{\chi^2}{(N-p)}, \tag{6.1}$$

where N is the number of data points included in the analysis and p is the number of fitted parameters, and the difference $(N-p)$ is known as the degrees of freedom of the system. Normalising χ^2 to obtain χ^2_{red} gives a method of testing the goodness of the fit. The closer the value is to one, the better the fit is thought to be.

We find for all values of the exponent n that the best fit values do in fact lie in the $R > 0$ regions.

For the case $n = 1$, the parameter space is 2-dimensional as d factors out of the system entirely. In this simple scenario, the convergence of the c_1 parameter is remarkably bad (left panel in Fig. 6.1). We find, consistently for each Markov chain generated, that there exists a range of c_1 values minimising χ^2. The χ^2 surface is extremely flat, and we find that the variation in the values of the χ^2 is small ($\sigma_{\chi^2} = 1.470$).

When $n = 2$, the parameter space is 3-dimensional. Once again, Ω_m converges quickly to $\Omega_m = 0.27 \pm 0.020$, however, c_1 and c_2 show no acceptable convergence in general (mid panel Fig. 6.1). In both cases the standard deviations of the posterior distributions are very large. As can be seen from Table 6.1, the best fit values of c_1 and c_2 are not similar to their mean values. The variation in the χ^2 values, $\sigma_{\chi^2} = 1.530$, is small in this case as well, implying that a wide range of values for c_1 and c_2 perform similarly when fitting the supernovae data. It is therefore possible for the best fit value, which minimizes the χ^2, to be quite different from the mean of the posterior.

Finally, for $n = 3$, where $\sigma_{\chi^2} = 1.364$, it can be seen that the results are very similar to those of $n = 2$. Whereas Ω_m successfully converges, c_1 and c_2 remain unconstrained (right panel Fig. 6.1).

The standard deviations of these two free parameters are large, so that the values which minimise χ^2 is not reflected in the statistics of the posteriors.

At this stage we must emphasise that although all the generated MCMC chains gave identical results for Ω_m, they provided inconsistent results for c_1 and c_2. The distributions of c_1 and c_2 were highly sensitive to the initial points of the various chains, which reiterates the fact that a wide range of values form part of an acceptable optimum region for the values of c_1 and c_2, some of which are not necessarily connected within the phase space. We have depicted the chain-dependence of the results for the $\{c_1, c_2\}$ parameters in Fig. 6.2 showing the results of four different chains for the cases $n = 2$ and $n = 3$. As can be seen, c_1 and c_2 show no tendency to converge to a preferred state. We are led to conclude that supernovae data does not impose strong enough constraints on the free parameters of the Hu-Sawicki model.

n	c_1		c_2		$\Omega_{m,0}$		χ^2_{min}	χ^2_{red}
1	347 ± 300	745	-	-	0.270 ± 0.020	0.270	542.683	0.979
2	825 ± 200	1052	303 ± 200	49	0.272 ± 0.020	0.270	542.683	0.981
3	947 ± 300	1388	3515 ± 500	3675	0.264 ± 0.018	0.270	542.689	0.981
ΛCDM	-	-	-	-	0.27 ± 0.02	0.27	542.685	0.978

Table 6.1: MCMC analysis results for the fitting of Hu-Sawicki model to Union 2 SNIa data. The free parameters c_1,c_2 and Ω_m are estimated, for each case where n is fixed, $n = 1, 2, 3$. We include the results for ΛCDM for comparison. Each free parameter is represented by two columns, the left showing the mean and 1σ of the resulting posterior, and the right showing its best fit value. The best fit values lie in the white regions in Fig. 5.11 and 5.12 for both $n = 2, 3$ exponents respectively, therefore providing the appropriate cosmological expansion behaviour at late time.

6.2 SNIa and BAO data constraints on the GV parameter space

In the same way as the HS model, we analysed the GV model (5.14). Several chains were generated by sampling from the distribution at (5.47), to minimise the free parameters $\{n, \sigma, \beta\}$ of the model at (5.1). However, before proceeding with the random journey through the parameter space, through analytic inspection and numeric experimentation, we found the following statements on parameter sets yielding regular cosmologies to be true:

- $\beta = 0$ is undefined, $-1 < \beta < 1$ are singular.
- Larger values of β improve the similarity of the model to ΛCDM.
- Increasing β, where all of $n, \alpha, \sigma = 1$, results in a decrease in the amplitude of oscillations in the Ricci scalar.

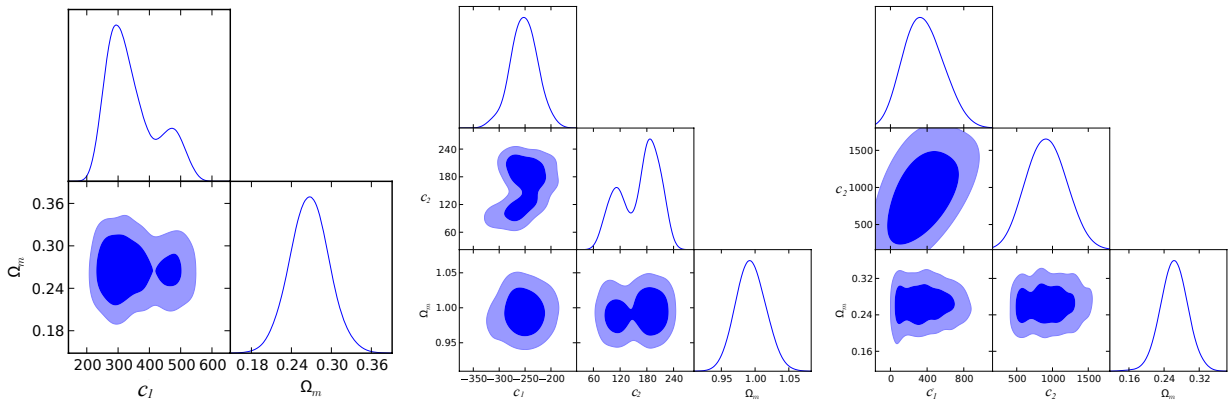

Figure 6.1: Constraints for the posterior distributions and contours for each free parameter, in each case of n, $n = 1$ (left panel), $n = 2$ (central panel) and $n = 3$ (right panel). For $n = 1$, parameter c_2 vanishes from the system. We find $\Omega_m = 0.27$, and c_1 is unconstrained for a wide range of values. For the case $n = 2$, again $\Omega_m = 0.27$ and c_1 is unconstrained for a wide range of values. For $n = 3$, $\Omega_m = 0.264$, whereas c_1 and c_2 remain unconstrained.

Thus the weak prior I place on β is $\beta < -1$ or $\beta > 1$. For safe values of β, we can say the following about the exponent n:

- $1 < n < 3$ are regular,
- $n \leq 0$ are singular,
- For most viable values of β, $n > 3$ is singular. For small values of β, $n > 3$ is not only regular, but preferred.

These points result in a weak prior on n: $n > 0$. The singularity detection method used previously for the HS model, was also implemented here. The sectors of the parameter space corresponding to $\beta < -1$ and $\beta > 1$ were sampled separately, so as to avoid the singular band at (-1,1). The minimum χ^2 values, however, do lie in the $(\beta > 0)$ sector.

6.2.1 SNIa Results

Investigating the 3 dimensional (n, σ, β) parameter space

There are three free parameters of interest for the GV model; the exponents, β and n, and σ which is related to the mass of the scalar field, and is identified through Ω_m in the HS model analysis. The

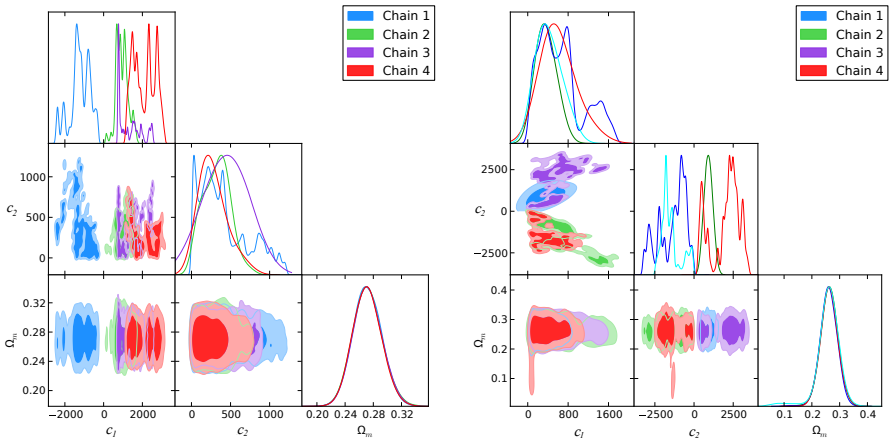

Figure 6.2: Above, we plot the results of four MCMC chains corresponding to the cases $n = 2$ and $n = 3$ to illustrate the lack of a convergence to a best fit value for the parameters c_1 and c_2 in both cases.

parameter α which scales the correction in (5.1) may be absorbed into either β or σ, and is therefore fixed to one ($\alpha = 1$) in favour of reducing the parameter space.

To investigate this 3 dimensional parameter space, several MCMC chains were generated of 10^5 steps, initialised at unique points. The weak priors justified in the previous section were implemented, but otherwise the space was unrestricted. In Figure 6.3, we show an example of a chain generated by moving through the (n, σ, β) space and minimising χ^2 as defined at Equation (5.47). Several ranges of the parameters were tested by increasing and decreasing the standard deviations of the normal distributions sampled for each parameter.

In this case the χ^2 surface was once again very flat, with values similar to that obtained for the HS model using the same data. The exact set of parameters which best fit the SNIa data with a $\chi^2 = 543.25$ are $(n, \sigma, \beta) = (3.97, 2.02, 2.74)$, having $\chi^2_{red} = 0.980$.

The main result from this analysis was a lack of convergence to a best fitting set of parameters, with the posterior appearing dependent on the initial point, and the length of the chain.

For this reason, it may be constructive to fix one of the three parameters, and test if correlations between the remaining parameters emerge from an MCMC.

Investigating the Exponents of the GV Model

Following the results of the previous section, we fix $\sigma = 1$, corresponding to $\sigma = cH_0^2 = 1$. This was done to investigate whether there are any direct relationships between the exponents of the GV

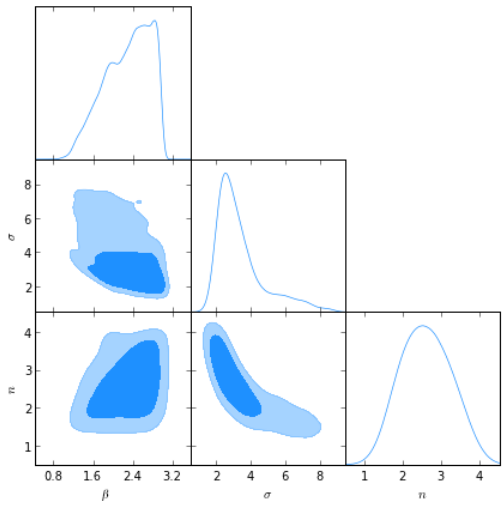

Figure 6.3: A corner plot showing an example of contours and marginalised posterior distributions generated by an MCMC (M-H) analysis for the 3 dimensional parameter space of the GV model, corresponding to n, σ, β, using SNIa Union 2.1 data. The exponent n may be estimated by the normal distribution $n \sim \mathcal{N}(2.6, 0.7)$. A clear peak in the σ posterior is noticed, where the mean value of σ for the chain corresponds to $\mu_\sigma = 3.5$ and a variance, $\text{var}_\sigma = 2.2$, with its best fitting value at $\sigma_{\chi^2_{min}} = 2.0$. There appears to be a peak in the distribution for the β exponent as well, however after many trials it was found that a wide range of values for β are acceptable in terms of minimising the χ^2 parameter, and no real convergence occurred.

model (5.1) which are preferred by SNIa data. For the purpose of the analysis, we restricted n to lie within [1,7], and left β unrestricted in both $\beta < -1$ and $\beta > 1$.

It was found that the global minimum lies in the $\beta > 1$ region of the GV (n, β) parameter space. In this posterior distribution for n, two peaks in the Likelihood, $\mathcal{L} = \exp^{-\frac{1}{2}\chi^2}$, can be noted in the left panel of Figure 6.4. The first and largest peak is located at $n = 3.25$ and the second smaller peak at $n = 6.38$.

Testing a very large portion of the parameter space for β, the contours exhibit the fact that although, as seen previously in the 3D analysis, a wide range of β values are acceptable, the highest point of the distribution occurs for the smaller values of β considered, corresponding to the largest values of n. To make this point clear, in this SNIa MCMC analysis of the 2D parameter space, we find the best fitting model to be $(n, \beta)|_{\chi^2_{min}} = (6.99, 4.95)$ at a minimum $\chi^2 = 542.90$. This gives a reduced $\chi^2_{red} = 0.98$. This result is in some tension with that of the previous section, where the model which minimised χ^2 was found to have $n \sim 3$, closer to the value of the larger peak in the n posterior distribution in Figure 6.4.

The higher the value of n, the better the model can mimic the data, since the largest values of n send the correction part of the GV $f(R)$ model to its ΛCDM limit faster than smaller values. When the sampling is allowed to test large values of n, it appears the best fit values for β are reduced. However, if we restrict $0 < n \leq 4$, while a very clear peak forms in the posterior distribution for

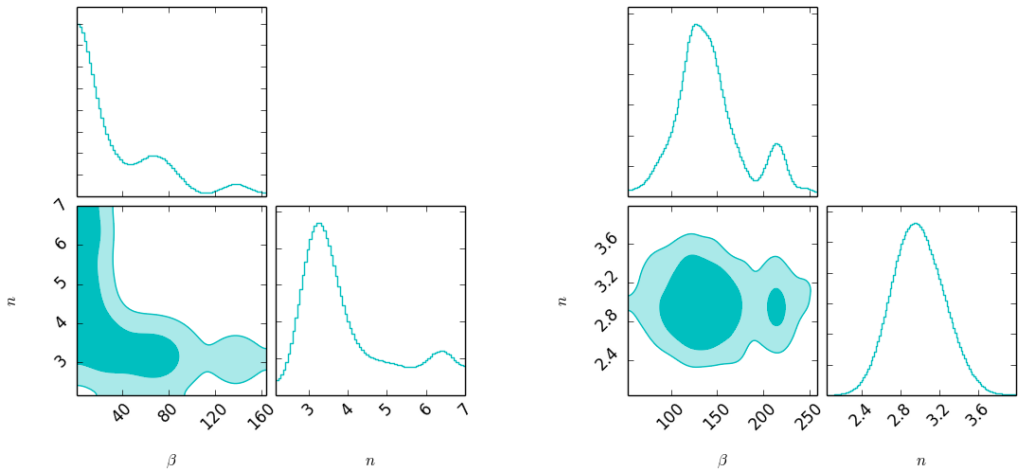

Figure 6.4: Typical corner plot of the (n, β) plane, generated by an MCMC routine to estimate the exponents in the GV model (5.1). The sample extends over $1 < \beta < 160$, $1 < n < 7$. The top and right bottom panels show the marginalised posterior distribution for either parameter. In particular, two peaks can be seen in the n posterior distribution, occurring over $n = 3.25$ and $n = 6.38$. These indicate a higher likelihood around these values for n according to SNIa data. The contours of the Likelihood $= \mathrm{e}^{-\frac{1}{2}\chi^2}$ surface, show that for small values of β, the whole range of $1 < n < 7$ are suitable, it appears $3 < n < 4$ are favoured for the widest range of β. The bump at the higher values of n point to the fact that the largest values of n will generate the best fit models, as higher order polynomials will tend to do. In the right panel, which shows a chain for restricted values of $1 < n < 4$, the maximum likelihood occurs for $n = 2.96$. In this case n may be approximated by a Normal distribution, $n \sim \mathcal{N}(2.96, 0.28)$

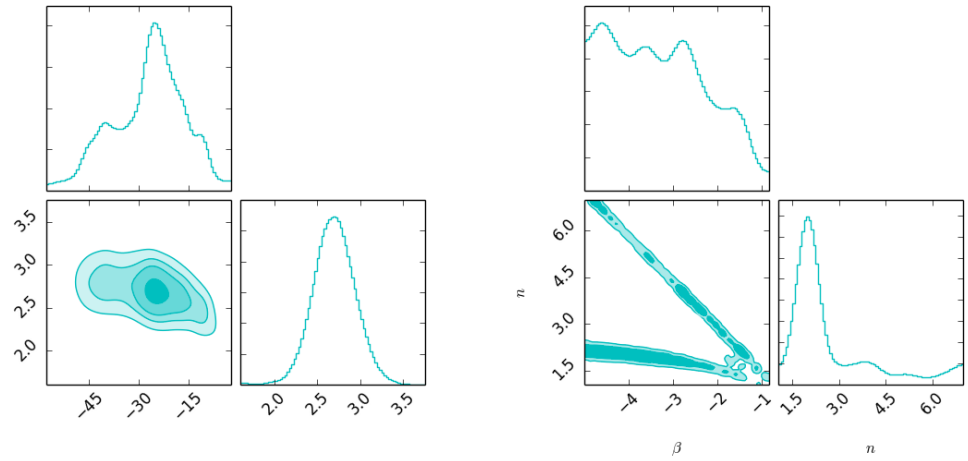

Figure 6.5: Corner plots showing the 2 dimensional MCMC contours for the GV model ($\beta < -1$ region) where the horizontal and vertical axes for the contour plot are β and n, respectively. The left panel shows the posterior distributions and contours, in the case where β is allowed a large range, specifically $\beta < -5$. In this sector n can be approximated with a Normal distribution, $n \sim \mathcal{N}(2.68, 0.26)$. But if we look at a focussed portion of the parameter space, where β is small, $-5 < \beta < -1$, it is clear to see the development of a line in the projected contours, corresponding to $n = -1.49, \beta - 0.091$. This line points to an exact correspondence between the parameters, which are favoured by the data used in the analysis, however this structure does not correspond to the global minimum. It is shown as a point of mild interest.

$n \sim \mathcal{N}(2.96, 0.28)$, β appears unconstrained and its values make little difference in the goodness of the model.

We find similar behaviour on the left hand side of $\beta = -1$, where the points in the chain cluster about $n \approx 3$, with a general lack of preference about the values of β. However one interesting feature which developed in the chain is the appearance of a narrow valley of locally minimised $\chi^2 \approx [548, 552]$ values, however, not corresponding to the global minimum. The equation of the line is estimated to be $n = -1.485\beta - 0.091$.

On this line, we have a set of models not remarkably different from the best fit models with a reduced $\chi^2_{red} \approx 0.948$. For clarity, we plot a contour, with the range of β restricted, to show the prominence of this line, relative to the rest of the parameter space in Figure 6.4. This feature is plotted for the record, to show there appears to be some correlation between n and $\beta < -1$ region of the parameter space.

6.2.2 BAO Results

We supplemented the results obtained using SNIa data by considering constraints on the exponents (n, β) of the GV model using the BAO data given in Table 5.1. Using an MCMC analysis, we once again tested a wide range of values β, for $1 < n < 7$, generate several MCMC chains. This time,

Data	n		β		χ^2_{min}	χ^2_{red}
SNIa	4.040 ± 1.200	6.943	38.665 ± 38.162	4.991	542.908	0.941
ΛCDM$_{SNIa}$	-	-	-	-	542.685	0.978
BAO	1.057 ± 0.052	1.000	1.237 ± 0.088	1.107	14.985	3.75
ΛCDM$_{BAO}$	-	-	-	-	4.51	1.13

Table 6.2: MCMC analysis results for the fitting of GV model (5.1) to Union 2.1 SNIa data. The free parameters n and β are estimated, while parameters associated with the mass scale, $\sigma = \alpha = 1.0$. We include the results for ΛCDM for comparison. Each free parameter is represented by two columns, the left showing the mean and 1σ constraints of the resulting posterior, and the right showing its best fit value.

for the 2 dimensional exponent parameter space of the GV model, we obtained somewhat tighter constraints for both β and n. We show the posterior distributions for these parameters generated with BAO data in Figure 6.6, along with the projected 1-σ and 2-σ contours. The best fit values in this case were obtained for a minimum $\chi^2_{BAO,min} = 14.99$ at $(n, \beta) = (1.0, 1.11)$ in the $\beta > 1$ sector. In a similar analysis performed for the ΛCDM model, the minimum $\chi^2_{BAO,min} = 4.51$, showing that this model does not improve the fit of the ΛCDM model to the data.

For the $\beta < -1$ sector, the minimum $\chi^2_{min} = 17.23$, consistent with the SNIa data having its global minimum in the $\beta > 1$ sector. This local minimum of the χ^2 distribution is located at $(n, \beta) = (3.99, -3.00)$.

As can be seen in Figure 6.6, the distribution of n could be approximated by a Normal distribution as $n \sim \mathcal{N}(1.04, 0.04)$. The χ^2 is minimised in the $\beta > 1$ sector, thus we only show this part of the parameter space, as $\beta < -1$ sector is rather uninteresting.

6.3 Conclusions

In this chapter, using data corresponding to background observables, namely SNIa and the BAO, we obtained new constraints of the parameters of a general class of viable broken power law theories for $f(R)$ gravity. Published in [111], we showed the results of an analysis to confirm that the HS model is unconstrained by background data.

The GV model, defined at (5.1) provided reasonable fits to the SNIa data with χ^2 values comparable to that obtained for the ΛCDM model. When fitting to the BAO data, we found the fit was significantly worse, however, through an MCMC analysis we were able to obtain tight constraints on the exponents of this GV model, which showed a preference for $n \approx 1.00, \beta \approx 1.25$, significantly reducing the effective parameter space of this model (See Fig. 6.6).

The SNIa data provided no real constraints on β, except to indicate that where the best fits were

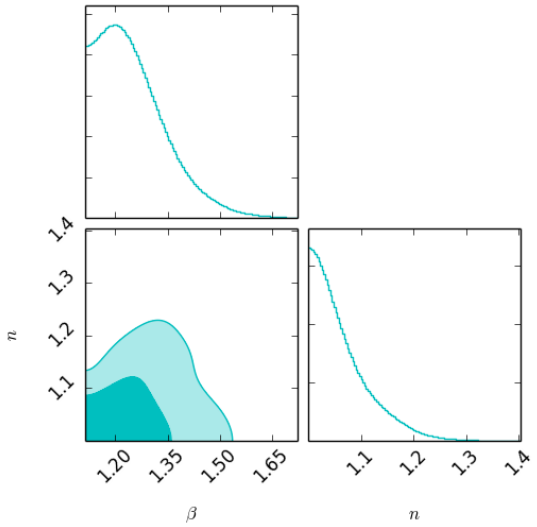

Figure 6.6: A corner plot showing the posterior distributions for the GV model parameters (n, β), and 1 and 2 σ regions of the projected χ^2 distribution, generated using BAO data for comparison. For this analysis the best fit values correspond to $(n, \beta)|_{bestfit} = (1.0, 1.11)$. This is a very interesting result, and corresponds to a model very close to the HS model, for $n = 1$.

for the highest values of $6 < n < 7$, β was restricted to smaller values, roughly within the range $1 < \beta < 20$. And the widest range of β parameters are allowed for $2.4 < n < 3.6$, in particular, the Normal distribution $n \sim \mathcal{N}(2.96, 0.28)$ is an excellent approximation of the posterior distribution of n in the uncapped range of $\beta > 1$ (see Fig. 6.4). In the next chapter we look at this 2 dimensional n, β parameter space from the perspective of a perturbations analysis on $f(R)$ models, by considering the matter power spectrum for linear scalar perturbations.

Chapter 7

Constraints of Viable $f(R)$ Models from LSS Data

Modifying the underlying theory of gravity changes the way gravitational potentials evolve, and is expected to leave a detectable signature in the large scale clustering of matter. We track the GV $f(R)$ model predictions for the scalar perturbations in the range of scales relevant to luminous red galaxies.

In this chapter I will discuss constraints coming from data representing the large scale structure in the observed universe. This complements the constraints on the model parameters obtained through an analysis of BAO and SNIa data, representing only background quantities.

Since, the HS model is indeed a subset of the GV model's parameter space, its inclusion is implicit in the study discussed in this chapter, through only the parameters (β, σ, n). Once again we choose to fix the value of $\sigma = 1$.

We considered scalar perturbations in the metric $f(R)$ theories through the 1+3 covariant gauge invariant formalism. As presented in Chapter 4, the equations are given by

$$\ddot{\Delta}^k_m - \left[(3w-2)H + \frac{\dot{R}f''}{f'}\right]\dot{\Delta}^k_m + \left[w\frac{k^2}{a^2} + (w-1)\frac{\rho_m}{f'} - w\frac{f}{f'}\right]\Delta^k_m$$
$$= \frac{(w+1)}{2}\left[-1 - \frac{2k^2}{a^2}\frac{f''}{f'} + \left(f - 2\rho_m + 6\dot{R}f''\right)\frac{f''}{f'2} - 6\dot{R}H\frac{f'''}{f'}\right]\mathcal{R}^k - \frac{3(1+w)}{f'}Hf''\dot{\mathcal{R}}^k, \quad (7.1)$$

$$\ddot{\mathcal{R}}^k + \left(2\dot{R}\frac{f'''}{f''} + 3H\right)\dot{\mathcal{R}}^k + \left[\frac{k^2}{a^2} + \ddot{R}\frac{f'''}{f''} + \dot{R}^2\frac{f^{(iv)}}{f''} + 3H\dot{R}\frac{f'''}{f''} + \frac{f'}{3f''} - \frac{R}{3}\right]\mathcal{R}^k$$
$$= -\left[\frac{1}{3}(3w-1)\frac{\rho_m}{f''} + \frac{w}{w+1}\left(2\ddot{R} + 2\dot{R}^2\frac{f'''}{f''} + 6\dot{R}H\right)\right]\Delta^k_m + \frac{1-w}{1+w}R\dot{\Delta}^k_m. \quad (7.2)$$

Interestingly, the $f(R)$ modification affords the ability to have positive growth of density perturbations in a universe where the expansion rate is accelerating. Thus the evolution of gravitational

potentials will not be stunted by the expansion of space. The ISW effect in these models are therefore a point of interest [155].

In terms of the dimensionless expansion normalised dynamical variables defined by Equations (5.18) and (5.19), the above equations may be written as the following first order differential equations

$$\frac{\mathrm{d}}{\mathrm{d}z}p(z) = -\frac{(\Omega - y)}{z+1}p(z) + \frac{3\Omega}{(z+1)^2}\Delta^k(z) + \frac{1}{2}\frac{1}{h^2 v(z+1)\Gamma}q(z) - \left[\frac{1}{6}\frac{\hat{k}^1(z+1)^2 + 3h^2(\Gamma v - v + 1) + 18A\Gamma h^4 vx}{vh^4\Gamma(z+1)^2}\right]\mathcal{R}^k(z), \tag{7.3}$$

$$\frac{\mathrm{d}}{\mathrm{dz}}q(z) = \frac{v\left(12A\Gamma h^2 x + 1\right)}{z+1}q(z) - \frac{6xvh^4\Gamma}{z+1}p(z) + \frac{6h^4 v\Omega\Gamma}{(z+1)^2}\Delta^k(z) - \left[\frac{\hat{k}^2}{h^2} - \frac{2v}{(z+1)^2}\left[18h^4 vx^2\Gamma^2(A^2 - B) - 3h^2 A\Gamma(\Omega + 2v - 4y) - \Gamma + 1\right]\right]\mathcal{R}^k(z). \tag{7.4}$$

where

$$p(z) = \frac{\mathrm{d}}{\mathrm{d}z}\Delta^k(z), \tag{7.5}$$

$$q(z) = \frac{\mathrm{d}}{\mathrm{d}z}\mathcal{R}^k(z), \tag{7.6}$$

and the functions Γ, A and B are defined as

$$\Gamma = \frac{f'(R)}{Rf''(R)}, \tag{7.7}$$

$$A = \frac{f'''(R)}{f''(R)}, \tag{7.8}$$

$$B = \frac{f^{(iv)}(R)}{f''(R)}. \tag{7.9}$$

In the background equations (5.21)-(5.22), Γ represents the model, and must be expressed in terms of the dynamical system variables in order to close the system. When considering the perturbations, we have two additional non-disappearing terms, comprising of third and fourth derivatives of the function, $f(R)$. These terms must also be expressed in terms of the dynamical variables in order to close the system. Thus, the above set of equations is a completely general system which can be solved for any $f(R)$ theory of gravity, provided Γ, A and B can be expressed in terms of the dynamical system variables at (5.18)- (5.19), to obtain the scale and redshift evolution of scalar perturbations.

7.1 Constructing the linear $f(R)$ matter density power spectrum

The linear matter power spectrum for $f(R)$ theories is related to that of the ΛCDM linearly through a transfer function , $T(k)$, encapsulating the scale dependence of the perturbations,

$$P_k^{f(R)} = T(k) P_k^{\Lambda CDM}|_{equality}, \tag{7.10}$$

In this way, the success of ΛCDM in the radiation dominated eras is preserved, and the modification need not have any effect on high redshift phenomena. We compute the transfer functions for each model by solving the Equations (7.3) - (7.6) for Δ^k, and constructing $T(k) = \left| \frac{\Delta_m^k(0)}{\Delta_m^{0.01}(0)} \right|^2$.

For this analysis, we assumed that the universe is spatially flat and contains only cold dark matter. The ΛCDM matter power spectrum used in Equation (7.10) corresponds to the fit used in [151] .

Initial Conditions

In principle, we would like to study the way the scalar perturbations evolve completely, throughout the expansion history. This would mean integrating the system (7.3)-(7.6) from a very high redshift, somewhere around matter-radiation equality, to the present day. However, due to the nature of the theory; with high frequency and large amplitude oscillations in the Ricci scalar growing with increasing redshift, and the derivatives of the dynamic quantities being very small, we began the integration of the $f(R)$ perturbation equations from $z = 20$.

All the models in this class have indistinguishable cosmological backgrounds. For a given set of parameters (n_x, β_x) which can produce a singularity - free background from $z = 2000$ to $z = 0$, we may :

- obtain the solution to (7.3)-(7.6) pertaining to this model specified by $n = n_x$ and $\beta = \beta_x$ in Equation (5.1) ,
- evaluate that solution at $z_0 = 20$, and obtain the values for the perturbations and their derivatives at $z_0 : \Delta^k(z_0 = 20)$, $\frac{\mathrm{d}\Delta_m^k}{\mathrm{d}z}(z_0 = 20)$, $\mathcal{R}_m^k(z_0 = 20)$, $\frac{\mathrm{d}\mathcal{R}_m^k}{\mathrm{d}z}(z_0 = 20)$,
- use these values, or at least their order of magnitude, as the initial conditions in the resolution of the same system (7.3)-(7.6), from $z = 20$ to $z = 0$ for any set of parameters.

This reduced the compute time of the rest of the analysis, in which we constructed the χ^2 surface over the $n - \beta$ parameter space, by calculating the model at each point of a grid and comparing it to the data.

The initial conditions obtained are given in the first row of Table 7.1. The second row, IC 2, gives the same order of magnitude as IC 1, and are the initial conditions which we make use of when constructing the grid. The third row gives an experimental set, included just as a case of interest - if the matter density perturbation and its derivative are of the same order of magnitude as that of the curvature perturbation at $z = 20$. We present transfer functions and power spectra resulting from using these three sets of initial conditions in Figure 7.1 for the HS model, and in Figure 7.2 for the GV model.

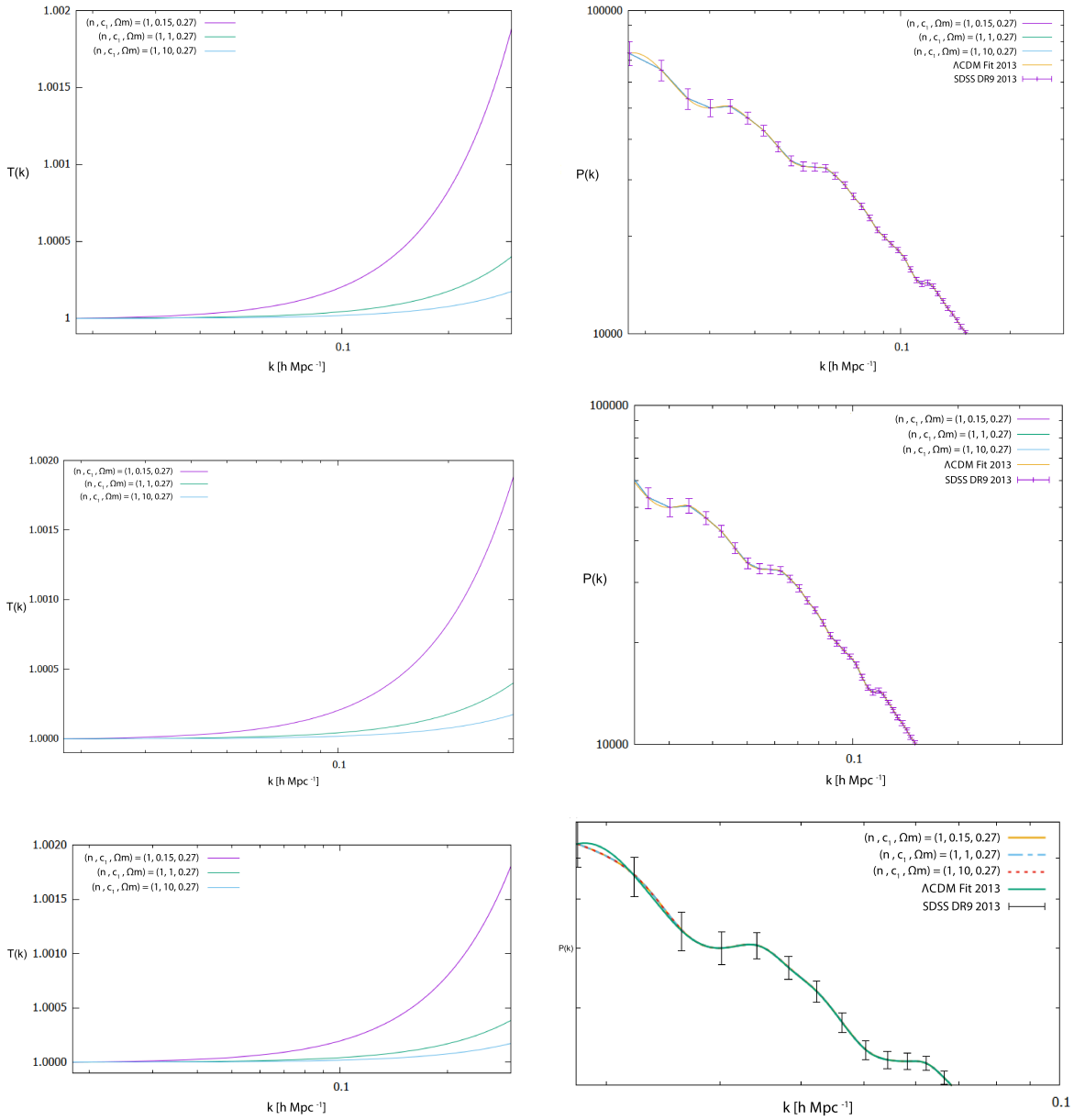

Figure 7.1: The transfer functions, $T(k) = |\Delta^k/\Delta^{0.01}|^2$, for the Hu Sawicki model for the three sets of initial conditions IC1, IC2 and IC3 are plotted in the left panels, for three different parameter sets HS_A, HS_B and HS_C, normalised to coincide at large scales, where k is in units of $h\text{Mpc}^{-1}$. These show the evolution of perturbations after radiation-matter equality, where the initial conditions for the $f(R)$ system were obtained as described in Section 7.1. The general behaviour is the same for all three cases; we have growth at small scales, and suppression for $k < 0.1$. Increasing the value of c_1 appears to cause a larger suppression at small scales. The right panels picture the corresponding theoretical power spectra, plotted with the ΛCDM fit [151], and the SDSS-III [156] power spectrum data in the range $k = [0.005, 0.29]h\text{Mpc}^{-1}$. The theoretical power spectra were normalised at $k = 0.01h\text{Mpc}^{-1}$ for comparison. All models give good fits to the data, due to the flatness of the transfer functions produced. In particular, the $f(R)$ models, in all three IC scenarios only deviate from the ΛCDM model in the range $k = [0.005, 0.02]h\text{Mpc}^{-1}$.

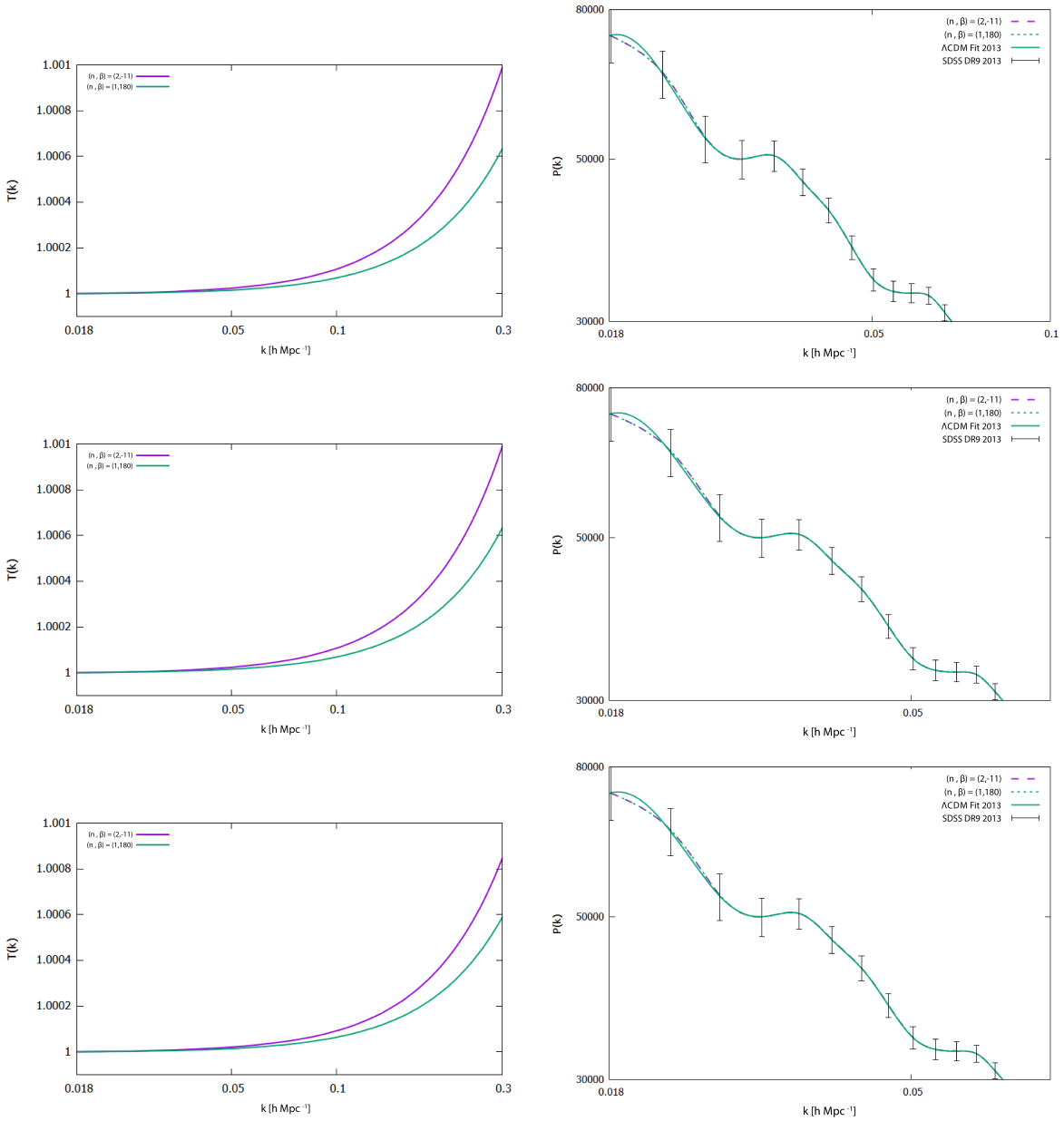

Figure 7.2: The transfer functions, $T(k) = |\Delta^k/\Delta^{0.01}|^2$, for the GV model given by (5.1), for the three sets of initial conditions IC1, IC2 and IC3, are plotted in the left panels, for two different parameter sets GV_A and GV_B, normalised to coincide at large scales. These show the evolution of perturbations after radiation-matter equality, where the initial conditions for the $f(R)$ system were obtained as described in Section 7.1. The behaviour is the similar for all three cases, as well as those calculated in the HS model. Once again, we have growth at small scales. Note that both parameter sets have comparable χ^2 values. The right panels picture the corresponding theoretical power spectra, plotted with the ΛCDM fit [151], and the SDSS-III [156] power spectrum data in the range $k = [0.005, 0.29]h\text{Mpc}^{-1}$. The theoretical power spectra were normalised at $k = 0.01h\text{Mpc}^{-1}$ for comparison. All models give good fits to the data, and are dominated by the ΛCDM fit, due to the flatness of the transfer function. In particular, the $f(R)$ models, in all three IC scenarios only deviate from the ΛCDM model in the range $k = [0.005, 0.02]h\text{Mpc}^{-1}$

Initial Conditions	$\Delta^k(z_0)$	$\Delta^{k\prime}(z)\|_{z_0}$	$\mathcal{R}^k(z_0)$	$\mathcal{R}^k(z)\|_{z_0}$
IC 1	0.1	-0.1	1.0	0.1
IC 2	0.2	-0.17	3.0	0.3
IC 3	1.0	1.0	0.1	0.1

Table 7.1: IC 1 and IC 2 are the same order of magnitude, and were obtained by integrating the system of perturbation equations at (7.3) - (7.6) from $z_i = 2000$, setting all the initial values of the background quantities to their values at $z = 2000$. IC 3 sets both curvature and matter density perturbations to the same order of magnitude (that of the curvature perturbation), just as a case of interest.

	n	c_1	Ω_m
$\mathrm{HS_A}$	1.0	0.15	0.27
$\mathrm{HS_B}$	1.0	1.0	0.27
$\mathrm{HS_C}$	1.0	10.0	0.27

Table 7.2: A list of the examples of parameters used to show the behaviour of $T(k)$ and $P(k)$ for the Hu-Sawicki model.

	n	β
$\mathrm{GV_A}$	2	180
$\mathrm{GV_B}$	1	-11

Table 7.3: A list of the examples of parameters for the GV model (5.1), used to show the behaviour of $T(k)$ and $P(k)$.

7.2 LSS constraints on the GV parameter space

For a restricted rectangular range for the 2D parameter space of the GV model, we constructed a χ^2 surface by computing its value at regular grid points. This method was previously used as a preliminary test for the MCMC parameter optimisation routine, however we find it sufficient to scan the regions previously constrained by the background data, in this LSS analysis.

A (n, β) grid of dimensions (100×200) was defined to extend between : (i) $1 < n < 7$, $1 < \beta < 200$, and (ii) $1 < n < 7, -200 < \beta < -1$, in order to test a large and inclusive portion of the parameter space, to locate any unexpected local minima. Regarding the avoiding of singular models, in this case, we use the same method as before of testing the background. If during the scanning of the grid a singular model is identified, we assigned it a high value for χ^2, essentially excluding them from concern. The χ^2 parameter defined as

$$\chi^2 = \Delta^T C^{-1} \Delta, \tag{7.11}$$

where $\Delta = P(k)^{f(R)} - P(k)^{obs}$, using the covariance matrix provided in the 2013 SDSS data set [151], [152], was computed at every point on the grid. Then using a 2D nearest neighbour interpolation method, three important iso-sections of the χ^2 surface were identified, plotted in Figure 7.3, corresponding to the 1σ and 2σ significance intervals in the parameter space considered. These plots show clearly the structure of the distribution of the χ^2 parameter in this analysis, highlighting the location of the minimum in the exponent parameter space of the GV model.

The dark blue sections contain models for which the χ^2 parameter is minimised, and is bound by lowest level curve, the teal section contains 68% of the distribution, and the light green section contains 95% of the distribution, effectively representing the 1 and 2σ confidence intervals of the χ^2 distribution. The mean, μ_{chi^2}, and standard deviation, σ_{χ^2}, values of the entire χ^2 grid, as well as the minimum values for χ^2, differ in the $\beta < -1$ and $\beta > 1$ regions of the parameter space. They are respectively:

	$\beta < -1$	$\beta > 1$
χ^2_{min}	8.33	8.32
μ_{χ^2}	8.35	8.35
σ_{χ^2}	0.01	0.02

From the above statistics, it is possible to gauge that the surface is quite flat, and it appears almost all models make similar fits to to the SDSS III DR9 data, with the χ^2 parameter calculated differing marginally throughout the parameter space considered.

- There is a very wide range of the GV model parameters β and n which can produce excellent fits to LSS LRG power spectrum data in the range $k = [0.018, 0.290]$.

- In the $\beta > 0$ region: for $2.65 < n < 3.4$, $\beta > 1$ is unconstrained. As seen in the SNIa analysis, there is an interval of β values for which large values of n make the best fits. Specifically, models where $25 < \beta < 35$, $n > 3.2$ minimise the χ^2 parameter. This results in the formation of a boomerang like minimum of the χ^2 surface, as can be seen in Figure 7.3. $(n, \beta) = (5.33, 25.43)$ corresponds to the model in the grid which has the lowest value for $\chi^2_{min} = 8.32$. We may pay less attention to the largest values of n, since they were included for a sense of completeness in the parameter space analysis, but in fact, it is quite usual to fix $2 < n < 4$ to produce perfectly viable backgrounds. The larger the value of n, the better the model will be mimic ΛCDM, and thus in this data set, the better the overall fit to data will be, however the actual effect of this value in the physics of the theory reaches a peak by $n = 4$.

- Even though the global minimum occurs in the $\beta-$ positive part of the parameter space, we show the contours obtained in the same way as before for the β negative space, as we had done with the previous data sets. Note that the values of χ^2_{min} and χ^{mean} are different in both panels of Figure (7.3), even though they are represented by the same set of colours. Interestingly, once

again there is the appearance of a band, − not a line, as appeared with the SNIa − in this sector. For negative values of β the exponent n within $(2.0, 3.25)$ correspond to a minimum $\chi^2_{min} = 8.35$.

From the above analysis, we have presented constraints on the exponents of the GV model using SDSS III DR9 matter power spectrum data. There appears to be a relationship between β and n which correspond to the best fit models to this data. This will form part of a useful constraint on the model parameters, in order to obtain expansion histories which are singularity free and viable. The degrees of freedom in this analysis d.o.f=69, and the reduced $\chi^2 = 0.12$. This small value indicates that the model is overfitting the data.

Such an analysis should be supplemented by considering a more realistic theoretical value for the σ parameter, which simulates a mass for the scalar field. The codes used to generate these results may easily be generalised to extend the analysis, when more intuition about the nature of these parameters is at hand.

Finally, we remark that the most notable result is the discovery of a preferred range of n values, which minimise residuals between data and model. The n parameter, as previously discussed plays the important role of setting the transition between the desired background and the effects of the $f(R)$ modification. Regarding β, on the other hand, we can say without losing generality, that its value may be set arbitrarily while testing these models, as far as SNIa, BAO and LRG LSS data is concerned.

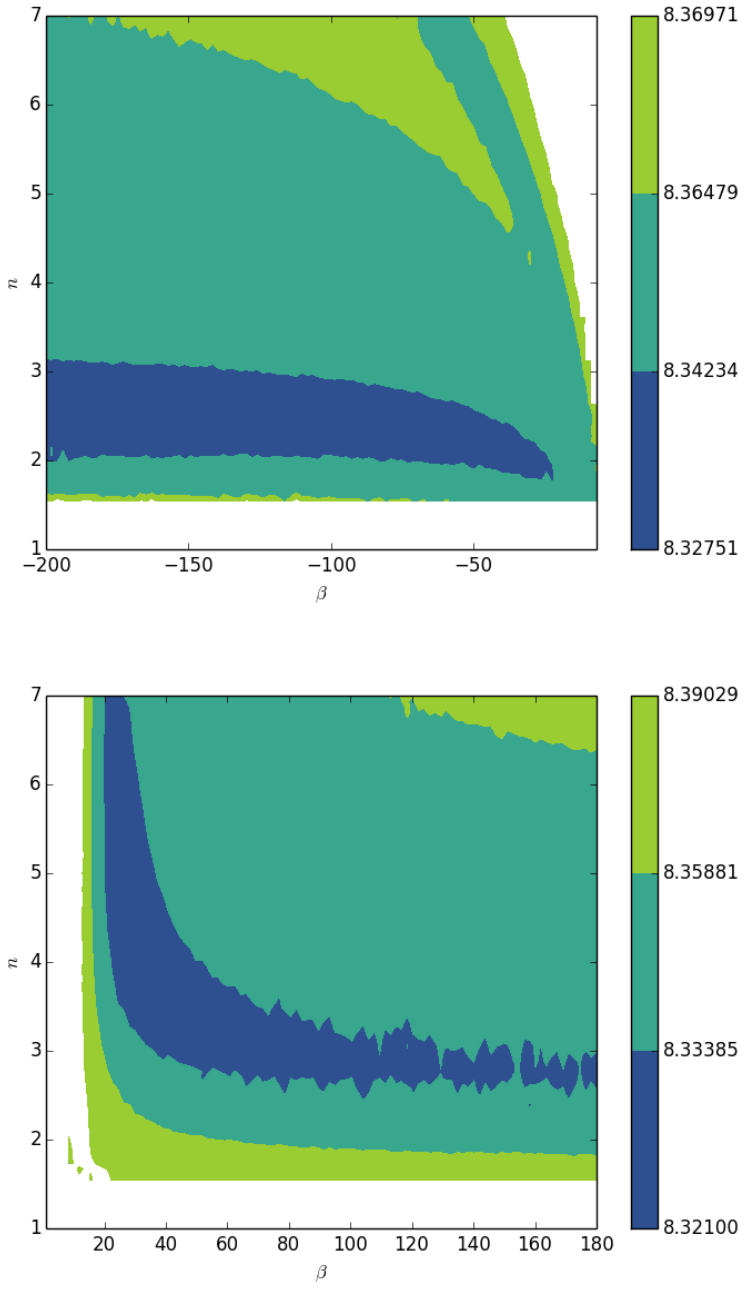

Figure 7.3: Contours of the χ^2 surface over the 2D (n, β) parameter space for the GV model at (5.1). The top and bottom panels show the regions for $\beta < -1$ and $\beta > 1$ respectively. The dark blue region contains all points between the absolute minimum of the surface and the lowest 2.5 percentile. The teal region is bounded by the 1σ confidence interval, and finally the leaf green region is bounded by the 2σ confidence interval. The global minimum is located in the $\beta > 1$ region; $\chi^2_{min} = 8.3$ for $(n, \beta) = (5.33, 25.43)$.

Chapter 8

Conclusions

This thesis focused on investigating the parameter space of viable broken power law models for the $f(R)$ class of modified gravity theories. Modifications to Einstein's GR is currently a popular field of research in many areas of physics, from quantum theories of gravity to astrophysics to Cosmology. The $f(R)$ modification is derived by replacing the Ricci scalar, R, in the EH gravitational action with a general function, which could in principle be *any* function of R. It is now known that this modification can be equivalent to adding an extra scalar field to the theory, which turns out to be the first derivative of $f(R)$, under the condition that the second derivative of f is non zero. In fact, at least pertaining to Dark Energy models, almost all modifications can be generalised under the umbrella of effective field theories. Over the years, it became understood that only very special models for $f(R)$ are worth studying in a cosmological and astrophysical sense. Only certain forms for the function can produce satisfactory physical effects, such as reproducing the gravitational field in and around a compact object, accelerating the universe at late times as well as generating an expansion history similar to the observable universe. In particular, a generally favoured approach is to assume that the theory already contains GR as a limit. In many theories a curvature dependent corrective term comprises the modification added to R in the EH action for gravity. Since one of the important ways to study the effects of this kind of modification is to examine dynamical changes in gravitating and large scale systems, the behaviour of the gravitational field in $f(R)$ theories and the interaction between the emergent scalar field and matter has been widely considered in a range of different physical phenomena. Degeneracy between $f(R)$ models is probably going to be the biggest bottleneck for these theories, since in principle there are plenty of clever ways to come up with satisfying the basic requirements.

The application considered in this thesis was in relation to generating an expansion history similar to the observed expansion history of the Universe. This also implied, at the very least, the mimicking of the ΛCDM model. The ΛCDM model is popular because it *is* able to produce a universe in concordance with cosmological observations, however faces its own phenomenological and motivational drawbacks.

Following previous research [7], [6], we considered a general class of broken power law models, which are designed to reduce to GR, in low curvature regimes, and tend to a GR + cosmological constant type model when the curvature is large relative to the local environment. This model also includes within its parameter space, previously considered "viable" models. The redshift evolution of the Hubble rate and the deceleration parameter, in the class of models considered here, described by (5.1) , have very similar behaviour to that of the ΛCDM model. Deviations in the Hubble parameter begin to develop only at very low redshifts, $0 < z < 1$, while, the deceleration parameter, showing larger deviations at low redshifts, still converges towards a value of $\frac{1}{2}$ from around a value of $z = 6$, consistent with the ΛCDM parametrisation. The exact behaviour will depend on the choices of model parameters, but this behaviour is typical of all the values which were tested.

We attempted to address the problem of degeneracy within the broken power law space of $f(R)$ theories, by considering three sets of real observational data.

We looked at $f(R)$ theories in a metric formulation, considering a flat, FLRW, matter dominated ($w = 0$) spacetime. We also continued in units such that $c = h = \kappa = 1$. The equations of motion for the scale factor obtained by these gravity field equations were recast in terms of expansion normalised dimensionless variables that convert the 2nd order system of differential equations into a set of first order autonomous differential equations. This new dynamical system is simpler to handle. Using a new set of variables through which to express the cosmological field equations is an approach taken in order to simplify calculations. I specifically used a set of variables defined in [4] to solve for the background of the models. I emphasise that the background used in this analysis are exact and not approximated by the ΛCDM model. We also studied the linear scalar perturbations for these models, using the $1 + 3$ formalism, and then cast these perturbation evolution equations in terms of the dynamical systems variables used for the background.

We performed a parameter optimisation analysis for the HS model using SNIa data. For three integer values of the exponent, $n = 1, 2, 3$, using a Metropolis Hastings MCMC algorithm, we estimated the best fit values for the remaining parameters of the model, c_1, c_2, and m^2 (which was related to the matter density fraction, Ω_m). We presented contours of the χ^2 surface, generated when comparing SNIa data to the theoretical predictions of the distance modulus. These confirm that the parameter values have very little baring on the background behaviour of the resultant universe, and as they were constructed to do so, a wide range of parameters are able to mimic the ΛCDM model. The MCMC chains showed no convergence for c_1 and c_2, while Ω_m was fit excellently by a Gaussian distribution, centred about $\mu_{\Omega_m} = 0.27$ with $\sigma_{\Omega_m} = 0.02$. We concluded that these results were unsurprising given that the HS model has an almost indistinguishable background from that of ΛCDM, and that we had selected a relationship between the model parameters which fixed the cosmological constant limit to be 2Λ. The χ^2 surface is very flat, for both the HS and GV models. For the GV model, the SNIa data confirmed that larger values of $4 < n < 7$ are preferred for smaller values of β, and that a wide range of β values are acceptable along the axis of $3 < n < 4$.

An interesting result was obtained in a numeric attempt to find a possible "prior" on the parameter space of the HS model. This was done to avoid parameters which result in a cosmological singularity, and regions in the parameter space that were more likely to have singular points. On scanning the parameter space we found that there were distinct regions which only contained singular points, and these regions were contained within continuous curves. The curves were dependent on the parameter values as well. This was also useful because it helped us avoid spaces which were completely singular in the MCMC analysis. It would be an interesting exercise to find the equations of these curves and understand more about why the specific relation of parameters separate a singular region from parameters that give singularity free expansion histories, as well as determine these regions in the parameter space of the GV model. Such an exercise may give broader insight into which models may be excluded altogether.

Another interesting feature, in the GV parameter space, is the appearance of a line, where minimised χ^2 points cluster, in the $\beta < 0$ portion. Its appearance hints that it may form as part of the boundary of a region corresponding to completely singular models. Further analysis can easily make this clear.

The BAO MCMC analysis on the 2 dimensional exponent subspace of the GV model indicates the following constraints on the parameters n and β : $n = 1.04 \pm 0.04$, and $\beta = 1.24 \pm 0.09$, if we compute the statistics of the best fit Normal distributions to these parameters posteriors. This is a satisfactory approximation, for our purposes of obtaining an idea of the best fit models according to this data.

Using SDSS III DR9 matter power spectrum data, we produced level curves of the χ^2 surface over the (n, β) plane. We found that there is a relationship between the exponents of the GV model which has a higher likelihood compared to the rest of the parameter space. This relationship, shown in the Figure 7.3, may be roughly encapsulated by the following conditions: when $2.65 < n < 3.4$, the value of β which optimises the fit is any value beyond $\beta > 25$, when $3.4 < n$, β is constrained within the interval $25 < \beta < 35$. While the exact values may be scaled by including a value of the mass scale different from one (we set $\sigma = 1$), the correlation which forms between β and n gives insight into an analytic relationship of the parameters of the GV model. This is another point of analysis which may be interesting to clarify.

These results are useful in identifying regions of the parameter space for which future studies may focus their attention. Since $n = 2$ corresponds to the Starobinsky class for $f(R)$ gravity, we see that in the regions of parameter space for which β is negative, the SNIa and LRG data still include the Starobinsky model, while BAO data in the $\beta > 0$ region, distinctly excludes it. We find, for the case $\sigma = 1$, that $\beta > 1$ is favoured in the SNIa and LRG analysis, and mildly so with the BAO analysis. $\beta = 1$ represents the Hu-Sawicki model, and these results may hint to it being excluded from the more general class of viable broken power law models which we considered here. However, if σ was included and constrained with these analyses, we may be able to infer a stronger constraint on β.

The framework used to carry out the analysis is quite general, and is easily extendible for other models, different cosmological parameters and initial conditions. It makes use of no approximations for the $f(R)$ backgrounds, as has been common practice in previous studies, for example [?], [?]. It would be extremely interesting to use CMB, weak gravitational lensing data, the ISW effect and even gravitational waves to place a full set of constraints on the parameter space of this class of $f(R)$ models, and in this way find the class of theories most likely given observational cosmological data. This is a point left for future work.

During the completion of this work, several other results were published, with a similar goal in mind; to place observational constraints on popular viable models for $f(R)$ gravity. For example, in [157] recently released cosmic chronometer data was used with the joint light curves SNe Ia sample, and Baryonic Acoustic Oscillation data points to place constraints on viable $f(R)$ models. In particular, the HS and Starobinksy models were considered, which are included in the GV parameter space that was studied here. The models were recast in terms of a distortion parameter, quantifying their respective deviation from the ΛCDM model, at a background level. It was found that small but non zero values for this parameter were slightly favoured for the HS and Starobinsky models, however zero was well within the 95% confidence interval in both cases. They concluded that the HS and Starobinsky models can coincide, to a large degree, with the ΛCDM model, which is of course consistent with what I have found from my own calculations. The authors also studied the Tsujikawa model - a tanh correction to the standard gravitational action-, and the exponential $f(R)$ correction, for which the respective distortion parameters were significantly larger than zero, indicating an observable deviation from ΛCDM behaviour is favoured in those models with respect to the data used [157].

A similar study was performed in [158]; MGCAMB (the modified gravity patch to CAMB) was used to compute observables such as the matter power spectrum for the Starobinsky and exponential $f(R)$ models. Furthermore, CosmoMC was employed to estimate a parameter quantifying the $f(R)$ model's deviation from theΛCDM background. Using Planck 2015 cosmic microwave background radiation data, Baryonic Acoustic Oscillations (BOSS) and SNIa (SNLS) data, they concluded that these data sets favoured deviations from ΛCDM model [158].

As was mentioned earlier, $f(R)$ gravity forms a subclass of Modified Gravity/Dark Energy models, and these theories have been unified under an Effective Field Theory approach [159], [160], in which a single action represents all modifications and all dark energy models, via a set of EFT functions. That is, all modifications, which introduce one extra scalar degree of freedom and have a well defined Jordan frame, can be transformed into the EFT language, with no approximations required.

This powerful perspective on the Dark Energy problem has already been implemented into the Einstein-Boltzmann solver, CAMB/CosmoMC in EFTCAMB/EFTCosmoMC [161]. In [162], an implementation of this public software is used to analyse the evolution of linear density perturbations in the Hu-Sawicki scenario. Using the code, the authors compare the model predictions with Planck

Model	n	σ	β	χ^2	χ^2_{red}
$f_{\rm GV}(n,\sigma,\beta)$ - SNIa	3.97	2.01	2.74	543.25	0.98
$f_{\rm GV}(n,\beta)$ - SNIa	6.99	-	4.95	542.90	0.98
$f_{\rm GV}(n,\beta)$ - BAO	1.0	-	1.11	14.98	3.75.
$f_{\rm GV}(n,\beta)$ - LRG	5.39	-	25.42	8.3	0.12

Table 8.1: Summarising the *best fit values* corresponding to the minimum χ^2 parameters in each separate data analysis. While BAO data actually produces tight constraints on the parameters of the model, the reduced χ^2 parameter at 3.75 reveals that these models provide a poor fit to the data points considered. Maximum likelihood for the GV model, given the SNIa data, was obtained for $n \approx 7$, the largest value in the range of n considered, for $\beta \approx 5$. However, this quoted result may be misleading, since the posterior distribution of n in this case, clearly demonstrated an accumulated likelihood for $2.4 < n < 3.6$. The reduced χ^2 parameter for the LRG data indicates that the model is overfitting the data.

2015 data, CMB lensing, the WiggleZ galaxy survey and the CFHTLenS weak lensing survey measurements, to place constraints on the value of the scalaron at the present epoch, and parameters representing structure growth rates.

These are just a few of several similar studies, all aimed at using observational data to limit the parameter space of alternative theories of gravity through statistical means. This field of study is more dynamic than ever before, and researchers look toward new methods of studying the implications of these complicated theories (see, for example, [80]) supplemented by vast data sets, to improve our understanding of the forces at work in our universe.

The results in this thesis form part of an emerging tapestry of observational constraints on the theoretical landscape of MG/DE theories. Future work involving larger, more numerous data sets and more intuitive parameter choices, may build upon the framework developed and the conclusions obtained to gain a clearer understanding of the role $f(R)$ gravity has to play in cosmology and astrophysics.

Bibliography

[1] Kandhai S. and Dunsby P. K. S. *Cosmological dynamics of viable f(R) theories of gravity*. 2015.

[2] Carloni S. et al. *Some remarks on the dynamical systems approach to fourth order gravity*. *Gen. Rel. Grav.*, 41:1757–1776, 2009.

[3] Abdelwahab M. et al. *Cosmological dynamics of exponential gravity*. *Class. Quant. Grav.*, 25:135002, 2008.

[4] Abdelwahab M. et al. *Cosmological dynamics of fourth order gravity: A compact view*. *Phys. Rev.*, D85:083511, 2012.

[5] Goheer N. et al. *Dynamical systems analysis of anisotropic cosmologies in R^n-gravity*. *Class. Quant. Grav.*, 24:5689–5708, 2007.

[6] Hu W. and Sawicki I. *Models of f(R) Cosmic Acceleration that Evade Solar-System Tests*. *Phys. Rev.*, D76:064004, 2007.

[7] Miranda V. et al. *Viable Singularity-Free f(R) Gravity Without a Cosmological Constant*. *Phys. Rev. Lett.*, 102:221101, 2009.

[8] Frolov A. V. *A Singularity Problem with f(R) Dark Energy*. *Phys. Rev. Lett.*, 101:061103, 2008.

[9] Weinberg S. *Gravitation and Cosmology: Principles and Applications of the General Theory of Relativity*. New York: Wiley, 1972.

[10] Wald R. *General Relativity*. The University of Chicago Press, 1984.

[11] Ellis G. F. R. and van Elst H. *Cosmological models: Cargese lectures 1998*. *NATO Sci. Ser. C*, 541:1–116, 1999.

[12] Fanti C. et al. *Isotropy of radio sources in the B2 catalogue*. *AAP*, 67:175–184, July 1978.

[13] Ghosh S. and Jain P. *Testing the Isotropy of the Log N–log S Slope for the NVSS Radio Catalog*. *Astrophys. J.*, 843(1):13, 2017.

[14] Sotiriou T. P. and Faraoni V. *f(R) Theories Of Gravity*. *Rev. Mod. Phys.*, 82:451–497, 2010.

[15] Sanders R.H. *The Dark Matter Problem: A Historical Perspective*. Cambridge University Press, 2010.

[16] de Swart et al. *How Dark Matter Came to Matter*. 2017. Nature Astron.1, 0059.

[17] Zwicky F. *Die Rotverschiebung von Extragalaktischen Nebeln. Helvetica Physica Acta*, 6:110–127, 1933.

[18] Smith S. *The Mass of the Virgo Cluster*. *ApJ*, 83:23, January 1936.

[19] Faber S. M. and Gallagher J. S. *Masses and mass-to-light ratios of galaxies. Ann. Rev. Astronomy and Astrophysics*, 17:135–187, 1979.

[20] Khlopov M. et al. *Particle Dark Matter Candidates. Mod. Phys. Lett.*, A32:1702001, 2017.

[21] Perlmutter, S. et al. Discovery of a supernova explosion at half the age of the Universe and its cosmological implications. *Nature*, 391:51–54, 1998.

[22] Perlmutter S. et al. *Measurements of Omega and Lambda from 42 high redshift supernovae. Astrophys. J.*, 517:565–586, 1999.

[23] Jarosik N. et al. *Seven-year Wilkinson Microwave Anisotropy Probe (WMAP) Observations: Sky Maps, Systematic Errors, and Basic Results*. *The Astrophysical Journal Supplement Series*, 192:14, February 2011.

[24] Komatsu E. et al. *Seven-year Wilkinson Microwave Anisotropy Probe (WMAP) Observations: Cosmological Interpretation. The Astrophysical Journal Supplement Series*, 192:18, February 2011.

[25] Larson D. et al. *Seven-year Wilkinson Microwave Anisotropy Probe (WMAP) Observations: Power Spectra and WMAP-derived Parameters. The Astrophysical Journal Supplement Series*, 192:16, February 2011.

[26] Sachs R. K. and Wolfe A. M. *Perturbations of a Cosmological Model and Angular Variations of the Microwave Background*. *ApJ*, 147:73, January 1967.

[27] Giannantonio T. et al. *Combined analysis of the integrated Sachs-Wolfe effect and cosmological implications. Phys. Rev.*, D77:123520, 2008.

[28] Novosyadlyj B. et al. *Dark Energy: Observational Evidence and Theoretical Models*. Academperiodyka, Kyiv, 2013.

[29] Velten H. E. S. et al. *Aspects of the cosmological "coincidence problem". Eur. Phys. J.*, C74(11):3160, 2014.

[30] de Blok W. J. G. *The Core-Cusp Problem. Advances in Astronomy*, 2010:789293, January 2010.

[31] Bullock J. S. *Notes on the Missing Satellites Problem. arXiv e-prints*, page arXiv:1009.4505, September 2010.

[32] Stelle K. S. *Renormalization of Higher Derivative Quantum Gravity. Phys. Rev.*, D16:953–969, 1977.

[33] Utiyama R. and De Witt B. S. *Renormalization of a classical gravitational field interacting with quantized matter fields. J. Math. Phys.*, 3:608–618, 1962.

[34] Birrell N. D. and Davies P. C. W. *Quantum Fields in Curved Space*. Cambridge Monographs on Mathematical Physics. Cambridge Univ. Press, Cambridge, UK, 1984.

[35] Buchbinder I. L. et al. *Effective action in quantum gravity*. 1992.

[36] Vilkovisky G. A. *Effective action in quantum gravity. Class. Quant. Grav.*, 9:895–903, 1992.

[37] Starobinsky A. A. *A New Type of Isotropic Cosmological Models Without Singularity. Phys. Lett.*, B91:99–102, 1980. [771(1980)].

[38] Brandenberger R. H. *A Nonsingular universe*. In *International School of Astrophysics, 'D. Chalonge': 2nd Course: Current Topics in Astrofundamental Physics Erice, Italy, September 6-13, 1992*, pages 102–112, 1992.

[39] Eisenstein D. J. et al. *Detection of the Baryon Acoustic Peak in the Large-Scale Correlation Function of SDSS Luminous Red Galaxies. Astrophys. J.*, 633:560–574, 2005.

[40] Riess, A. G. et al. *Type Ia supernova discoveries at $z > 1$ from the Hubble Space Telescope: Evidence for past deceleration and constraints on dark energy evolution. Astrophys. J.*, 607:665–687, 2004.

[41] Spergel, D. N. et al. *Wilkinson Microwave Anisotropy Probe (WMAP) three year results: implications for cosmology. Astrophys. J. Suppl.*, 170:377, 2007.

[42] Clifton, T. et al. *Modified Gravity and Cosmology. Phys. Rept.*, 513:1–189, 2012.

[43] Faraoni V. and Capozziello S. *Beyond Einstein Gravity*, volume 170. Springer, Dordrecht, 2011.

[44] Lovelock, D. *The Einstein tensor and its generalizations. J. Math. Phys.*, 12:498–501, 1971.

[45] Cognola, G. et al. Dark energy in modified gauss-bonnet gravity: Late-time acceleration and the hierarchy problem. *Phys. Rev. D*, 73:084007, Apr 2006.

[46] Nojiri S. and Odintsov S. D. *Modified Gauss-Bonnet theory as gravitational alternative for dark energy. Phys. Lett.*, B631:1–6, 2005.

[47] de la Cruz-Dombriz A. and Saez-Gomez D. *On the stability of the cosmological solutions in $f(R,G)$ gravity*. *Class. Quant. Grav.*, 29:245014, 2012.

[48] Brans C. and Dicke R. H. *Mach's Principle and a Relativistic Theory of Gravitation*. *Phys. Rev.*, 124:925–935, Nov 1961.

[49] C. H. Brans. Mach's principle and a relativistic theory of gravitation. ii. *Phys. Rev.*, 125:2194–2201, Mar 1962.

[50] García-Bellido, J. et al. *Fluctuations of the gravitational constant in the inflationary Brans-Dicke cosmology*. *Phys. Rev. D*, 50:730–750, Jul 1994.

[51] Cembranos, J. A. R. et al. *Quantum Corrections to the Cosmological Evolution of Conformally Coupled Fields*. *JCAP*, 0907:025, 2009.

[52] L. H. Ford. *Inflation driven by a vector field*. *Phys. Rev. D*, 40:967–972, Aug 1989.

[53] Maroto A. L. Jiménez J. B. Cosmic vector for dark energy. *Phys. Rev. D*, 78:063005, Sep 2008.

[54] Koivisto T. and Mota D. F. *Vector Field Models of Inflation and Dark Energy*. *JCAP*, 0808:021, 2008.

[55] Alcaraz J. et al. *Limits on the brane fluctuations mass and on the brane tension scale from electron-positron colliders*. *Phys. Rev. D*, 67:075010, Apr 2003.

[56] Dvali G. R. et al. *4-D gravity on a brane in 5-D Minkowski space*. *Phys. Lett.*, B485:208–214, 2000.

[57] Lindén, T. L. J. *A scalar field theory of gravitation*. *International Journal of Theoretical Physics*, 5(5):359–368, Sep 1972.

[58] Faraoni, V. *Cosmology in scalar tensor gravity*, volume 139. 2004.

[59] Dicke, R. H. Brans, C. *Mach's principle and a relativistic theory of gravitation*. *Phys. Rev.*, 124:925–935, 1961. [,142(1961)].

[60] Blaschke D. and Dabrowski M. P. *Conformal relativity versus Brans-Dicke and superstring theories*. *Entropy*, 14:1978–1996, 2012.

[61] Khoury J. et al. Chameleon cosmology. *Phys. Rev.*, D69:044026, 2004.

[62] Perivolaropoulos L. *PPN Parameter gamma and Solar System Constraints of Massive Brans-Dicke Theories*. *Phys. Rev.*, D81:047501, 2010.

[63] Hohmann M. et al. *Post-Newtonian parameters γ and β of scalar-tensor gravity with a general potential*. *Phys. Rev.*, D88(8):084054, 2013. [Erratum: Phys. Rev.D89,no.6,069901(2014)].

[64] Capozziello, S. et al. *Dark energy: The Equation of state description versus scalar-tensor or modified gravity*. *Phys. Lett.*, B634:93–100, 2006.

[65] Sotiriou T. P. *f(R) gravity and scalar-tensor theory*. *Class. Quant. Grav.*, 23:5117–5128, 2006.

[66] T. P. Sotiriou. *Curvature scalar instability in f(R) gravity*. *Phys. Lett.*, B645:389–392, 2007.

[67] Carroll S. M. et al. *Is cosmic speed - up due to new gravitational physics?* *Phys. Rev.*, D70:043528, 2004.

[68] Bertotti, B. et al. *A test of general relativity using radio links with the Cassini spacecraft*. *Nature*, 425:374–376, 2003.

[69] Amendola L. et al. *Are f(R) dark energy models cosmologically viable ?* *Phys. Rev. Lett.*, 98:131302, 2007.

[70] Amendola, L. et al. *Power-laws f(R) theories are cosmologically unacceptable*. *Int. J. Mod. Phys.*, D16:1555–1561, 2007.

[71] Amendola, L. et al. *Conditions for the cosmological viability of f(R) dark energy models*. *Phys. Rev.*, D75:083504, 2007.

[72] Odintsov S. D. Nojiri S. Modified f(R) gravity consistent with realistic cosmology: From matter dominated epoch to dark energy universe. *Phys. Rev.*, D74:086005, 2006.

[73] Nojiri S. and Odintsov S. D. *Modified gravity and its reconstruction from the universe expansion history*. *J. Phys. Conf. Ser.*, 66:012005, 2007.

[74] Evans J. D. et al. *Standard Cosmological Evolution in a Wide Range of f(R) Models*. *Phys. Rev.*, D77:083514, 2008.

[75] De Witt B. S. *Dynamical theory of groups and fields*. *Conf. Proc.*, C630701:585–820, 1964. [Les Houches Lect. Notes13,585(1964)].

[76] Chiba T. *1/R gravity and scalar - tensor gravity*. *Phys. Lett.*, B575:1–3, 2003.

[77] O' Hanlon J. *Mach's principle and a new gauge freedom in Brans-Dicke theory*. *J. Phys.*, A5:803–811, 1972.

[78] Teyssandier P. and Tourrenc Ph. *The Cauchy problem for the $R+R^2$ theories of gravity without torsion*. *J. Math. Phys.*, 24:2793, 1983.

[79] Wands D. *Extended gravity theories and the Einstein-Hilbert action*. *Class. Quant. Grav.*, 11:269–280, 1994.

[80] Lazkoz R. et al. *$f(R)$ gravity modifications: from the action to the data*. *Eur. Phys. J.*, C78(3):213, 2018.

[81] Basilakos S. and Nesseris S. *Conjoined constraints on modified gravity from the expansion history and cosmic growth*. *Phys. Rev.*, D96(6):063517, 2017.

[82] Jaime, L. et al. *Cosmology in $f(R)$ exponential gravity*. *Springer Proc. Phys.*, 157:363–371, 2014.

[83] Dunsby P. K. S. et al. *On the LCDM Universe in f(R) gravity*. *Phys. Rev.*, D82:023519, 2010.

[84] Chiba T. et al. *Solar System constraints to general f(R) gravity*. *Phys. Rev.*, D75:124014, 2007.

[85] Khoury J. and Weltman A. *Chameleon fields: Awaiting surprises for tests of gravity in space*. *Phys. Rev. Lett.*, 93:171104, 2004.

[86] Sokolowski L. M. *Stability of a metric f(R) gravity theory implies the Newtonian limit*. *Acta Phys. Polon.*, B39:2879–2901, 2008.

[87] Appleby S. A. et al. *Curing singularities in cosmological evolution of f(R) gravity*. *JCAP*, 1006:005, 2010.

[88] Cline J. M. et al. *The Phantom menaced: Constraints on low-energy effective ghosts*. *Phys. Rev.*, D70:043543, 2004.

[89] Nariai H. *Gravitational instability of regular model-universes in a modified theory of general relativity*. *Prog. Theor. Phys.*, 49:165–180, 1973.

[90] Gurovich V. Ts. and Starobinsky A. A. *Quantum Effects and Regular Cosmological Models*. *Sov. Phys. JETP*, 50:844–852, 1979.

[91] Dolgov A. D. and Kawasaki M. *Can modified gravity explain accelerated cosmic expansion?* *Phys. Lett.*, B573:1–4, 2003.

[92] V. Faraoni. *Matter instability in modified gravity*. *Phys. Rev.*, D74:104017, 2006.

[93] V. Faraoni. *de Sitter space and the equivalence between f(R) and scalar-tensor gravity*. *Phys. Rev.*, D75:067302, 2007.

[94] V. Faraoni. *f(R) gravity: Successes and challenges*. In *18th SIGRAV Conference Cosenza, Italy, September 22-25, 2008*, 2008.

[95] Appleby S. A. and Battye R. A. *Do consistent $F(R)$ models mimic General Relativity plus Λ?* *Phys. Lett.*, B654:7–12, 2007.

[96] Starobinsky, A. A. *Disappearing cosmological constant in f(R) gravity*. *JETP Lett.*, 86:157–163, 2007.

[97] Tsujikawa, S. *Observational signatures of f(R) dark energy models that satisfy cosmological and local gravity constraints*. *Phys. Rev.*, D77:023507, 2008.

[98] Jaime, L. G. et al. *f(R) Cosmology revisited*. 2012.

[99] Salgado M. *The Cauchy problem of scalar tensor theories of gravity*. *Class. Quant. Grav.*, 23:4719–4742, 2006.

[100] Ehlers J. et al. *Isotropic solutions of the Einstein-Liouville equations*. *J. Math. Phys.*, 9:1344–1349, 1968.

[101] Stoeger W. R. et al. *Proving almost homogeneity of the universe: An Almost Ehlers-Geren-Sachs theorem*. *Astrophys. J.*, 443:1, 1995.

[102] Clarkson C. A. et al. *The Cosmic microwave background and scalar tensor theories of gravity*. *Phys. Rev.*, D64:063510, 2001.

[103] Maartens R.and Taylor D. R. *Fluid dynamics in higher order gravity*. *Gen. Rel. Grav.*, 26:599–613, 1994.

[104] G. F. R. Ellis. *General Relativity and Cosmology. Proceeding of the XLVII Enrico Fermi Summer School Ed. R K Sachs.* Academic Press New York, 1971. p 104 - 182.

[105] Ehlers J. *Contributions to the relativistic mechanics of continuous media*. *Gen. Rel. Grav.*, 25:1225–1266, 1993. [Abh. Akad. Wiss. Lit. Mainz. Nat. Kl.11,793(1961)].

[106] Maartens R. *Linearization instability of gravity waves?* *Phys. Rev.*, D55:463–467, 1997.

[107] Carloni S. et al. The Evolution of density perturbations in f(R) gravity. *Phys. Rev.*, D77:024024, 2008.

[108] Kodama H. and Sasaki M. *Cosmological Perturbation Theory*. *Progress of Theoretical Physics Supplement*, 78:1–166, 01 1984.

[109] de la Cruz-Dombriz, A. et al. *On tidal forces in f(R) theories of gravity*. *Phys. Rev.*, D89(6):064029, 2014.

[110] Synge J. L. *On the deviation of geodesics and null-geodesics, particularly in relation to the properties of spaces of constant curvature and indefinite line-element. Annals of Mathematics*, pages 705–713, 1934.

[111] de la Cruz-Dombriz A. et al. *Theoretical and observational constraints of viable f(R) theories of gravity*. *Phys. Rev.*, D93(8):084016, 2016.

[112] Albareti F. D. et al. *On the non-attractive character of gravity in f(R) theories*. *JCAP*, 1307:009, 2013.

[113] de la Cruz-Dombriz A. Albareti F. D., Cembranos J. A. R. *Focusing of geodesic congruences in an accelerated expanding Universe*. *JCAP*, 1212:020, 2012.

[114] E. M. Lifshitz. On the gravitational stability of the expanding universe. *Zhurnal Eksperimentalnoi i Teoreticheskoi Fiziki*, 16:587–602, 1946.

[115] Lifshitz E. M. and Khalatnikov I. M. *Investigations in relativistic cosmology*. *Adv. Phys.*, 12:185–249, 1963.

[116] Bardeen J. M. *Gauge Invariant Cosmological Perturbations*. *Phys. Rev.*, D22:1882–1905, 1980.

[117] Miedema P. G. *Relativistic Cosmological Perturbation Theory and the Evolution of Small-Scale Inhomogeneities*. 2011.

[118] Bruni M. et al. *Cosmological perturbations and the physical meaning of gauge invariant variables*. *Astrophys. J.*, 395:34–53, 1992.

[119] Ananda K. N. et al. *A detailed analysis of structure growth in $f(R)$ theories of gravity*. *Class. Quant. Grav.*, 26:235018, 2009.

[120] Bruni M., Dunsby P. K. S., Ellis G. F. R. *Cosmological perturbations and the physical meaning of gauge-invariant variables*. *ApJ*, 395:34–53, August 1992.

[121] Carloni S. *Covariant gauge invariant theory of Scalar Perturbations in $f(R)$-gravity: a brief review*. *Open Astron. J.*, 3:76–93, 2010.

[122] Navarro I. and Van Acoleyen K. *f(R) actions, cosmic acceleration and local tests of gravity*. *JCAP*, 0702:022, 2007.

[123] De Felice A. and Tsujikawa S. *f(R) theories*. *Living Rev. Rel.*, 13:3, 2010.

[124] Ellis G. F. R Wainwright J. *Dynamical Systems in Cosmology*. Cambridge Univ. Press, Cambridge, UK, 1997.

[125] Place, C. M. Arrowsmith, D. K. *An Introduction to Dynamical Systems*. Cambridge University Press, 1990.

[126] Faraoni V. de Souza J. C. C. *The phase space view of f(R) gravity*. *Class. Quant. Grav.*, 24:3637–3648, 2007.

[127] Carloni S. and Dunsby P. K. S. *A Dynamical system approach to higher order gravity*. *J. Phys.*, A40:6919–6926, 2007.

[128] Carloni S. et al. *Cosmological dynamics of scalar-tensor gravity*. *Class. Quant. Grav.*, 25:035008, 2008.

[129] Alho A. et al. On dynamical systems approaches and methods in $f(R)$ cosmology. *JCAP*, 1608(08):064, 2016.

[130] Carloni S. et al. *Unifying the study of background dynamics and perturbations in $f(R)$-gravity*. 2008.

[131] Filippenko A. V. and Riess A. G. *Type ia supernovae and their cosmological implications*. 1999.

[132] Hlozek R. Bassett B. A. Baryon Acoustic Oscillations. [arXiv:0910.5224] 2009.

[133] Riess, A. G. et al. *Observational evidence from supernovae for an accelerating universe and a cosmological constant*. *Astron. J.*, 116:1009–1038, 1998.

[134] Riess, A. G. et. al. *Tests of the accelerating Universe with near-infrared observations of a high-redshift type Ia supernova*. *Astrophys. J.*, 536:62, 2000.

[135] Suzuki, N. et al. *The Hubble Space Telescope Cluster Supernova Survey. V. Improving the Dark-energy Constraints above $z > 1$ and Building an Early-type-hosted Supernova Sample*. *apj*, 746:85, February 2012.

[136] Astier, P. *et al. The Supernova Legacy Survey: measurement of Ω_M, Ω_Λ and w from the first year data set*. *Astronomy and Astrophysics*, 447:31–48, February 2006.

[137] Wood-Vasey, W. M. et al. *Observational constraints on the nature of Dark Energy: First Cosmological Results from the ESSENCE Supernova Survey*. *ApJ*, 666:694–715, September 2007.

[138] Kessler, R. et al. *First-Year Sloan Digital Sky Survey-II Supernova Results: Hubble Diagram and Cosmological Parameters*. *The Astrophysical Journal Supplement Series*, 185:32–84, November 2009.

[139] Amanullah, R. et al. *Spectra and Hubble Space Telescope Light Curves of Six Type Ia Supernovae at $0.511 < z < 1.12$ and the Union2 Compilation*. *ApJ*, 716:712–738, June 2010.

[140] Tegmark M. Eisenstein D. J., Hu W. *Cosmic Complementarity: H_0 and Ω_m from Combining Cosmic Microwave Background Experiments and Redshift Surveys*. *ApJL*, 504:L57–L60, September 1998.

[141] Blake, C. et al. *The WiggleZ Dark Energy Survey: mapping the distance-redshift relation with baryon acoustic oscillations*. *Monthly Notices of the Royal Astronomical Society*, 418:1707–1724, December 2011.

[142] Blake C. et al. *Cosmological baryonic and matter densities from 600000 SDSS luminous red galaxies with photometric redshifts*. *Monthly Notices of the Royal Astronomical Society*, 374:1527–1548, February 2007.

[143] Meiksin A. and Peacock J. A. White M. *Baryonic signatures in large-scale structure*. *Monthly Notices of the Royal Astronomical Society*, 304:851–864, April 1999.

[144] Padmanabhan N. and White M. *Calibrating the baryon oscillation ruler for matter and halos*. *Phys. Rev. D*, 80(6):063508, September 2009.

[145] Staveley-Smith L. et al. *The 6dF Galaxy Survey: baryon acoustic oscillations and the local Hubble constant*. *Monthly Notices of the Royal Astronomical Society*, 416(4):3017–3032, 09 2011.

[146] Percival W J. et al. *Baryon acoustic oscillations in the Sloan Digital Sky Survey Data Release 7 galaxy sample*. *Monthly Notices of the Royal Astronomical Society*, 401(4):2148–2168, 01 2010.

[147] Padmanabhan, N. et al. *A 2 per cent distance to $z = 0.35$ by reconstructing baryon acoustic oscillations – I. Methods and application to the Sloan Digital Sky Survey*. *Monthly Notices of the Royal Astronomical Society*, 427(3):2132–2145, 12 2012.

[148] Abebe, A. et al. *Large Scale Structure Constraints for a Class of f(R) Theories of Gravity*. *Phys. Rev.*, D88:044050, 2013.

[149] Ho, S. et al. *Clustering of Sloan Digital Sky Survey III Photometric Luminous Galaxies: The Measurement, Systematics, and Cosmological Implications*. *ApJ*, 761:14, December 2012.

[150] Guth A. H. *Inflationary universe: A possible solution to the horizon and flatness problems*. *Phys. Rev. D*, 23:347–356, Jan 1981.

[151] Anderson, L. et al. *The clustering of galaxies in the SDSS-III Baryon Oscillation Spectroscopic Survey: baryon acoustic oscillations in the Data Releases 10 and 11 Galaxy samples*. *Mon. Not. Roy. Astron. Soc.*, 441(1):24–62, 2014.

[152] Eisenstein D. J. et al. *SDSS-III: Massive Spectroscopic Surveys of the Distant Universe, the Milky Way, and Extra-Solar Planetary Systems*. *AJ*, 142:72, September 2011.

[153] Kobayashi T. and Maeda K. *Relativistic stars in f(R) gravity, and absence thereof*. *Phys. Rev.*, D78:064019, 2008.

[154] Saez-Gomez D. *Cosmological evolution, future singularities and Little Rip in viable f(R) theories and their scalar-tensor counterpart*. *Class. Quant. Grav.*, 30:095008, 2013.

[155] P. Zhang. *Testing gravity against the early time integrated Sachs-Wolfe effect. Phys. Rev. D*, 73:123504, Jun 2006.

[156] Ross, A. J. et al. *The clustering of galaxies in the SDSS-III Baryon Oscillation Spectroscopic Survey: analysis of potential systematics. Monthly Notices of the Royal Astronomical Society*, 424(1):564–590, 07 2012.

[157] Nunes, R. C. et al. *New observational constraints on $f(R)$ gravity from cosmic chronometers. JCAP*, 1701(01):005, 2017.

[158] Chen Y. et al. *Matter Power Spectra in Viable $f(R)$ Gravity Models with Dynamical Background. Eur. Phys. J.*, C79(2):93, 2019.

[159] Gubitosi G. et al. *The effective field theory of dark energy. Journal of Cosmology and Astroparticle Physics*, 2013(02):032–032, feb 2013.

[160] Bloomfield J. *A simplified approach to general scalar-tensor theories. Journal of Cosmology and Astroparticle Physics*, 2013(12):044–044, dec 2013.

[161] Hu B. et al. *Effective Field Theory of Cosmic Acceleration: an implementation in CAMB. Phys. Rev.*, D89(10):103530, 2014.

[162] Hu B. et al. *Testing Hu–Sawicki f(R) gravity with the effective field theory approach. Mon. Not. Roy. Astron. Soc.*, 459(4):3880–3889, 2016.